T2R2 東京科学大学 リサーチリポジトリ
Science Tokyo Research Repository

論文 / 著書情報
Article / Book Information

題目(和文)	コンパクトMIMOシステム用最適低雑音受信機の設計
Title(English)	Optimal Low Noise Receiver Design for Compact MIMO System
著者(和文)	ｼﾞﾖﾝｼﾞｴﾎ
Author(English)	Jaeho Jeong
出典(和文)	学位:博士（工学）, 学位授与機関:東京工業大学, 報告番号:甲第9628号, 授与年月日:2014年9月25日, 学位の種別:課程博士, 審査員:鈴木　博,安藤　真,高田　潤一,府川　和彦,廣川　二郎,阪口　啓
Citation(English)	Degree:, Conferring organization: Tokyo Institute of Technology, Report number:甲第9628号, Conferred date:2014/9/25, Degree Type:Course doctor, Examiner:,,,,,
学位種別(和文)	博士論文
Type(English)	Doctoral Thesis

Powered by T2R2 (Science Tokyo Research Repository)

Doctoral Dissertation

Optimal Low Noise Receiver Design for Compact MIMO System

September 2014

Supervisor

Professor Hiroshi Suzuki

Associate Professor Kei Sakaguchi

Department of Electrical & Electronic Engineering

Graduate School of Engineering

Tokyo Institute of Technology

Jaeho Jeong

Acknowledgements

I would like to express my profound gratitude to all of my family, colleagues and supervisors for their constant support. I am profoundly thankful to Professor Kiyomichi Araki, who was an initial adviser, for his invaluable guidance, consideration, and support, as well as he inspires me tremendous research ideas under his supervision. He has instructed not only the fundamental background of mobile communications but also how to approach the various conceptual problems.

I also deeply thank to Professor Suzuki Hiroshi for his supervision, patient and consideration. I sincerely thank to Associate Professor Kei Sakaguchi for his great comments and novel viewpoints during all seminars. I would like to deeply thank the committee members of my dissertation, Professor Makoto Ando, Professor Jun-ichi Takada, Professor Kazuhiko Fukawa, and Associate Professor Jiro Hirokawa for their perseverance and time in evaluating this dissertation and their valuable comments.

Furthermore, I am very grateful to Assistant Professor Tran Gia Khanh for reviewing my research and providing fruitful insights during our discussions on my works. And, I would like to express my gratitude to Dr. Chang YuYuan and all lab members for their friendship and help over the past years.

Finally, I am indebted to my parents for supporting given throughout my life. Without their unconditional help, the thesis not have been completed successfully.

Abstract

Multiple-input multiple-output (MIMO) systems deploy multiple antennas at both the transmitter and receiver to improve the spectral efficiency and link reliability of wireless communications. With the development of communication theory, the study of MIMO technique has become more feasible, though several problems need to be solved as ever at the receive end mostly. The insufficient antenna spacing due to the small aspect of the receive end causes the mutual coupling (MC) strongly, which deteriorates performance of the MIMO system.

To alleviate the problem, this thesis focus on the low noise MIMO receiver with mutually coupled antennas. We first address a noise matching problem for MIMO receiver with mutual coupling in the presence of correlated fading and noise. To minimize the noise figure, matching network scheme is employed. As the optimal matching network minimizing the noise figure is hard to realize in practice, we develop an even-odd mode matching method with simple design procedure, high performance and easy implementation. For the effect of practical matching circuit, the matching circuit in lossy condition is investigated using Q-factor of circuit parameters with planar network structure in a specific condition.

We furthermore propose a novel low noise model of single front-end MIMO (SF-MIMO) receiver system with parasitic antenna element (PAE) which includes arbitrary signal and noise coupling. Single front-end architecture with PAE in compact array system is investigated for enhancing spectral efficiency and miniaturizing the receiver. The proposed model articulates physical noise sources and relates their spatial correlation with array receive antennas, parasitic element, front-end and matching circuit. After that, the optimal PAE value is derived to maximize channel capacity. Finally, we demonstrate that SF-MIMO system with PAE impacts on performance through analytical and numerical results.

Contents

Chapter 1 Introduction **1**

1.1 Introduction and motivation 1

1.2 Main contribution and thesis structure 3

Chapter 2 MIMO Communication with Correlated Fading **7**

2.1 Introduction 7

2.2 Channel model 8

2.3 MIMO channel capacity 15

2.4 Summary 20

Chapter 3 Low Noise Matching Design **21**

3.1 Introduction 21

3.2 System model 22

3.3 Design for matching circuit 26

3.4 Numerical results 32

3.5 Summary 38

Chapter 4 Matching Circuit in Realization **39**

4.1 Introduction 39

4.2 Multi-port circuit realization 39

4.3 symmetrical matching circuit 43

4.4 Lossy matching circuit 45

4.5 Numerical results 46

4.6 Summary 54

Chapter 5 Single Front-end Receiver with Parasitic Antenna Element 55
5.1 Introduction 55
5.2 Channel model for SF-SIMO with PAE 57
5.3 Channel model for SF-MIMO with PAE 59
5.4 Circuit model 62
5.5 Optimal noise matching 65
5.6 Numerical results 67
5.7 Summary 75

Chapter 6 Conclusion 77
6.1 Summary of the research 77
6.2 Future research topics 79

Appendix I SISO Channel Capacity 81

Appendix II Correlation Coefficient 82

Appendix III Thermal Noise Characteristic 88

Appendix IV Constant Noise Factor Circle 90

Appendix V Lossy Matching Network 92

Appendix VI List of Publications 94

Reference 97

List of Figures

1.1 Diagram of a typical MIMO communication system. 1
1.2 The organization of this dissertation. 6

2.1 Illustration of wireless propagation model in urban environment. 9
2.2 Scattering parameter representation by wave impedance for each spherical eigen-mode. 12
2.3 Correlation coefficient on two termination conditions. 14
2.4 Function formula $f(\lambda)$ for validity range of asymptotic forms. 18
2.5 Ergodic capacity boundary of rigorous form and asymptotic forms. 19

3.1 Circuit model with two multiple receivers. 22
3.2 Matching network classification. 27
3.3 Impedance matrix representation of a 2-element array. 29
3.4 Ergodic capacity as a function of even and odd mode eigenvalues. 35
3.5 Ergodic capacity as antenna separation (γ=10dB). 35
3.6 Ergodic capacity on SNR condition 36
3.7 Capacity comparison of rigorous form and two asymptotic forms. 37

4.1 Examples of multi-port circuit structure. 40
4.2 Classification of matching network. 41
4.3 Receiver model of symmetrical matching. 42
4.4 Circuit model for even-odd mode. 43
4.5 Circuit component values of symmetrical matching. 46
4.6 Ergodic channel capacity of 8 combinations ($Q = 10$). 48
4.7 Equivalent circuit for lossy matching network (case 2). 49
4.8 Matching circuit performance in different lossy condition. 49

4.9 Minimum required Q-factor as γ. 50
4.10 Signal degradation loss of even-odd mode. 50
4.11 Original noise figure by lossy condition. 51
4.12 Noise figure circle of symmetrical matching in lossy condition. 52
4.13 Smithchart of symmetrical matching on lossy condition ($Q = 10$). 53

5.1 Parasitic antenna elements system. 56
5.2 Single front-end system with PAE. 57
5.3 Channel representation for SIMO PAE system. 58
5.4 Channel model representation for SF-MIMO. 59
5.5 Switching mechanism for SF-MIMO. 61
5.6 Circuit model of a single front-end receiver with PAE. 62
5.7 Rothe-Dahlke model of single front-end. 64
5.8 Optimum PAE value for SIMO PAE system. 68
5.9 Optimum PAE value for MIMO PAE system. 69
5.10 Capacity comparison for fixed and optimal PAE in SF-MIMO PAE. 70
5.11 Capacity comparison with other systems (d=$\lambda_w/8$). 71
5.12 Capacity comparison with other systems (d=$\lambda_w/2$). 72
5.13 Frequency characteristic (d=$\lambda_w/8$, γ=10dB). 73
5.14 Capacity versus antenna distance (γ=10dB). 74

II.1 Schematic of an incident wave impinging across antenna array. 83
II.2 Concept of mutual coupling of an array antenna. 83
II.3 Self and mutual impedance using induced EMF method. 84
II.4 Schematic of coupling paths between array antennas. 85
II.5 Comparison of various correlation models. 86

III.1 Schematic of loss property with impedance matrix. 88

IV.1 NF circle of SISO antenna receiver. 90

V.1 Single receiver model for lossy matching network. 92

List of Tables

3.1 Antenna conditions. 34
3.2 Antenna parameters. 34
3.3 Front-end noise parameters. 34

4.1 Combination of matching network components. 47

Notations

In this thesis, uppercase boldface type is used for matrices and lowercase boldface is used for vectors; all scalar quantities are not in boldface. The other notations are listed as follow:

j	the imaginary unit in complex number
$\triangleq$	defined as equal to
$\gg$	much greater than
$\ll$	much less than
$\otimes$	Kronecker product
a^*	complex conjugate of a
$\log_2 a$	the base 2 log of a
$\arg\max(a)$	value of a that maximizes
$\mathbb{C}^{m\times n}$	the field of complex numbers where $m \times n$ is the size of the field
$\mathbf{a}^T$	transpose of vector $\mathbf{a}$
$\mathbf{A}^T$	transpose of matrix $\mathbf{A}$
$\mathbf{A}^\dagger$	conjugate transpose of matrix $\mathbf{A}$
$\mathbf{A}^{-1}$	inverse of matrix $\mathbf{A}$
$\mathbf{A}^{1/2}$	square root of matrix $\mathbf{A}$
$\Re(a)$	the real part of a complex number a
$\Re[\mathbf{A}]$	the real part of a complex matrix $\mathbf{A}$
$\mathrm{E}[\cdot]$	expectation operator
$\mathrm{tr}[\mathbf{A}]$	trace of matrix $\mathbf{A}$
$\det[\mathbf{A}]$	determinant of matrix $\mathbf{A}$
$\mathrm{diag}[\mathbf{A}]$	diagonal elements of matrix $\mathbf{A}$
$\mathrm{vec}[\mathbf{A}]$	columnwise vectorisation operation of a matrix $\mathbf{A}$
$\mathbf{I}_N$	$N \times N$ identity matrix

Chapter 1

Introduction

This thesis is devoted for low noise receiver design in compact MIMO system. This chapter briefly introduces the motivation and prior work in Section 1.1. Then section 1.2 present main contribution and thesis structure.

1.1 Introduction and motivation

Multiple-input multiple-output (MIMO) communication which employs multiple antennas at the transmitter (Tx) and the receiver (Rx) is a key technology enhancing spectral efficiency. The two characteristics of MIMO system over single-input single output (SISO) system are diversity technique which transmits same signal with multiple sub-channels and the information combination at the receiver [1] [2] and multiplexing technique which is realized by transmit-

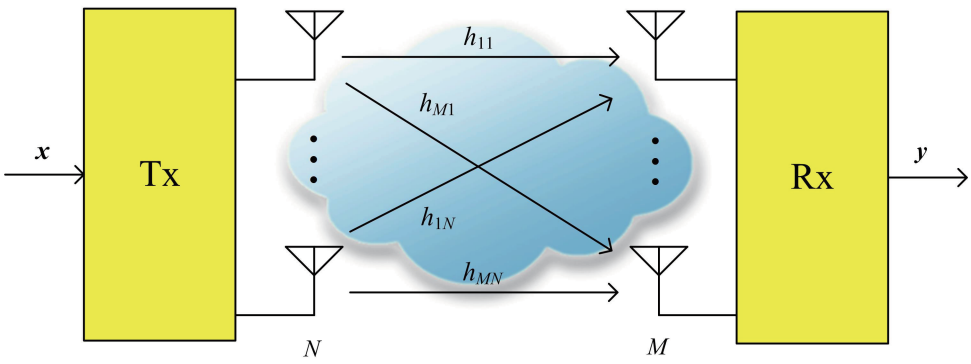


Figure 1.1 Diagram of a typical MIMO communication system.

ting different signals over different sub-channels simultaneously. As the diversity performance is an important factor in MIMO system, enough antenna spacing is necessity condition for a decent MIMO system performance. However, the integration of multiple antenna with radio-frequency (RF) front-end is affected by the limited design space, which results in impractical for compact mobile devices.

As the antenna elements become more compact with higher mutual coupling effect, previous authors concluded that the channel capacity deteriorates more severely due to a mismatch of impedance matrix [6, 16]. With closely spaced antennas, impairments such as fading correlation and mutual coupling become more remarkable. Transceivers designed for compact antenna arrays often employ special RF matching networks embedded between the antenna array and the rest of the RF chain for optimizing the system performance. Impedance mismatch between the RF front-end and the antenna increases the noise delivered to the antenna and hence decreases the performance of the entire system.

Conventional studies have proposed optimal transceiver design for MIMO systems in the presence of mutual coupling by utilizing multiport matching network [34]. Recent works have also paid attention to the noise and the mutual coupling effect at the receiver [27] [28]. The realistic noise model was considered to be consisted of two noise sources i.e. sky noise (external noise) and front-end noise (internal noise) [25] [26]. These papers demonstrated that the matching for minimizing noise figure matrix can be superior than maximizing the power transfer function. Although the coupled matching circuit showed the optimal performance, it is difficult to implement in practice due to the complexity of multi-layer realization across antenna ports of the antenna array [30]. To alleviate the complexity, simple single port matching system maximizing capacity has been studied with the common assumption that the coupled antenna impedance can be adequately represented using only the diagonal elements of the antenna impedance matrix for the case of isolated dipole [24, 31]. However, the works did not consider realistic noise sources and their performance were also deteriorated as compared to the optimal matching system as well.

On the other hand, in conventional MIMO architecture, a transceiver circuit is required for each antenna port, which increases the cost of RF front-end and power consumption. Under these technical problems including the requests for device miniaturization and cost reduction, Kalis proposed a MIMO transmitter using a single RF front-end by mapping multiple signal streams transmitted simultaneously on a set of basis radiation patterns [37]. The proposed single front-end (SF) architecture can be a suitable solution as an ideal architecture to alleviate

this problem. Moreover, the latest work has been studied that antenna switching with SF architecture enables data multiplexing without deterioration due to the switching penalty, owing to the analog beamforming effect of parasitic antenna element (PAE) [38].

1.2 Main contribution and thesis structure

The main contributions of this thesis can be summarized as follows:

- Matching networks for low noise receiver in compact MIMO system with correlated fading and noise are examined. Conventional matching network based on multiport circuit is difficult to implement in practice due to the complexity of multi-layer realization. Assuming symmetrical channel characteristic, symmetrical array antenna and identical front-end, a so-called symmetrical matching of optimal low noise receiver is proposed for simple design procedure, high performance and easy implementation.

- For practical usage of the matching circuit, we theoretically derive the corresponding realization circuit parameters with reduced RF complexity. Furthermore, lossy condition within the matching circuit is studied in a specific realistic simulation condition. The numerical results for the effect of the lossy matching circuit confirm the theoretical and simulation predictions through discrepancies as Q-factor of inductor elements.

- As a new alternative low noise receiver design for compact MIMO system, we proposed new architecture receive design with single front-end (SF) system with parasitic antenna element (PAE). Another characteristic is required by antenna switching for signal multiplexing and SF-MIMO system. PAE affected by mutual coupling between array antenna can compensate for the switching penalty due to analog beamforming.

Figure. 1.2 shows the thesis structure of the remaining parts as follows.

Chaper 2 presents an overview of the background related to the topic of this thesis. It starts from the introduction of wireless propagation channel. Then signal correlation models without mutual coupling and with mutual coupling are offered. Important MIMO channel model and MIMO capacity concept are discussed. As well as a rigorous form of the ergodic capacity, the asymptotic forms on 2×2 MIMO system are derived and calculated.

Chapter 3 studies a low noise matching model for compact MIMO system. System model using channel model, array antenna, front-end and matching network are employed. Matching

network which plays an important role for maximization channel capacity is addressed. Different methods with multiport matching, symmetrical matching and identical self matching are reviewed and compared via simulation. These results are published in

- J. Jeong, G. K. Tran and K. Araki, "A design of self noise matching circuit for compact MIMO system," *IEICE Technical Report*, MW2012-80, pp83-88, Sep, 2012
- J. Jeong, G. K. Tran and K. Araki, "Ergodic capacity with optimal matching for spatially correlated 2×2 MIMO systems in 3-D isotropic scattering environment," *APMC2014*, Nov, 2014

Chapter 4 describes multiport circuit realization of a two-element compact receiver. Two network topologies for multiport circuit realization are discussed. Although multiport matching circuit with coupled signal is difficult to realize, alternative optimal matching which is called as symmetrical matching is designed and lossy condition within the desired matching circuit is examined. In the end, the simulation results for verifying the effect of the proposed matching circuit are also included. These results are published in

- J. Jeong, G. K. Tran and K. Araki, "A study of matching circuit on a lossy condition for compact symmetrical MIMO receiver," *IEICE General Conference*, B-1-207, Mar, 2013
- J. Jeong, G. K. Tran and K. Araki, "Noise figure of matching circuit on lossy condition in 2x2 symmetrical MIMO receiver system," *IEICE Society conference*, BS-6-27, Sep, 2014
- J. Jeong, G. K. Tran and K. Araki, "Complexity-reduced low noise matching design for realizaion in compact MIMO receivers," *IEICE Transactions on Electronics, Recent Progress in Microwave and Millimeter-Wave Technologies*, Vol.E97-C, No.10, pp.-, Oct. 2014

Chapter 5 investigates a new architecture receive system with SF and PAE for compact two array antennas. Two different schemes with SF-SIMO PAE and SF-MIMO PAE are developed for maximization channel capacity. Then the numerical results for verifying the effect of the proposed systems are conducted at certain conditions. These results are published in

- J. Jeong, G. K. Tran and K. Araki, "Optimal low noise single front-end MIMO receiver system with parasitic antenna element," *IEICE Transactions on Electronics, Recent*

Progress in Microwave and Millimeter-Wave Technologies, Vol.E95-C, No.10, pp.1620-1626, Oct. 2012

- J. Jeong, Y. Miao, K. Sakaguchi and K. Araki, "Optimal low noise design for single front-end receiver with PAE," *2011 Korea-Japan Microwave Conference*, FR2-4-4, Nov. 2011

- J. Jeong and K. Araki, "Optimal low noise design for SF-MIMO receiver with parasitic antenna element (PAE)," *IEICE General Conference*, B-1-223, Mar, 2012

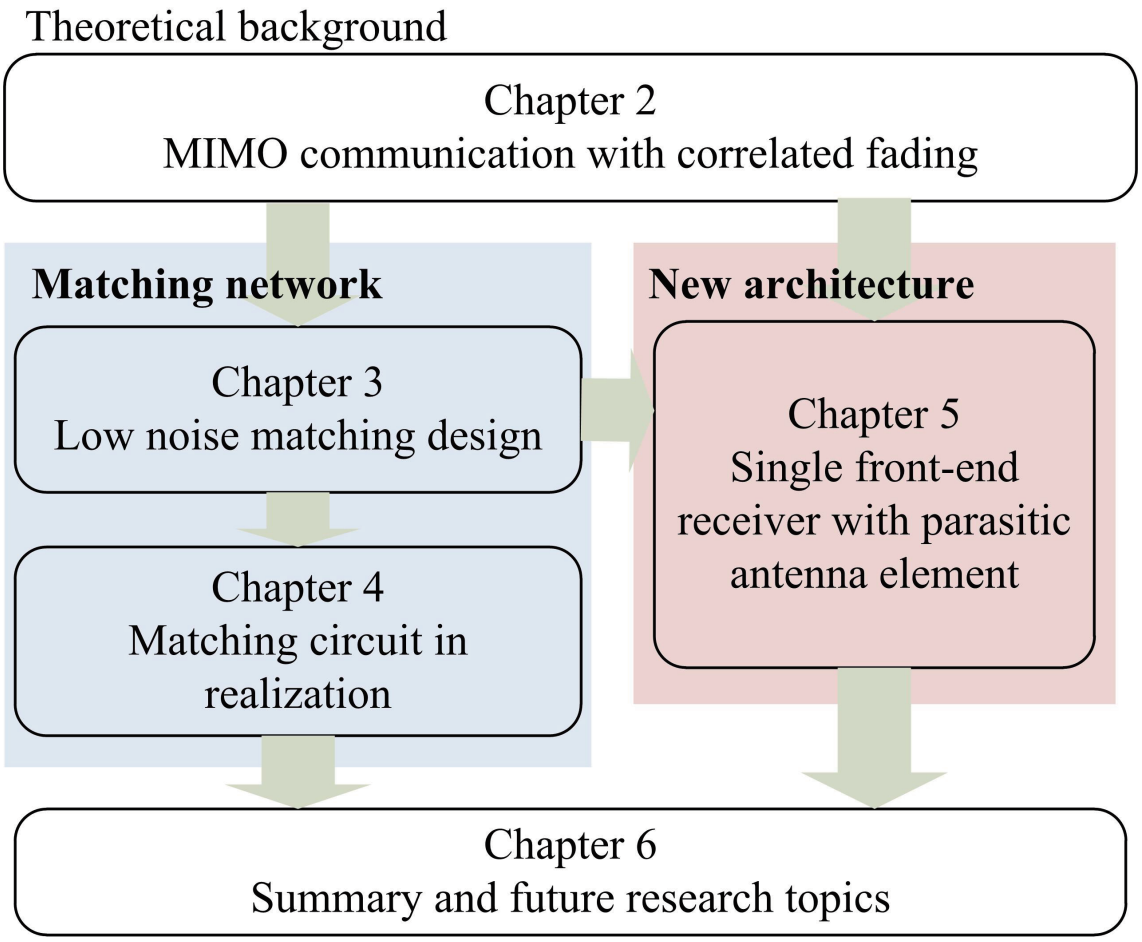


Figure 1.2 The organization of this dissertation.

Chapter 2

MIMO Communication with Correlated Fading

This chapter briefly offers fundamental background used for low noise design of compact MIMO system. We begin our study by introducing the MIMO system and compact antenna arrays with backgrounds of this thesis.

2.1 Introduction

While prior works on MIMO modeled the fading path gains as independent random variables, the recent observation led to explosion of research activity how fading path gain is correlated through the propagation environment or mutual coupling between the antennas and how this coupling effect affects. The impact of the fading correlation and the mutual coupling has been long studied in various multi-antenna systems such as diversity receiver and adaptive array [3] [4].

Initial literature dealt with MIMO capacity for fading correlation which is employed by a ray-tracing propagation model in receiver diversity [5]. This separable correlation model introduced the correlation between two fading path gains by product of two quantities with transmit and receive correlation [7]. While previous works above modeled for the propagation environment, they do not consider the interactions which may generate between antennas. From an induced electric field, the induced voltage in array antennas depends on the radiation pattern and converts to the terminal voltage by the array impedance matrix. In compact array antenna, the radiation pattern of each antenna may distort by the impact of other adjacent

antenna so that the antennas are coupled, called as the mutual coupling as an expression of non-diagonal impedance matrix [11]. Earlier studies showed that the mutual coupling effect can reduce signal correlation in insufficient antenna distance by distorting the radiation pattern of each element, so the authors concluded that the mutual coupling may increase the system capacity [12–16]. However, the capacity performance is simultaneously determined by inducing a mismatch between the characteristic impedance of the circuit and the array antenna input [17]. This contradictory result shows that the mutual coupling effect may affect the system performance as different conclusion [18].

The remainder of this chapter is organized as follows. We first introduces a stochastic wireless channel model specifies the fading and noise statistics. Since the focus of this thesis is on spatial correlation, the channel model is investigated with simplified channel not considering time and frequency domain. After introducing SISO channel model, we present a well-known MIMO channel model for the spatial correlation of fading. With the MIMO channel model, various correlation models are proved without mutual coupling and with mutual coupling which affects both the embedded element radiation patterns and the element input impedances. To carry out the system evaluation for the impact of the compact array, ergodic capacity is a widely used metric of such an evaluation. As well as a rigorous form of ergodic capacity for MIMO system, asymptotic forms for low/high SNR cases are derived and simulated for performance difference between rigorous and asymptotic forms.

2.2 Channel model

In this section, we consider a channel model for MIMO systems used throughout this dessertation. Most of the results of this section be found in wireless communication books [19] [20].

At first, we show propagation environment with a general wireless communication system in Fig. 2.1. A baseband signal $x(t)$ with the complex number transmits and receives through free space propagation environment. If we assume that the signal is deformed by noise component such as addictive white Gaussian noise (AWGN) $n(t)$ with power spectral density, then the received signal defines

$$r(t) = \sum_m \alpha_m(t) e^{-j2\pi f_c \tau_m(t)} x(t - \tau_m(t)) + n(t), \tag{2.1}$$

where $\alpha_m(t)$ and $\tau_m(t)$ are the amplitude and propagation delay of the m^{th} multipath component at time t. The propagation delay effects both the signal and the carrier $e^{j2\pi f_c t}$ with

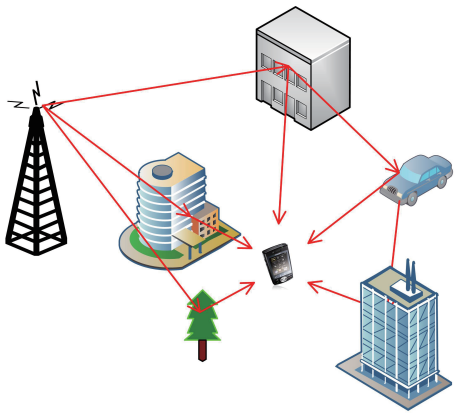


Figure 2.1 Illustration of wireless propagation model in urban environment.

the carrier frequency f_c in Hz. Since the wireless channel is linear, it can be described by the response $h(\tau, t)$ at time $t - \tau$, the input and output relationship is given by

$$r(t) = \int_{-\infty}^{\infty} h(\tau, t)x(t - \tau)d\tau + n(t). \tag{2.2}$$

Comparing Eq. (2.1) and Eq. (2.2), the impulse response for the fading multipath channel becomes

$$h(\tau, t) = \sum_m \alpha_m(t)e^{-j2\pi f_c \tau_m(t)}\delta(\tau - \tau_m(t)) + n(t), \tag{2.3}$$

and $\delta(t)$ is the Direc-delta function.

We assume the complex baseband signal $x(t)$ with bandwidth $B/2$. Samples $x[s] \triangleq x(s/B)$ taken every $1/B$ seconds can be defined by *Nyquist sampling theorem*. Then, we express *frequency flat channel* in discrete time as

$$r[s] = hx[s] + n[s], \quad s = 0, 1, \ldots, S - 1, \tag{2.4}$$

where $h \triangleq \sum_m \alpha_m e^{-j2\pi f_c \tau_m}$ is the *fading path gain* and $S \triangleq \lfloor T_c B \rfloor$ is the block length with *coherence time* T_c. And the noise model $n[s] \triangleq n(s/B)$ is an independent and identically distributed (i.i.d.) random variables sequence with variance $N_0 B$, where $n[s] \sim \mathcal{CN}(0, N_0 B)$. In practical systems, the phase $2\pi f_c \tau_m$ of each multipath component is defined by a uniformly distributed random variable. Assuming that a *rich scattering environment* with many i.i.d. multipaths by the central limit theorem $h \sim \mathcal{CN}(0, \sum_m \mathrm{E}[\alpha_m^2])$. So, this is called as *Rayleigh fading* model due to a Rayleigh distribution $|h|$.

Since this thesis does not consider the time domain, we simplify the channel model for SISO system regardless of the time from Eq. (2.4) as

$$r = hx + n, \tag{2.5}$$

where $h \sim \mathcal{CN}(0,1)$ and $n \sim \mathcal{CN}(0, N_0 B)$. We have normalized the fading path gain power to unity by absorbing the signal attenuation into the transmit power $P_t \triangleq \mathrm{E}|x|^2$.

Consider a MIMO system with N transmit antennas and M receive antennas. Denoting the impulse response between the j^{th} $(j = 1, 2, \ldots, N)$ transmit antenna and the i^{th} $(i = 1, 2, \ldots, M)$ receive antenna by h_{MN}, the MIMO channel is given by $M \times N$ matrix $\mathbf{H}$ with

$$\mathbf{H} = \begin{bmatrix} h_{11} & h_{12} & \cdots & h_{1N} \\ h_{21} & h_{22} & \cdots & h_{2N} \\ \vdots & \vdots & \ddots & \vdots \\ h_{M1} & h_{M2} & \cdots & h_{MN} \end{bmatrix}. \tag{2.6}$$

The vector $[h_{1j}\ h_{2j}\ \cdots\ h_{Mj}]^T$ is the spatial signature or channel induced by the jth transmit antenna across the receive antenna array. Assuming that the channel between each transmit and receive antenna pair is identical to the SISO model Eq. (2.5), the MIMO channel is expand in vector form by

$$\mathbf{r} = \mathbf{H}\mathbf{x} + \mathbf{n}, \tag{2.7}$$

where $\mathbf{r}, \mathbf{n} \in \mathbb{C}^M$ are the received signal and noise, respectively. The transmitted signal $\mathbf{x} \in \mathbb{C}^N$ with $P_{\mathrm{T}} r_{\mathrm{T}} = \mathrm{tr}(\mathbf{\Sigma}_{\mathrm{x}})$ noting that transmit power P_{T} and the transmit impedance r_{T}, where $\mathbf{\Sigma}_{\mathrm{x}} \triangleq \mathrm{E}[\mathbf{x}\mathbf{x}^{\dagger}]$. Since the channel matrix and noise vector are jointly ZMCSCG, it can specify the correlation between these elements, i.e. the *spatial correlation*. This section focuses on the channel matrix as the *noise correlation matrix* $\Sigma_{\mathbf{n}} \triangleq \mathrm{E}[\mathbf{n}\mathbf{n}^{\dagger}]$ will be defined in next section.

Under the channel model $\mathbf{H}$ to be ZMCSCG with unit variance, we get the spatially white channel $\mathbf{H} = \mathbf{H}_{\mathrm{w}}$ called as the i.i.d. Rayleigh fading model. It is the adopted model in the evaluation of MIMO system performance because of its analytical tractability. Some properties of $\mathbf{H}_{\mathrm{w}}$ are summarized as

$$\mathrm{E}\left\{[\mathbf{H}_{\mathrm{w}}]_{ij}\right\} = 0, \tag{2.8}$$

$$\mathrm{E}\left\{|[\mathbf{H}_{\mathrm{w}}]_{ij}|^2\right\} = 1, \tag{2.9}$$

$$\mathrm{E}\left\{[\mathbf{H}_{\mathrm{w}}]_{ij}[\mathbf{H}_{\mathrm{w}}]^*_{kl}\right\} = 1 \quad \text{if } i \neq k \text{ or } j \neq l. \tag{2.10}$$

In real propagation environment, the MIMO channel is affected by gain imbalances between channel elements and the presence of a LOS (line-of-sight). These include inadequate antenna spacing or scattering distribution leading to spatial correlation. Correlated channels imply that elements of $\mathbf{H}$ are correlated and the channel can be modeled by

$$\mathrm{vec}(\mathbf{H}) = \mathbf{\Psi}^{1/2}\mathrm{vec}(\mathbf{H}_{\mathrm{w}}), \tag{2.11}$$

where $\mathbf{H}_{\mathrm{w}}$ is the spatially white $M \times N$ MIMO channel. *Covariance matrix* $\mathbf{\Psi}$ is expressed by the $MN \times MN$ block matrix as

$$\mathbf{\Psi} = \begin{bmatrix} \mathrm{E}[\mathbf{h}_1\mathbf{h}_1^{\dagger}] & \cdots & \mathrm{E}[\mathbf{h}_1\mathbf{h}_N^{\dagger}] \\ \vdots & \ddots & \vdots \\ \mathrm{E}[\mathbf{h}_N\mathbf{h}_1^{\dagger}] & \cdots & \mathrm{E}[\mathbf{h}_N\mathbf{h}_N^{\dagger}] \end{bmatrix}. \tag{2.12}$$

where $\mathbf{h}_i$ denotes the i^{th} column of $\mathbf{H}$, so the $(k,l)^{\mathrm{th}}$ element of $\mathrm{E}[\mathbf{h}_i\mathbf{h}_j^{\dagger}]$ is $\mathrm{E}[\mathrm{h}_{ki}\mathrm{h}_{ij}^{*}]$. And $\mathbf{\Psi}$ is a positive semi-definite hermitian matrix. If $\mathbf{\Psi} = \mathbf{I}_N$, then $\mathbf{H} = \mathbf{H}_{\mathrm{w}}$. If we further assume that the transmitter does not affect the spatial properties of the received signal, $\mathbf{\Psi}$ can be separated by

$$\mathbf{\Psi} = \mathbf{\Psi}_{\mathrm{T}}^{T} \otimes \mathbf{\Psi}_{\mathrm{R}}, \tag{2.13}$$

where $\mathbf{\Psi}_{\mathrm{T}}$ and $\mathbf{\Psi}_{\mathrm{R}}$ are the covariance matrix of the transmitter and receiver, respectively. Eq. (2.13) represents that $\mathbf{H}$ is still the Rayleigh fading model with following covariance property as

$$\mathrm{E}[\mathrm{h}_{ki}\mathrm{h}_{ij}^{*}] = (\mathbf{\Psi}_{\mathrm{T}})_{ij}(\mathbf{\Psi}_{\mathrm{R}})_{kl}. \tag{2.14}$$

Referring to the Kronecker correlation model [8], $\mathbf{H}$ can be revised by

$$\mathbf{H} = \mathbf{\Psi}_{\mathrm{R}}^{1/2}\mathbf{H}_{\mathrm{w}}\mathbf{\Psi}_{\mathrm{T}}^{1/2}, \tag{2.15}$$

This model implies that receive antenna correlation $\mathbf{\Psi}_{\mathrm{R}}$ is equal to the covariance of the $M \times 1$ receive vector channel when excited by any transmit antenna, and is therefore the same for all transmit antennas.

The main topic of this dissertation is focusing on fading correlation for compact MIMO receivers. If we assume no transmit correlation $\mathbf{\Psi}_{\mathrm{T}} = \mathbf{I}_N$, we can substitute $\mathbf{\Psi}_{\mathrm{R}} = \mathbf{\Sigma}_{\mathrm{h}}$ for simplifying the analysis. Therefore, the columns of $\mathbf{H}$ in Eq. (2.7) are i.i.d. ZMCSCG random vectors with correlation matrix $\mathbf{\Sigma}_{\mathrm{h}}$, denoted by $\mathbf{h}_i \sim \mathcal{CN}(\mathbf{0}, \mathbf{\Sigma}_{\mathrm{h}})$.

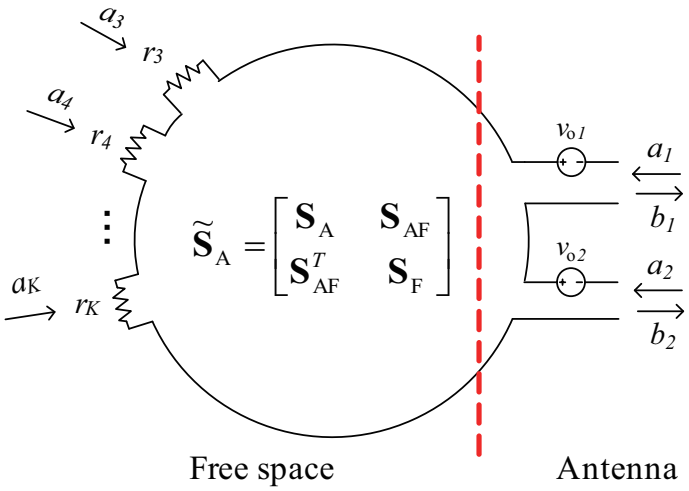


Figure 2.2 Scattering parameter representation by wave impedance for each spherical eigen-mode.

Considering a 2×2 MIMO system, we summarize the propagation channel is represented by

$$\mathbf{H} = \mathbf{\Sigma}_{\mathrm{h}}^{1/2}\mathbf{H}_{\mathrm{w}}, \quad \mathbf{\Sigma}_{\mathrm{h}} = \mathrm{E}[\mathbf{h}_i\mathbf{h}_i^{\dagger}] = \alpha \begin{bmatrix} 1 & \rho \\ \rho & 1 \end{bmatrix}, \tag{2.16}$$

where average power transfer coefficient α from transmitter to receiver and correlation coefficient and ρ observed at the receiver side.

To derive $\mathbf{\Sigma}_{\mathrm{h}}$ in the termination-dependent condition (perfect match and open-circuit), let us consider the extended antenna scattering matrix $\tilde{\mathbf{S}}_{\mathrm{A}}$ including antenna and free space characteristics in Fig. 2.2, which has incident and reflected wave vector $\mathbf{a}_{\mathrm{L}} = [a_1, a_2, \cdots, a_K]^T$, $\mathbf{b}_{\mathrm{L}} = [b_1, b_2, \cdots, b_K]^T$, as follows

$$\mathbf{b}_{\mathrm{L}} = \tilde{\mathbf{S}}_{\mathrm{A}}\mathbf{a}_{\mathrm{L}}, \quad \tilde{\mathbf{S}}_{\mathrm{A}} = \begin{bmatrix} \mathbf{S}_{\mathrm{A}} & \mathbf{S}_{\mathrm{AF}} \\ \mathbf{S}_{\mathrm{AF}}^T & \mathbf{S}_{\mathrm{F}} \end{bmatrix}, \quad \mathbf{S}_{\mathrm{A}} = \begin{bmatrix} S_{\mathrm{A11}} & S_{\mathrm{A12}} \\ S_{\mathrm{A21}} & S_{\mathrm{A22}} \end{bmatrix}, \tag{2.17}$$

where $\mathbf{S}_{\mathrm{AF}} \in \mathbb{C}^{2\times(K-2)}$ and $\mathbf{S}_{\mathrm{F}} \in \mathbb{C}^{(K-2)\times(K-2)}$ defines sub-matrices of antenna, antenna-free space and free space region, respectively. Using antenna boundary $\mathbf{a}_{\mathrm{A}} = \mathbf{\Gamma}\mathbf{b}_{\mathrm{A}}$ with reflection coefficient matrix $\mathbf{\Gamma}$, noting that $\mathbf{a}_{\mathrm{A}} = [a_1, a_2]^T$ and $\mathbf{b}_{\mathrm{A}} = [b_1, b_2]^T$, we describe the received signals of antenna side as,

$$\mathbf{b}_{\mathrm{A}} = \mathbf{S}_{\mathrm{A}}\mathbf{a}_{\mathrm{A}} + \mathbf{S}_{\mathrm{AF}}\mathbf{a}_{\mathrm{F}} = (\mathbf{I}_2 - \mathbf{S}_{\mathrm{A}}\mathbf{\Gamma})^{-1}\mathbf{S}_{\mathrm{AF}}\mathbf{a}_{\mathrm{F}}, \tag{2.18}$$

where incident wave vector $\mathbf{a}_{\mathrm{F}} = [a_3, a_4, \cdots, a_K]^T$ assumes random variable characteristic on free space. If the physical antenna size is given, finite number of spherical eigen-modes is enough to present the interaction between free space and antenna. The number $(K-2)$ of the free space port defines as follows [9],

$$K = 2N_{\mathrm{T}}(N_{\mathrm{T}}+2) + \mathrm{q}, \tag{2.19}$$

where $N_{\mathrm{T}} = \lfloor k_0 r_0 \rfloor + n_1$ is the truncation index with correction of truncated error n_1, $k_0 = 2\pi/\lambda$ is the wave number, r_0 is the radius of a spherical volume containing the two receive antennas and q is the truncated error.

Using the voltage $\mathbf{v}_0 = [v_{01}, v_{02}]^T = 2\sqrt{z_0}(\mathbf{a}_{\mathrm{A}} + \mathbf{b}_{\mathrm{A}})$, where z_0 is the characteristic impedance, we can derive the receive correlation matrix $\mathbf{\Sigma}_{\mathrm{h}}$ using the covariance matrix of the general voltage normalized by $P_{\mathrm{T}} r_{\mathrm{T}}/2$ as follows,

$$\begin{aligned}
\mathbf{\Sigma}_{\mathrm{h}} &= \frac{2}{P_{\mathrm{T}} r_{\mathrm{T}}} \mathrm{E}[\mathbf{v}_0 \mathbf{v}_0^{\dagger}] \\
&= \frac{2z_0}{P_{\mathrm{T}} r_{\mathrm{T}}} (\mathbf{I}_2 + \mathbf{\Gamma})(\mathbf{I}_2 - \mathbf{S}_{\mathrm{A}}\mathbf{\Gamma})^{-1} \mathbf{S}_{\mathrm{AF}} \mathrm{E}[\mathbf{a}_{\mathrm{F}} \mathbf{a}_{\mathrm{F}}^{\dagger}] \mathbf{S}_{\mathrm{AF}}^{\dagger} (\mathbf{I}_2 - \mathbf{S}_{\mathrm{A}}\mathbf{\Gamma})^{-\dagger} (\mathbf{I}_2 + \mathbf{\Gamma})^{\dagger} \\
&= \frac{2z_0 P_{\mathrm{h}}}{P_{\mathrm{T}} r_{\mathrm{T}}} (\mathbf{I}_2 + \mathbf{\Gamma})(\mathbf{I}_2 - \mathbf{S}_{\mathrm{A}}\mathbf{\Gamma})^{-1} (\mathbf{I}_2 - \mathbf{S}_{\mathrm{A}}\mathbf{S}_{\mathrm{A}}^{\dagger}) (\mathbf{I}_2 - \mathbf{S}_{\mathrm{A}}\mathbf{\Gamma})^{-\dagger} (\mathbf{I}_2 + \mathbf{\Gamma})^{\dagger}.
\end{aligned} \tag{2.20}$$

Assuming 3-D i.i.d. direction of arrival (DoA) and phase, we achieve two properties i.e. the incident wave $\mathrm{E}[\mathbf{a}_{\mathrm{F}} \mathbf{a}_{\mathrm{F}}^{\dagger}] = P_{\mathrm{h}} \mathbf{I}_2$ with the incident wave power $P_{\mathrm{h}} = P_{\mathrm{T}}\alpha$ and the unitary condition of antenna and free space $\mathbf{S}_{\mathrm{A}}\mathbf{S}_{\mathrm{A}}^{\dagger} + \mathbf{S}_{\mathrm{AF}}\mathbf{S}_{\mathrm{AF}}^{\dagger} = \mathbf{I}_2$.

At first, perfect match case $\mathbf{\Gamma} = \mathbf{0}$ on the antenna termination can be expressed by

$$\mathbf{\Sigma}_{\mathrm{h,match}} = \frac{2z_0 P_{\mathrm{h}}}{P_{\mathrm{T}} r_{\mathrm{T}}} (\mathbf{I}_2 - \mathbf{S}_{\mathrm{A}}\mathbf{S}_{\mathrm{A}}^{\dagger}), \tag{2.21}$$

The correlation coefficient of perfect match case identities with Blanch's model [49] on matching condition by 50Ω (cf., Appendix II).

$$\rho_{\mathrm{match}}^2 = \frac{|S_{\mathrm{A11}}^* S_{\mathrm{A12}} + S_{\mathrm{A21}}^* S_{\mathrm{A22}}|^2}{\{1 - (|S_{\mathrm{A11}}|^2 + |S_{\mathrm{A21}}|^2)\}\{1 - (|S_{\mathrm{A22}}|^2 + |S_{\mathrm{A12}}|^2)\}}. \tag{2.22}$$

On the other hand, open-circuit condition $\mathbf{\Gamma} = \mathbf{I}_2$ becomes

$$\mathbf{\Sigma}_{\mathrm{h,open}} = \frac{2z_0 P_{\mathrm{h}}}{P_{\mathrm{T}} r_{\mathrm{T}}} (\mathbf{I}_2 - \mathbf{S}_{\mathrm{A}})^{-1} (\mathbf{I}_2 - \mathbf{S}_{\mathrm{A}}\mathbf{S}_{\mathrm{A}}^{\dagger}) (\mathbf{I}_2 - \mathbf{S}_{\mathrm{A}})^{-\dagger} = \frac{8z_0 P_{\mathrm{h}}}{P_{\mathrm{T}} r_{\mathrm{T}}} \mathbf{R}_{\mathrm{A}}, \tag{2.23}$$

where $\mathbf{Z}_{\mathrm{A}} = \mathbf{R}_{\mathrm{A}} + j\mathbf{X}_{\mathrm{A}}$ is the antenna impedance matrix as follows,

$$\mathbf{Z}_{\mathrm{A}} = \begin{bmatrix} z_{\mathrm{A11}} & z_{\mathrm{A12}} \\ z_{\mathrm{A12}} & z_{\mathrm{A11}} \end{bmatrix}. \tag{2.24}$$

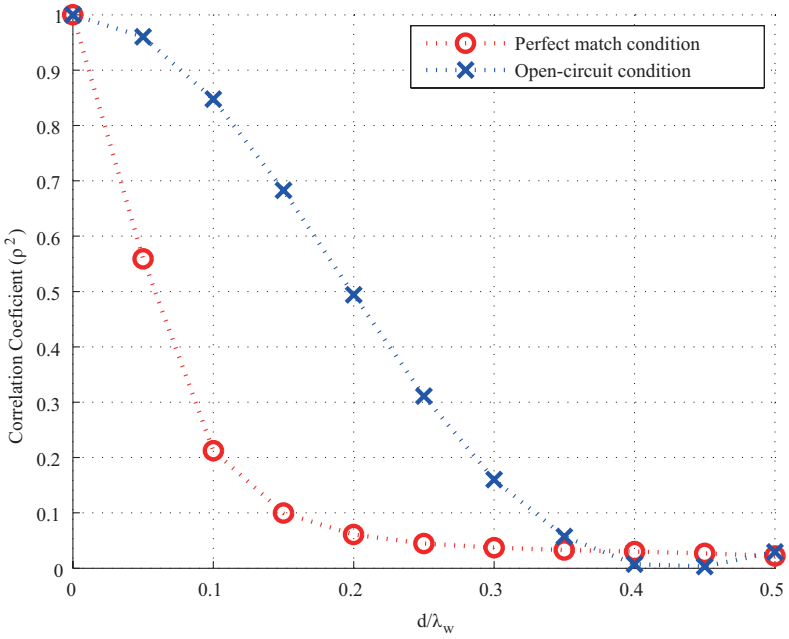


Figure 2.3 Correlation coefficient on two termination conditions.

The open-circuit correlation coefficient using the normalized mutual resistance has been proposed [21]

$$\rho_{\text{open}} = \frac{\Re(z_{\text{A12}})}{\Re(z_{\text{A11}})}, \tag{2.25}$$

The mutual impedance between two minimum scattering antennas with normalized far fields in the sense that total radiated power from each element defines [22]

$$z_{\text{A12}} = \int_0^{2\pi} \int_0^{\pi} g_1(\theta,\phi) g_2^*(\theta,\phi) e^{j\frac{2\pi}{\lambda_{\text{w}}} d\sin\theta\cos\phi} \sin\theta \, \mathrm{d}\theta \mathrm{d}\phi, \tag{2.26}$$

where the antenna pattern $g_i(\theta,\phi)$ is defined as the voltage induced in the i^{th} dipole antenna with i.i.d. DoA and phase. Note that d is the mutual antenna distance and λ_{w} is wavelength of the signal. For open-circuit termination case, the normalized mutual resistance and the correlation coefficient of Eq. (2.25) are identical. Figure 2.3 shows the correlation coefficient on two different scenarios of perfect match and open-circuit termination based on two half wave dipole antenna parameter by induced EMF method [11]. There is a significant difference since it is the mutual coupling which causes the difference between the perfect match and open-circuit termination cases.

Therefore, $\mathbf{\Sigma}_{\mathrm{h}}$ is determined by antenna property, termination condition and incoming wave stochastic property. If the incoming wave has another stochastic property, $\mathbf{a}_{\mathrm{F}}$ depends on another propagation model, i.e. 3-D uniform DoA and polarization.

2.3 MIMO channel capacity

To evaluate the performance upper bound in communication system, the capacity concept has been employed by *Shannon' theory* in 1948, which is based on information theory [29]. In this section the frequency flat deterministic and time invariant channels are considered. Consider the input-output relation of a single-input single-output (SISO) system as

$$y = hx + n, \tag{2.27}$$

where x and y are the input and output signal, respectively. And h is the SISO channel and n is the addictive Gaussian noise with zero mean and σ^2 variance at the receiver. Then the SISO system *Shannon capacity* becomes

$$C = \log_2\left(1 + \frac{P|h|^2}{\sigma^2}\right) \text{ bps/Hz}, \tag{2.28}$$

where the channel SNR $\frac{P|h|^2}{\sigma^2}$ with P is the average transmit power. Similar to SISO case, consider the receive signal vector of a MIMO channel as

$$\mathbf{y} = \mathbf{H}\mathbf{x} + \mathbf{n}. \tag{2.29}$$

If the vector $\mathbf{x}$ and $\mathbf{n}$ are gaussian distribution vector, $\mathbf{y}$ is also gaussian distribution vector. For simplicity, the covariance of $\mathbf{y}$ with independent $\overline{\mathbf{x}} = 0$ and $\overline{\mathbf{n}} = 0$ becomes

$$\mathbf{\Sigma}_{\mathrm{y}} = \mathbf{H}^{\dagger}\mathbf{\Sigma}_{\mathrm{x}}\mathbf{H} + \mathbf{\Sigma}_{\mathrm{n}}. \tag{2.30}$$

The mutual information between input signal vector $\mathbf{x}$ and output signal vector $\mathbf{y}$ is equal to channel capacity expressed by entropy $\mathbf{y}$

$$\begin{aligned} I(\mathbf{x};\mathbf{y}) &= H(\mathbf{y}) - H(\mathbf{y}|\mathbf{x}) \\ &= \log_2\det\mathbf{\Sigma}_{\mathrm{y}} - \log_2\det\mathbf{\Sigma}_{\mathrm{n}} \\ &= \log_2\det(\mathbf{I}_N + \mathbf{H}^{\dagger}\mathbf{\Sigma}_{\mathrm{x}}\mathbf{H}\mathbf{\Sigma}_{\mathrm{n}}^{-1}). \end{aligned} \tag{2.31}$$

Assuming equal power P, the instantaneous capacity for a MIMO system is expressed by

$$\begin{aligned} C &= \log_2 \det(\mathbf{I}_N + \frac{P}{N}\mathbf{H}^\dagger \mathbf{\Sigma}_{\mathrm{n}}^{-1}\mathbf{H}) \\ &= \log_2 \det(\mathbf{I}_N + \frac{P}{N}\mathbf{H}_{\mathrm{w}}^\dagger \mathbf{\Sigma}_{\mathrm{h}}^{1/2}\mathbf{\Sigma}_{\mathrm{n}}^{-1}\mathbf{\Sigma}_{\mathrm{h}}^{1/2}\mathbf{H}_{\mathrm{w}}), \end{aligned} \tag{2.32}$$

The ergodic capacity becomes

$$C = \mathop{\mathrm{E}}_{\mathbf{H}_{\mathrm{w}}} \left[\log_2 \det \left(\mathbf{I}_N + \mathbf{H}_{\mathrm{w}}^\dagger \mathbf{\Sigma} \mathbf{H}_{\mathrm{w}} \right) \right], \tag{2.33}$$

where $\mathbf{\Sigma}$ is defined as the SNR matrix as follows,

$$\mathbf{\Sigma} = \frac{P}{N}\mathbf{\Sigma}_{\mathrm{h}}^{1/2}\mathbf{\Sigma}_{\mathrm{n}}^{-1}\mathbf{\Sigma}_{\mathrm{h}}^{1/2}, \tag{2.34}$$

where N denotes the transmit antenna number. A closed form expression for Eq. (2.33) was derived in [27]. If $M = N$ and the $\mathbf{\Sigma}$ has distinct eigenvalues $(\lambda_1, \lambda_2, \cdots, \lambda_{\mathrm{N}})$, the rigorous ergodic capacity is redefined by

$$C = \frac{\sum_{k=1}^{N} \det \mathbf{A}_k}{\prod_{i=1, j>i}^{N} \lambda_i^i \lambda_j^j (1 - \lambda_i/\lambda_j)}, \quad [\mathbf{A}_k]_{ij} = \begin{cases} \frac{1}{(j-1)!} \int_0^\infty u^{j-1} e^{-u/\lambda_i} \log(1+u)\, du, & j = k \\ \lambda_i^j, & j \neq k \end{cases} \tag{2.35}$$

2.3.1 Approaximation of channel capacity

Assuming 2×2 MIMO system, let revise a original definition of ergodic capacity as

$$C = \mathop{\mathrm{E}}_{\mathbf{H}_{\mathrm{w}}} \left[\log_2 \det \left(\mathbf{I}_2 + \mathbf{H}_{\mathrm{w}}^\dagger \mathbf{U}^\dagger \begin{bmatrix} \lambda_1 & 0 \\ 0 & \lambda_2 \end{bmatrix} \mathbf{U}\mathbf{H}_{\mathrm{w}} \right) \right], \tag{2.36}$$

where λ_1 and λ_2 mean distinct eigenvalue of $\mathbf{\Sigma}$ from Eq. (2.34). If $\mathbf{H}_{\mathrm{w}}$ is spatially white, $\mathbf{H}'_{\mathrm{w}} = \mathbf{U}\mathbf{H}_{\mathrm{w}}$ is also same property with unitary matrix $\mathbf{U}$. Next, the determinants of $\mathbf{A}_1, \mathbf{A}_2$ from Eq. (2.35) are defined as

$$[\mathbf{A}_1]_{ij} = \begin{bmatrix} f(\lambda_1) & \lambda_1^2 \\ f(\lambda_2) & \lambda_2^2 \end{bmatrix}, \quad [\mathbf{A}_2]_{ij} = \begin{bmatrix} \lambda_1^1 & \lambda_1^2 f'(\lambda_1) \\ \lambda_2^1 & \lambda_2^2 f'(\lambda_2) \end{bmatrix}, \tag{2.37}$$

where the function formula $f(\lambda)$ is derived through integral function Ei as

$$f(\lambda) = \int_0^\infty e^{-\frac{u}{\lambda}} \log(1+u)\, du = \lambda \int_0^\infty \frac{e^{-\frac{u}{\lambda}}}{1+u}\, du = -\lambda e^{\frac{1}{\lambda}} Ei\left(-\frac{1}{\lambda}\right),$$

Therefore, the simplified rigorous ergodic capacity is expressed as

$$C = \frac{\lambda_2^2 f(\lambda_1) - \lambda_1^2 f(\lambda_2) + \lambda_1 \lambda_2^2 f'(\lambda_2) - \lambda_2 \lambda_1^2 f'(\lambda_1)}{\lambda_1 \lambda_2 (\lambda_2 - \lambda_1)}. \tag{2.38}$$

Two asymptotic cases for approximation from rigorous capacity expression of Eq. (2.38) are considered. At first, when $\lambda \ll 1$ at low SNR case, $f_{\mathrm{L}}(\lambda)$ is redefined using antiderivative definition as

$$e^{\frac{1}{\lambda}} Ei\left(-\frac{1}{\lambda}\right) \sim \sum_{n=1}^{\infty}(n-1)!\lambda^n,\ n=1,2,\cdots \tag{2.39}$$

$$f_{\mathrm{L}}(\lambda) = \lambda^2 - \lambda^3 + 2\lambda^4 - \cdots, \tag{2.40}$$

then, from Eq. (2.38) the asymptotic capacity for low SNR becomes

$$C_{\mathrm{L}} = 2(\lambda_1+\lambda_2) + \lambda_1\lambda_2 - 3(\lambda_1^2+\lambda_2^2+\lambda_1\lambda_2) + \cdots. \tag{2.41}$$

On the other hand, when $\lambda \gg 1$ at high SNR case, $f_{\mathrm{H}}(\lambda)$ is expressed through *Bessel's function* as

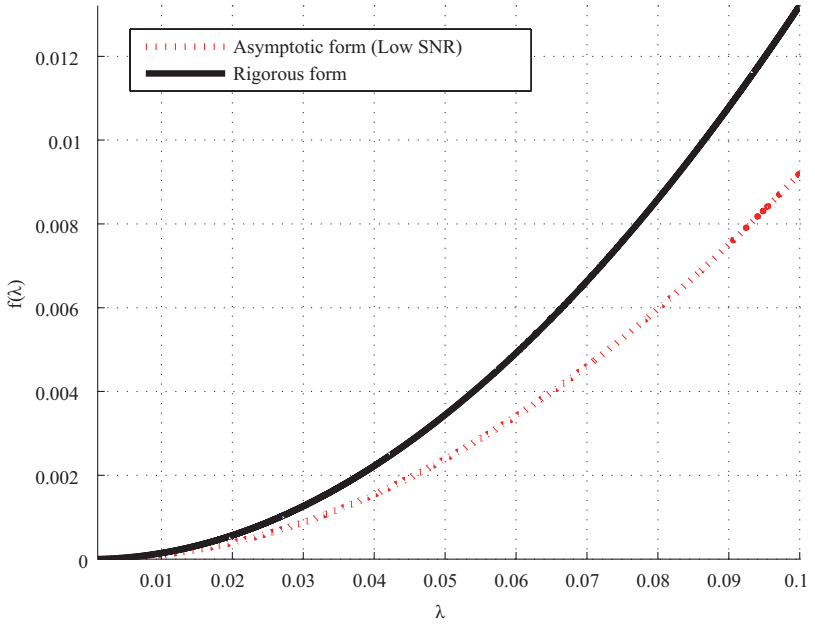
$$Ei\left(-\frac{1}{\lambda}\right) = \gamma_{\mathrm{e}} + \log_2\frac{1}{\lambda} - e^{-\frac{1}{\lambda}}\sum_{n=1}^{\infty}\frac{1}{n!}\left(\sum_{r=1}^{n}\frac{1}{r}\right)\left(\frac{1}{\lambda}\right)^n \tag{2.42}$$

$$f_{\mathrm{H}}(\lambda) = \lambda(\log_2(\lambda) - \gamma_{\mathrm{e}}), \tag{2.43}$$

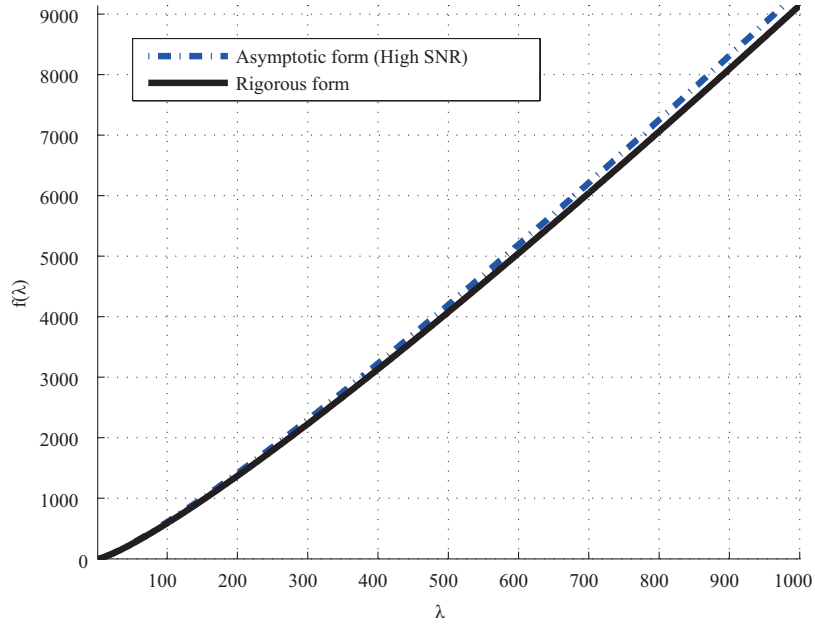
where γ_{e} is *Euler's* constant $(0.57721\cdots)$. So, from Eq. (2.38) the asymptotic capacity for low SNR is given by

$$C_{\mathrm{H}} = \log_2\lambda_1\lambda_2 - 2\gamma_{\mathrm{e}}, \tag{2.44}$$

Since our focus in this section is a validity of upper-bound and low-bound system performance discussed above, we need to perform a comparison with rigorous form and asymptotic forms of ergodic capacity We first confirm function formula $f(\lambda)$ with respect to eigenvalue variable λ in induced three scenarios with asymptotic expressions and rigorous form, shown as Fig. 2.4(a) and Fig. 2.4(b). The result shows a validity range of the asymptotic forms that very extreme low SNR ($\lambda \ll 1$) may deviate a little according to rigorous form while high SNR case almost match. The calculation of the asymptotic forms is much quicker to evaluate on MATLAB simulation, e.g. time ratio (rigorous form : 1, Low SNR : 1/572 and high SNR : 1/286). After that, we compare ergodic capacity compared with rigorous form asymptotic form as two distinct eigenvalues λ_1, λ_2. We immediately notice that low SNR ergodic capaticy of Fig. 2.5(a) is slightly different as both two eigenvalues are increasing, whereas high SNR case agree very well with each other in Fig. 2.5(b).

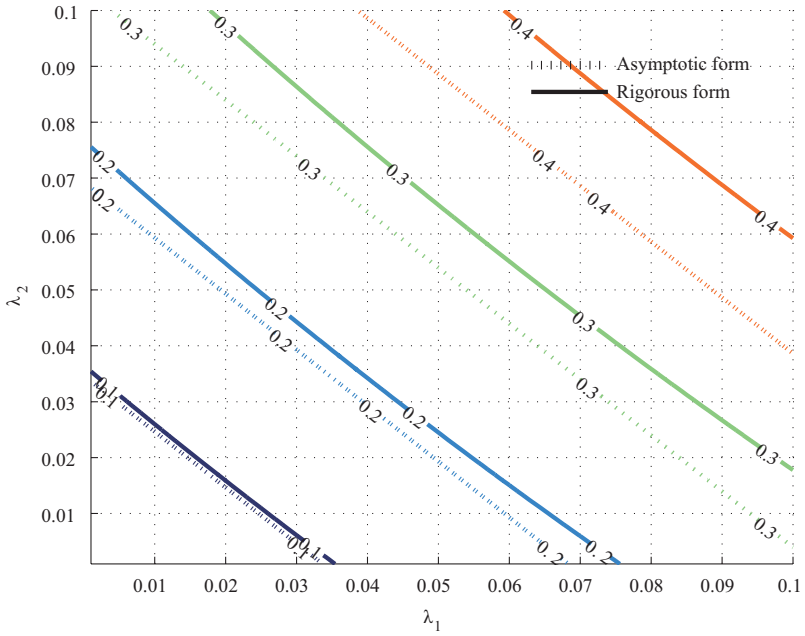


(a) Low SNR ($0 < \lambda < 0.1$)

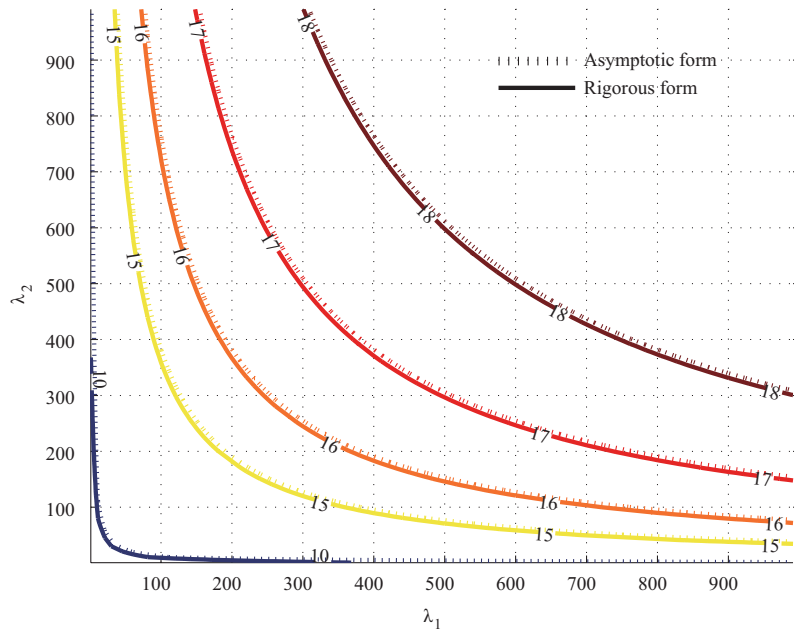


(b) High SNR ($1 < \lambda < 1000$)

Figure 2.4 Function formula $f(\lambda)$ for validity range of asymptotic forms.



(a) Low SNR ($0 < \lambda < 0.1$)



(b) High SNR ($1 < \lambda < 1000$)

Figure 2.5 Ergodic capacity boundary of rigorous form and asymptotic forms.

2.4 Summary

This chapter has reviewed the characteristics of wireless propagation channel for SISO and MIMO systems. MIMO systems were investigated with various signal correlation models and performance evaluation approaches. Basic antenna theory including array antenna parameters, mutual coupling and ergodic capacity of system evaluation method was discussed. The mutual coupling may decrease the signal correlation between fading path gains by distorting radiation pattern between array antenna. Furthermore, asymptotic forms of ergodic capacity for low and high SNR regimes were addressed. By using the asymptotic forms, we can reduce computation time for calculating the ergodic capacity. We consider how mutual coupling would affect system performance for optimal MIMO receiver design in next chapter.

Chapter 3

Low Noise Matching Design

3.1 Introduction

Conventional studies considered the mutual coupling effect on the power with the impedance mismatch resulting in power loss. For compensating the penalty with the power loss, matching network was introduced for maximizing power transfer providing complete decoupling of the array [18,23]. It was proven that the matching circuit for maximization of power transfer, the so-called multiport conjugate match, can realize zero output correlation and lossless power transfer from array antennas to the load for any antenna spacing and improve significant capacity performance for very compact antenna spacings [16, 18, 32, 33].

However, it has been paid little attention to the noise sources since the above studies presented to introduce increasingly detailed models of fading correlation. While most of the literatures mentioned above considered a spatial white noise model with noise correlation, i.e. external noise so-called as sky noise, it was not until recently that internal noise generated in the receiver also employed. For example, the front-end noise by amplifiers, mixers and filters spread apart neighbor receive chain due to coupled antennas. Recently, a special noise modeling for MIMO system receivers was proposed in [24]. They introduced coupling noise sources with the previous mutual coupling and standard amplifier noise model. It was shown that minimizing noise factor outweighs maximizing power transfer for matching network. Some work investigated system evaluation of the impact of antenna noise and amplifier noise individually [25,26]. He showed that the matching network is more effective on system capacity when the amplifier noise source is dominant. Furthermore, recent noise modeling for MIMO receivers was considered mutual coupling effect with distortion of radiation pattern at closely

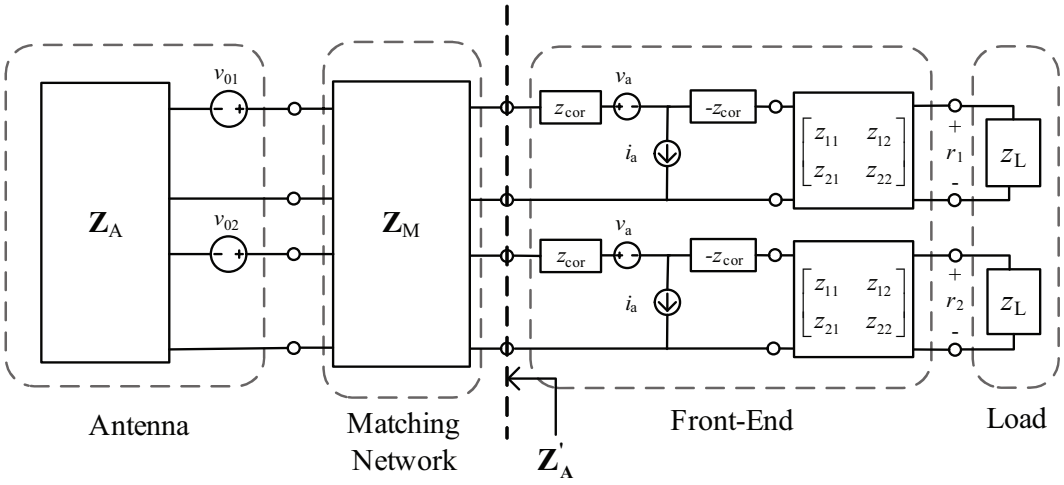


Figure 3.1 Circuit model with two multiple receivers.

antenna spacing and standard front-end model with arbitrary coupling and noise correlation between its ports [27, 28].

In this chapter, we first present a general low noise matching circuit for compact MIMO receiver. Assuming symmetrical channel characteristic, symmetrical array antenna and identical front-end, a so-called symmetrical matching for maximizing the ergodic channel capacity is proposed. Finally, numerical analysis with specific simulation condition is conducted to verify the effectiveness of the proposed models.

3.2 System model

We assume coupling occurs only between two array antennas; there is no coupling between front-end chains such as the amplifiers. We further assume a narrowband system, so all impedances are constant over the system bandwidth and all signals can be expressed in complex baseband form. A circuit model of this two branch receiver in illustrated in Fig. 3.1. Both the antenna array and identical front-ends are represented by equivalent noisy circuit models.

3.2.1 Channel representation

Considering a 2×2 MIMO system, we first represent the propagation channel matrix $\mathbf{H} \in \mathbb{C}^{2\times 2}$ as follows,

$$\mathbf{H} = \begin{bmatrix} h_{11} & h_{12} \\ h_{21} & h_{22} \end{bmatrix} = [\mathbf{h}_1 \ \mathbf{h}_2], \tag{3.1}$$

where the column vectors $\mathbf{h}_1, \mathbf{h}_2$ with independent and identically distributed (i.i.d) zero mean elements are respectively the signal signature from each transmit antenna. Assuming the Kronecker model with spatial correlation at the receiver side, the receive correlation matrix of the propagational channel $\mathbf{\Sigma}_{\mathrm{h}} = \mathrm{E}\left[\mathbf{H}\mathbf{H}^{\dagger}\right]$ can be expressed as [7],

Furthermore, the signal signature can be represented as

$$\mathbf{h}_1 = \mathbf{\Sigma}_{\mathrm{h}}^{1/2}\mathbf{h}_{\mathrm{w}_1}, \quad \mathbf{h}_2 = \mathbf{\Sigma}_{\mathrm{h}}^{1/2}\mathbf{h}_{\mathrm{w}_2}, \tag{3.2}$$

where $\mathbf{h}_{\mathrm{w}_1}, \mathbf{h}_{\mathrm{w}_2} \in \mathbb{C}^2$ are column vectors with i.i.d elements following normal distribution $\mathcal{CN}(0,1)$. The overall channel matrix $\mathbf{H}$ is rewritten as

$$\mathbf{H} = \mathbf{\Sigma}_{\mathrm{h}}^{1/2}\mathbf{H}_{\mathrm{w}}, \tag{3.3}$$

where $\mathbf{H}_{\mathrm{w}} = [\mathbf{h}_{\mathrm{w}_1} \ \mathbf{h}_{\mathrm{w}_2}]$.

3.2.2 Array antenna model

An antenna converts an incident electromagnetic field into a voltage across the antenna terminals. When the array antennas are closely spaced, the terminal voltage of the antenna depends on the field as well as the currents flowing through neighboring antennas. Let $\mathbf{v}, \mathbf{i} \in \mathbb{C}^2$, respectively, denote the voltage and current vectors impinging on the antenna array. Using Thevenin equivalent network model for the array, we define

$$\mathbf{v} = \mathbf{Z}_{\mathrm{A}}\mathbf{i} + \mathbf{v}_0, \tag{3.4}$$

where $\mathbf{Z}_{\mathrm{A}} = \mathbf{R}_{\mathrm{A}} + j\mathbf{X}_{\mathrm{A}}$ is the antenna impedance matrix as follows,

$$\mathbf{Z}_{\mathrm{A}} = \begin{bmatrix} z_{\mathrm{A11}} & z_{\mathrm{A12}} \\ z_{\mathrm{A21}} & z_{\mathrm{A22}} \end{bmatrix}, \tag{3.5}$$

In Eq. (3.4), $\mathbf{v}_0 = [v_{01}\ v_{02}]^T$ is the open-circuit voltage at the input of the two receive antennas. The open-circuit voltage is related to the incident electric field which can be expressed in the following form,

$$\mathbf{v}_0 = \mathbf{H}\mathbf{x} + \mathbf{n}_0, \tag{3.6}$$

where $\mathbf{x} \in \mathbb{C}^2$ is the transmit signal and $\mathbf{n}_0 = [n_{01}\ n_{02}]^T$ denotes the external noise component which represents either the induced thermal radiation or interference. For thermal noise in an isotropic environment, the noise voltage can be modeled as, $\mathbf{n}_0 \sim \mathcal{CN}(\mathbf{0}, \mathbf{\Sigma}_{\mathrm{n}_0})$, where $\mathbf{\Sigma}_{\mathrm{n}_0} = 4k_{\mathrm{B}}T_0B\Re[\mathbf{Z}_{\mathrm{A}}]$, $k_{\mathrm{B}} = 1.38 \times 10^{-23}$J/K is the Boltzman's constant, $T_0 = 290$K is the standard noise temperature, and B is the bandwidth in Hz.

3.2.3 Matching network

We consider 4-port matching network between the array antenna and the front-end, as shown in Fig. 3.1. The matching network has the impedance matrix $\mathbf{Z}_{\mathrm{M}} \in \mathbb{C}^{4\times4}$ as follows,

$$\mathbf{Z}_{\mathrm{M}} = \begin{bmatrix} \mathbf{Z}_{\mathrm{M11}} & \mathbf{Z}_{\mathrm{M12}} \\ \mathbf{Z}_{\mathrm{M21}} & \mathbf{Z}_{\mathrm{M22}} \end{bmatrix}, \quad \mathbf{Z}_{\mathrm{M}ij} \in \mathbb{C}^{2\times2} \tag{3.7}$$

The ideal matching circuit is formed with passive, reactive elements so it is noiseless, lossless, and reciprocal, $\mathbf{Z}_{\mathrm{M11}} = -\mathbf{Z}_{\mathrm{M11}}^{\dagger} = \mathbf{Z}_{\mathrm{M11}}^{T}$, $\mathbf{Z}_{\mathrm{M22}} = -\mathbf{Z}_{\mathrm{M22}}^{\dagger} = \mathbf{Z}_{\mathrm{M22}}^{T}$ and $\mathbf{Z}_{\mathrm{M21}} = -\mathbf{Z}_{\mathrm{M12}}^{\dagger} = \mathbf{Z}_{\mathrm{M12}}^{T}$. The revised antenna impedance matrix with multiport matching network is derived as follows,

$$\mathbf{Z}_{\mathrm{A}}^{'} = -\mathbf{M}\mathbf{Z}_{\mathrm{M12}} + \mathbf{Z}_{\mathrm{M22}}, \quad \mathbf{M} = \mathbf{Z}_{\mathrm{M21}}(\mathbf{Z}_{\mathrm{A}} + \mathbf{Z}_{\mathrm{M11}})^{-1}. \tag{3.8}$$

3.2.4 Front-end

An amplifiers is usually well-modeled within its dynamic range a linear, noisy two port network. It is given by Thevenin equivalent network with impedance matrix as

$$\begin{bmatrix} z_{11} & z_{12} \\ z_{21} & z_{22} \end{bmatrix}, \tag{3.9}$$

and open circuit noise voltages n_1 and n_2 at the input and output ports, respectively. The well-known Rothe-Dahlke model is generally used to amplifier model instead of Thevenin equivalent network model [45]. The noise voltage source and noise current source at the

input port, denoted by v_{a} and i_{a} are related to the other parameters i.e. the equivalent noise resistance r_{a} and the equivalent noise conductance g_{a} by the follwing relationship,

$$r_{\mathrm{a}} = \frac{\mathrm{E}[|v_{\mathrm{a}}|^2]}{4k_{\mathrm{B}}T_0B}, \quad g_{\mathrm{a}} = \frac{\mathrm{E}[|i_{\mathrm{a}}|^2]}{4k_{\mathrm{B}}T_0B}. \tag{3.10}$$

Noise correlation between the input and the output port is characterized by the correlation impedance $z_{\mathrm{cor}} = r_{\mathrm{cor}} + jx_{\mathrm{cor}}$. The amplifiers in Fig. 3.1 are identical and uncoupled, so the joint distributions of the two amplifier voltage and current sources are $\mathbf{v}_{\mathrm{a}} \sim \mathcal{CN}(\mathbf{0}, 4k_{\mathrm{B}}\,T_0B\,r_{\mathrm{a}}\mathbf{I}_2)$ and $\mathbf{i}_{\mathrm{a}} \sim \mathcal{CN}(\mathbf{0}, 4k_{\mathrm{B}}\,T_0B\,g_{\mathrm{a}}\mathbf{I}_2)$, An important amplifiers noise metric is the noise factor F which means as the ratio of the output noise power to the noise power contributed by a source alone, if a source impedance $z_{\mathrm{A}} = r_{\mathrm{A}} + jx_{\mathrm{A}}$ is a single antenna impedance connected to the input port as

$$F = 1 + \frac{r_{\mathrm{a}} + g_{\mathrm{a}}|z_{\mathrm{A}} + z_{\mathrm{cor}}|^2}{\Re(z_{\mathrm{A}})}, \tag{3.11}$$

The noise factor is useful because it relates the input and output signal to noise ratios (SNR) of the amplifier, given in dB by noise figure NF= $10\log_{10}(F)$. Note that F obtains its minimum value $F_{\min}$ when $z_{\mathrm{A}} = z_{\mathrm{opt}}$ characterized by the front-end are derived in [44] as follows,

$$F_{\min} = 1 + 2\left\{g_{\mathrm{a}}r_{\mathrm{cor}} + \sqrt{g_{\mathrm{a}}r_{\mathrm{a}} + (g_{\mathrm{a}}r_{\mathrm{cor}})^2}\right\}, \tag{3.12}$$

$$z_{\mathrm{opt}} = \sqrt{\frac{r_{\mathrm{a}}}{g_{\mathrm{a}}} + r_{\mathrm{cor}}^2} - jx_{\mathrm{cor}}. \tag{3.13}$$

Note the parameters $F_{\min}, g_{\mathrm{a}}$ and z_{opt} are typically used to characterize the noise statistics of low noise amplifier (LNA) and is redefined by

$$F = F_{\min} + \frac{g_{\mathrm{a}}|z_{\mathrm{A}} - z_{\mathrm{opt}}|^2}{\Re(z_{\mathrm{A}})}. \tag{3.14}$$

3.2.5 Ergodic capacity with noise factor matrix

We derive the ergodic channel capacity for this two branch antenna receiver model as,

$$C = \underset{\mathbf{H}_{\mathrm{w}}}{\mathrm{E}}\left[\log_2 \det\left(\mathbf{I}_2 + \mathbf{H}_{\mathrm{w}}\mathbf{\Sigma}\mathbf{H}_{\mathrm{w}}^{\dagger}\right)\right], \tag{3.15}$$

where $\mathbf{\Sigma}$ is defined as the SNR matrix as follows,

$$\mathbf{\Sigma} = \frac{P_{\mathrm{T}}r_{\mathrm{T}}}{4Nk_{\mathrm{B}}\,T_0B}\mathbf{\Sigma}_{\mathrm{h}}^{1/2}\mathbf{R}_{\mathrm{A}}^{-1/2}\mathbf{F}^{-1}\mathbf{R}_{\mathrm{A}}^{-1/2}\mathbf{\Sigma}_{\mathrm{h}}^{1/2}, \tag{3.16}$$

where N denotes the transmit antenna number. For deriving noise factor matrix, consider the output voltage $\mathbf{r} = [r_1\ r_2]^T$ with identical front-end,

$$\mathbf{r} = \left[z_{\mathrm{L}}\left\{z_{12}\mathbf{T} - z_{22}\mathbf{I}_2 - z_{\mathrm{L}}\mathbf{I}_2\right\}^{-1}\mathbf{T}\right](\tilde{\mathbf{v}}_0 + \mathbf{z}), \tag{3.17}$$

where $\mathbf{T} = z_{21}(\mathbf{Z}'_{\mathrm{A}} + z_{11}\mathbf{I}_2)^{-1}$ and $\tilde{\mathbf{v}}_0$ is the revised open circuit voltage vector regarding the matching network which is defined as,

$$\tilde{\mathbf{v}}_0 = \mathbf{MHx} + \mathbf{Mn}_0. \tag{3.18}$$

Also, $\mathbf{z} = \mathbf{v}_{\mathrm{a}} + (\mathbf{Z}'_{\mathbf{A}} + z_{\mathrm{cor}}\mathbf{I}_2)\mathbf{i}_{\mathrm{a}}$ is the internal noise generated by the well-known front-end model [45] which is characterized by mutually independent noise sources in subsec. 3.2.4.

Therefore, the total noise can be separated as two uncorrelated noise sources i.e. the external noise by the antenna and internal noise by the front-end as,

$$\mathbf{n} \triangleq \mathbf{Mn}_0 + \mathbf{z}, \tag{3.19}$$

with the noise covariance matrix $\mathbf{\Sigma}_{\mathrm{n}} = \mathrm{E}[\mathbf{nn}^{\dagger}]$,

$$\mathbf{\Sigma}_{\mathrm{n}} = 4k_{\mathrm{B}}T_0B\{\mathbf{MR}_{\mathrm{A}}\mathbf{M}^{-\dagger} + r_{\mathrm{a}}\mathbf{I}_2 + g_{\mathrm{a}}(\mathbf{Z}'_{\mathrm{A}} + \mathrm{z}_{\mathrm{cor}}\mathbf{I}_2)(\mathbf{Z}'_{\mathrm{A}} + \mathrm{z}_{\mathrm{cor}}\mathbf{I}_2)^{\dagger}\}. \tag{3.20}$$

Therefore, the noise factor matrix $\mathbf{F}\in\mathbb{C}^{2\times2}$ for multiport network can be given by

$$\begin{aligned}\mathbf{F} &= \left(\mathbf{\Sigma}_{\mathrm{n}}|_{\mathbf{z}=\mathbf{0}}\right)^{-1/2}\mathbf{\Sigma}_{\mathrm{n}}\left(\mathbf{\Sigma}_{\mathrm{n}}|_{\mathbf{z}=\mathbf{0}}\right)^{-1/2} \\ &= \mathbf{I}_2 + \mathbf{R}_{\mathrm{A}}^{-1/2}\mathbf{M}^{-1}\left[r_{\mathrm{a}}\mathbf{I}_2 + g_{\mathrm{a}}(\mathbf{Z}'_{\mathrm{A}} + \mathrm{z}_{\mathrm{cor}}\mathbf{I}_2)(\mathbf{Z}'_{\mathrm{A}} + \mathrm{z}_{\mathrm{cor}}\mathbf{I}_2)^{\dagger}\right]\mathbf{M}^{-\dagger}\mathbf{R}_{\mathrm{A}}^{-1/2},\end{aligned} \tag{3.21}$$

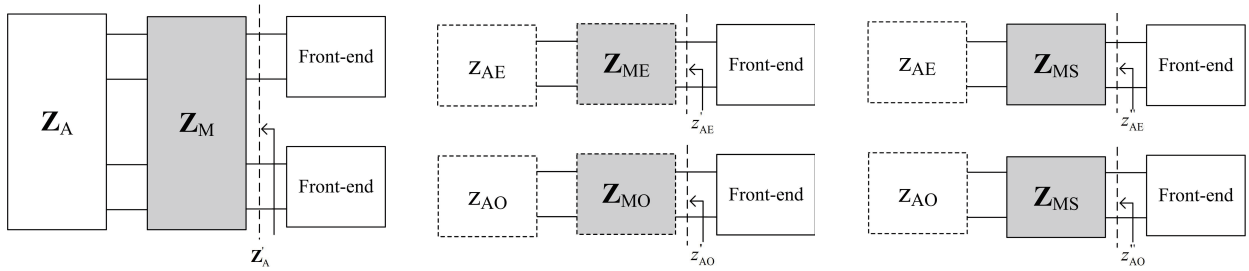
3.3 Design for matching circuit

Three matching methods to minimize the noise factor of two compact antenna array are introduced.

3.3.1 Multiport matching

We derive the set of noise factor matrices with lossless matching, called as multiport matching in Fig. 3.2(a) [28]. From Eq. (3.11), the noise factor of a single antenna receiver achieves its minimum $F_{\min}$ when the source impedance is $z_{\mathrm{opt}} = r_{\mathrm{opt}} + jx_{\mathrm{opt}}$. We expand the noise factor matrix for the multi-antenna system that we have mentioned above as

$$\mathbf{F} = \mathbf{F}_{\min}\mathbf{I}_2 + g_{\mathrm{a}}\mathbf{R}_{\mathrm{A}}^{-1/2}\mathbf{M}^{-1}(\mathbf{Z}'_{\mathrm{A}} - z_{\mathrm{opt}}\mathbf{I}_2)(\mathbf{Z}'_{\mathrm{A}} - z_{\mathrm{opt}}\mathbf{I}_2)^{\dagger}\mathbf{M}^{-\dagger}\mathbf{R}_{\mathrm{A}}^{-1/2}. \tag{3.22}$$



(a) Multiport matching (b) Symmetrical matching (c) Identical self matching

Figure 3.2 Matching network classification.

For the given positive definite matrix $\mathbf{\Sigma}_{\mathrm{h}}$ and $\mathbf{R}_{\mathrm{A}}$, the ergodic channel capacity is determined by the designable matrix $\mathbf{F}$ with positive definite. Let assume C_1 and C_2 be the channel capacity achieved with $\mathbf{F}_1$ and $\mathbf{F}_2$, respectively. [27] proved that if $\mathbf{F}_1 \succcurlyeq \mathbf{F}_2 \triangleq F_{\min}\mathbf{I}_2$ then $C_1 \leq C_2$ for arbitrary noise factor matrix $\mathbf{F}_1$ with equality if and only if $\mathbf{Z}'_{\mathrm{A}} = z_{\mathrm{opt}}\mathbf{I}_2$

One particular matching network example is given by

$$\begin{bmatrix} \mathbf{Z}_{\mathrm{M11}} & \mathbf{Z}_{\mathrm{M12}} \\ \mathbf{Z}_{\mathrm{M21}} & \mathbf{Z}_{\mathrm{M22}} \end{bmatrix} = j \begin{bmatrix} -\mathbf{X}_{\mathrm{A}} & (r_{\mathrm{opt}}\mathbf{R}_{\mathrm{A}})^{1/2} \\ (r_{\mathrm{opt}}\mathbf{R}_{\mathrm{A}})^{1/2} & x_{\mathrm{opt}}\mathbf{I}_2 \end{bmatrix} \tag{3.23}$$

Therefore, from Eq. (3.20) the total noise covariance matrix with the optimal matching network can be expressed as follows,

$$\mathbf{\Sigma}_{\mathrm{n,opt}} = 4k_{\mathrm{B}}T_0BF_{\min}\mathbf{R}_{\mathrm{A}}. \tag{3.24}$$

Assuming that incoming waves are 3-D model with independent, uniformly-distributed DoA, the deterministic SNR matrix $\mathbf{\Sigma}$ is defined by

$$\mathbf{\Sigma}_{\mathrm{n,opt}} = \frac{P_{\mathrm{T}}r_{\mathrm{T}}}{2}\mathbf{\Sigma}_{\mathrm{h}}^{1/2}\mathbf{\Sigma}_{\mathrm{n,opt}}\mathbf{\Sigma}_{\mathrm{h}}^{1/2} = \beta\mathbf{I}_2, \quad \beta = \frac{P_{\mathrm{h}}}{4k_{\mathrm{B}}T_0BF_{\min}}. \tag{3.25}$$

If we assume perfect lossless matching network which can transform any antenna impedance $\mathbf{Z}'_{\mathrm{A}}$ to $z_{\mathrm{opt}}\mathbf{I}_2$, then the SNR matrix $\mathbf{\Sigma}$ contains no information of antenna characteristics but only scattering property. Therefore, the theoretical ergodic capacity which is now determined by only β can be represented in Telatar's closed form [50],

$$C = 2\int_0^\infty \left(1 - 2u + \frac{u^2}{2}\right) e^{-u} log(1+\beta u)\, du. \tag{3.26}$$

3.3.2 Symmetrical matching

In this subsection, we present special assumptions of symmetrical channel characteristic, symmetrical array antenna and identical front-end for suboptimal design. Since designing multi-port matching network for minimizing the noise factor is highly difficult in practice, suboptimal alternatives, called as symmetrical matching and identical self matching are proposed as shown in Figs. 3.2(b) and 3.2(c), respectively. In these figures, assuming 2×2 symmetrical array antennas, for arbitrary 2 port impedance matrix, we set that z_{AE} and z_{AO} are the virtual antenna impedance called as even mode impedance and odd mode impedance, respectively.

At first, let set symmetrical channel characteristic as $\mathbf{\Sigma}_{\mathrm{h}} = \mathbf{U}\mathbf{\Lambda}_{\mathbf{\Sigma}_{\mathrm{h}}}\mathbf{U}^{\dagger}$. The special symmetric nature of $\mathbf{\Sigma}_{\mathrm{h}}$ allows its eigen-value decomposition (EVD) into the product of the unitary matrix $\mathbf{U}$ and the diagonal eigen-value matrix $\mathbf{\Lambda}_{\mathbf{\Sigma}_{\mathrm{h}}}$ specified as,

$$\mathbf{U} = \frac{1}{\sqrt{2}}\begin{bmatrix} 1 & 1 \\ 1 & -1 \end{bmatrix}, \ \mathbf{\Lambda}_{\mathbf{\Sigma}_{\mathrm{h}}} = \mathrm{diag}(\Sigma_{\mathrm{hE}}, \Sigma_{\mathrm{hO}}), \tag{3.27}$$

where Σ_{hE} and Σ_{hO} refer to the even and odd mode channel correlation expression.

Second, we assume two identical array antennas with same radiation pattern, such that the antenna impedance matrix from Eq. (3.5) has the special symmetric structure to be redefined as,

$$\mathbf{Z}_{\mathrm{A}} = \begin{bmatrix} z_{\mathrm{A11}} & z_{\mathrm{A12}} \\ z_{\mathrm{A12}} & z_{\mathrm{A11}} \end{bmatrix} = \mathbf{U}\mathbf{\Lambda}_{\mathrm{Z_A}}\mathbf{U}^{\dagger}, \tag{3.28}$$

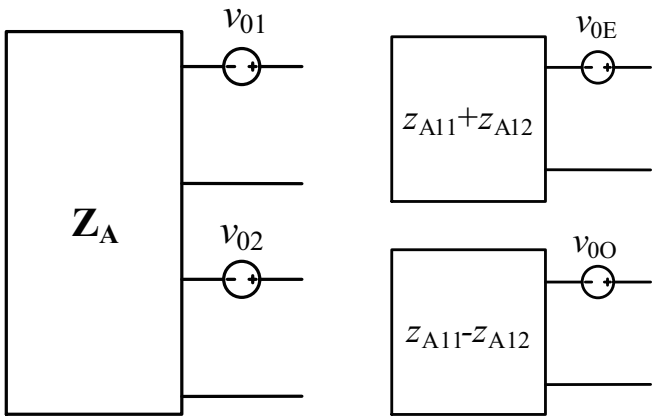
where $\mathbf{\Lambda}_{\mathrm{Z_A}} = \mathrm{diag}(\mathrm{z_{AE}},\ \mathrm{z_{AO}})$ with two diagonal components of the even and odd modes, respectively. We study additional constellation of noise correlation for even-odd mode decomposition. From array antenna impedance with mutual coupling of signal and noise in Fig. 3.3(a), the decomposed antenna impedance is simultaneously applied by circuit parameter and noise property in Fig. 3.3(b). The open-circuit voltage column vector $\mathbf{v}_0 = [v_{01}\ v_{02}]^T$ by *Nyquist formula* for original two port circuit is given by

$$\mathbf{\Sigma}_{\mathrm{n_0}} = \begin{bmatrix} \overline{|v_{01}|^2} & \overline{v_{01}v_{02}^*} \\ \overline{v_{01}^* v_{02}} & \overline{|v_{02}|^2} \end{bmatrix} = 4k_{\mathrm{B}}T_0 B\Re[\mathbf{Z}_{\mathrm{A}}] = 4k_{\mathrm{B}}T_0 B\begin{bmatrix} r_{\mathrm{A11}} & r_{\mathrm{A12}} \\ r_{\mathrm{A12}} & r_{\mathrm{A11}} \end{bmatrix} \tag{3.29}$$

On the other hand, we define the covariance value correspond to isolated two 1-port with even mode open-circuit voltage $v_{0\mathrm{E}}$ and odd mode open-circuit voltage $v_{0\mathrm{O}}$ for the noise sources of Fig. 3.3(b) as

$$\overline{|v_{0\mathrm{E}}|^2} = 4k_{\mathrm{B}}T_0 B\Re(\mathrm{z_{AE}}) = \overline{|v_{01}|^2} + \overline{v_{01}v_{02}^*} = \overline{v_{01}(v_{01}^* + v_{02}^*)}, \tag{3.30}$$

$$\overline{|v_{0\mathrm{O}}|^2} = 4k_{\mathrm{B}}T_0 B\Re(\mathrm{z_{AO}}) = \overline{|v_{01}|^2} - \overline{v_{01}v_{02}^*} = \overline{v_{01}(v_{01}^* - v_{02}^*)} \tag{3.31}$$



(a) Original (b) Decomposed

Figure 3.3 Impedance matrix representation of a 2-element array.

Off-diagonal component of the decomposed circuit become $\overline{v_{0\mathrm{E}}v_{0\mathrm{O}}^{*}}=0$, then $\overline{|v_{0\mathrm{E}}|^2}, \overline{|v_{0\mathrm{O}}|^2}$ are independent, respectively. So, the matching network impedance of Eq. (3.7) has the special symmetricity preserved for all sub matrices $\mathbf{Z}_{\mathrm{M}ij}$. From EVD property of the sub matrix $\mathbf{Z}_{\mathrm{M}ij}$, as shown in Fig. 3.2(b), symmetrical matching network $\mathbf{Z}_{\mathrm{ME}}$ and $\mathbf{Z}_{\mathrm{MO}}$ with reciprocal and lossless propoerty is represented by

$$\mathbf{Z}_{\mathrm{ME}}=\begin{bmatrix} z_{\mathrm{ME11}} & z_{\mathrm{ME12}} \\ z_{\mathrm{ME12}} & z_{\mathrm{ME22}} \end{bmatrix}, \quad \mathbf{Z}_{\mathrm{MO}}=\begin{bmatrix} z_{\mathrm{MO11}} & z_{\mathrm{MO12}} \\ z_{\mathrm{MO12}} & z_{\mathrm{MO22}} \end{bmatrix} \tag{3.32}$$

By the existance of the each matching networks, the revised antenna impedance matrix with the matching network is derived as $\mathbf{Z}_{\mathrm{A}}^{\prime}=\mathbf{U}\mathbf{\Lambda}_{\mathbf{Z}_{\mathrm{A}}^{\prime}}\mathbf{U}^{\dagger}$, where $\mathbf{\Lambda}_{\mathrm{Z}_{\mathrm{A}}^{\prime}}=\mathrm{diag}(z_{\mathrm{AE}}^{\prime},\ z_{\mathrm{AO}}^{\prime})$ as follows,

$$z_{\mathrm{AE}}^{\prime}=z_{\mathrm{ME22}}-\frac{z_{\mathrm{ME12}}^{2}}{z_{\mathrm{ME11}}+z_{\mathrm{AE}}}, \quad z_{\mathrm{AO}}^{\prime}=z_{\mathrm{MO22}}-\frac{z_{\mathrm{MO12}}^{2}}{z_{\mathrm{MO11}}+z_{\mathrm{AO}}}. \tag{3.33}$$

The revised even mode impedance $z_{\mathrm{AE}}^{\prime}$ and odd mode impedance $z_{\mathrm{AO}}^{\prime}$ resulted by the even-odd matching network are simultaneously equal to the desired impedance z_{opt} characterized by noise property of front-end from Eq. (3.14),

$$z_{\mathrm{AE}}^{\prime}=z_{\mathrm{AO}}^{\prime}=z_{\mathrm{opt}}. \tag{3.34}$$

The optimal matching condition minimizing noise factor under symmetrical antenna impedance and identical front-end is attained. Therefore, from Eq. (3.16) and Eq. (3.21) the noise factor matrix $\mathbf{F}$ and the SNR matrix $\mathbf{\Sigma}$ for symmetrical matching network can be given by

$$\mathbf{F}=\mathbf{U}\mathbf{\Lambda}_{\mathrm{F}}\mathbf{U}^{\dagger}, \quad \mathbf{\Sigma}=\mathbf{U}\mathbf{\Lambda}_{\Sigma}\mathbf{U}^{\dagger}, \tag{3.35}$$

where $\mathbf{\Lambda}_{\mathrm{F}} = \mathrm{diag}(F_{\mathrm{E}},\ F_{\mathrm{O}})$ and the SNR matrix is also preserved with the special symmetricity and can be decomposed into two eigen-values of even-odd mode i.e. $\mathbf{\Lambda}_{\Sigma} = \mathrm{diag}(\lambda_{\mathrm{E}},\ \lambda_{\mathrm{O}})$ by the same eigenmatrix $\mathbf{U}$. We derive a closed form expression for calculating the ergodic channel capacity can be derived as,

$$C = \frac{\lambda_{\mathrm{O}}^2 f(\lambda_{\mathrm{E}}) - \lambda_{\mathrm{E}}^2 f(\lambda_{\mathrm{O}}) + \lambda_{\mathrm{E}}\lambda_{\mathrm{O}}^2 f'(\lambda_{\mathrm{O}}) - \lambda_{\mathrm{O}}\lambda_{\mathrm{E}}^2 f'(\lambda_{\mathrm{E}})}{\lambda_{\mathrm{E}}\lambda_{\mathrm{O}}(\lambda_{\mathrm{O}} - \lambda_{\mathrm{E}})}, \tag{3.36}$$

$$f(\lambda) = \int_0^{\infty} e^{-\frac{u}{\lambda}} \log(1+u)\, du. \tag{3.37}$$

Furthermore, as $F_{\mathrm{E}} \geq F_{\min}$ and $F_{\mathrm{O}} \geq F_{\min}$ for arbitrary matching circuit, the designable boundaries of the even and odd mode eigenvalues are respectively

$$\lambda_{\mathrm{E}} \leq \frac{P_{\mathrm{T}} r_{\mathrm{T}} \Sigma_{\mathrm{hE}}}{8 k_{\mathrm{B}} T_0 B \Re(z_{\mathrm{AE}}) F_{\min}}, \quad \lambda_{\mathrm{O}} \leq \frac{P_{\mathrm{T}} r_{\mathrm{T}} \Sigma_{\mathrm{hO}}}{8 k_{\mathrm{B}} T_0 B \Re(z_{\mathrm{AO}}) F_{\min}}, \tag{3.38}$$

where r_{AE} and r_{AO} denote the real part of the even and odd mode antenna impedance, respectively. There are detail design processes for symmetrical matching network in the next chapter. Under these assumptions mentioned above, symmetrical matching can be derived to reduce RF complexity with optimal performance.

3.3.3 Identical self matching

Conventional identical self matching was proposed using a particular network composed by parameters of self antenna impedance and optimal impedance in [24], However, it is not optimal that each antenna achieves the minimum noise figure in isolation. In this sub-section, we propose a so-called identical self matching method for minimizing the determinant of the noise factor matrix. We assume an identical matching network $\mathbf{Z}_{\mathrm{MS}}$ shown in Fig. 3.2(c) which is also reciprocal and lossless.

$$\mathbf{Z}_{\mathrm{MS}} = \begin{bmatrix} z_{\mathrm{MS11}} & z_{\mathrm{MS12}} \\ z_{\mathrm{MS12}} & z_{\mathrm{MS22}} \end{bmatrix} \tag{3.39}$$

We perform transformation of antenna impedance matrix to derive the revised antenna impedances z''_{AE} and z''_{AO} regarding the identical matching circuit defined as,

$$z''_{\mathrm{AE}} = z_{\mathrm{MS22}} - \frac{z_{\mathrm{MS12}}^2}{z_{\mathrm{MS11}} + z_{\mathrm{AE}}},\ z''_{\mathrm{AO}} = z_{\mathrm{MS22}} - \frac{z_{\mathrm{MS12}}^2}{z_{\mathrm{MS11}} + z_{\mathrm{AO}}}. \tag{3.40}$$

To obtain the determinant of the noise factor matrix, Eq. (3.21) is rewritten as

$$\mathbf{F} = F_{\min}\mathbf{I}_2 + \left\{\sqrt{g_{\mathrm{a}}}\mathbf{R}_{\mathrm{A}}^{-1/2}\mathbf{M}^{-1}(z_{\mathrm{opt}}\mathbf{I}_2 - \mathbf{Z}'_{\mathrm{A}})\right\}\left\{\sqrt{g_{\mathrm{a}}}\mathbf{R}_{\mathrm{A}}^{-1/2}\mathbf{M}^{-1}(z_{\mathrm{opt}}\mathbf{I}_2 - \mathbf{Z}'_{\mathrm{A}})\right\}^{\dagger}. \tag{3.41}$$

Changing from the desired antenna impedance matrix $\mathbf{Z}'_{\mathrm{A}}$ to the revised antenna impedances z''_{AE} and z''_{AO}, for high SNR case the determinant of the noise factor matrix is given by,

$$\det[\mathbf{F}] = \left(F_{\min} + \frac{g_{\mathrm{a}}|z''_{\mathrm{AE}} - \mathrm{z}_{\mathrm{opt}}|^2}{\mathrm{r}''_{\mathrm{AE}}}\right)\left(F_{\min} + \frac{g_{\mathrm{a}}|z''_{\mathrm{AO}} - \mathrm{z}_{\mathrm{opt}}|^2}{\mathrm{r}''_{\mathrm{AO}}}\right), \tag{3.42}$$

where $z''_{\mathrm{AE}} = r''_{\mathrm{AE}} + jx''_{\mathrm{AE}}$ and $z''_{\mathrm{AO}} = r''_{\mathrm{AO}} + jx''_{\mathrm{AO}}$. For finding the optimum value of identical self matching, we use an exhaustive search method,

$$[z^{\mathrm{opt}}_{\mathrm{MS11}}\ z^{\mathrm{opt}}_{\mathrm{MS12}}\ z^{\mathrm{opt}}_{\mathrm{MS22}}] = \underset{z_{\mathrm{MS11}}, z_{\mathrm{MS12}}, z_{\mathrm{MS22}}}{\arg\max}\ (\det[\mathbf{F}]). \tag{3.43}$$

On the other hand, we consider a approximation method for minimizing noise factor using determinant of $\mathbf{F}$. Based on the constraint requirement of symmetrical antenna impedance discussed in Eq. (3.28) and Eq. (3.40), we obtain

$$\frac{|z''_{\mathrm{AE}} - z''_{\mathrm{AO}}|}{|z''_{\mathrm{AE}} + z''^{*}_{\mathrm{AO}}|} = \frac{|z_{\mathrm{AE}} - z_{\mathrm{AO}}|}{|z_{\mathrm{AE}} + z^{*}_{\mathrm{AO}}|} = \eta \tag{3.44}$$

For given $z''_{\mathrm{AO}} = z_{\mathrm{opt}}$, the target parameter $\mu = \frac{g_{\mathrm{a}}|z''_{\mathrm{AE}} - z_{\mathrm{opt}}|^2}{r''_{\mathrm{AE}}}$ of Eq. (3.42) should be minimized. With bilinear transform of Eq. (3.44), a center c_η and a radius r_η of *Apollonius circle* are given by

$$c_\eta = \frac{1+\eta^2}{1-\eta^2} r''_{\mathrm{AO}} + jx''_{\mathrm{AO}}, \quad r_\eta = \frac{2|\eta|}{1-|\eta|^2} r''_{\mathrm{AO}}. \tag{3.45}$$

Furthermore, another circle of μ is drawn by

$$c_\mu = z_{\mathrm{opt}} + \frac{\mu}{2}, \quad r_\mu = \sqrt{\mu r_{\mathrm{opt}} + \frac{\mu^2}{4}}. \tag{3.46}$$

If the two circles intersect with one point, μ becomes minimum. For $x''_{\mathrm{AO}} = x_{\mathrm{opt}}$, μ is given by

$$\mu = \frac{r_{\mathrm{opt}}}{\epsilon}\left\{\frac{(\epsilon^2+1)(1+\eta^2)}{1-\eta^2} + \frac{\epsilon^2-1}{1-\eta^2} - 2\epsilon\right\} \tag{3.47}$$

where $\epsilon = \frac{r_{\mathrm{opt}}}{r''_{\mathrm{AO}}} > 0$. The minimum of μ at $\epsilon = 1$ becomes

$$\min(\mu) = \frac{4r_{\mathrm{opt}}\eta^2}{1-\eta^2}. \tag{3.48}$$

3.4 Numerical results

In this section, we conduct numerical analysis in some specific conditions, i.e. symmetrical channel characteristic, symmetrical receive antennas and identical front-end to verify the proposed system. From the antenna parameters on Table 3.1 and Table 3.2, Ansoft HFSS is used to calculate the antenna impedance, the S parameter as well as the radiation pattern descriptions for the dipole antennas. Furthermore, the channel correlation matrix $\mathbf{\Sigma}_{\mathrm{h}}$ is given assuming that incoming waves are 3-D model with independent, uniformly-distributed direction-of-arrival phases and no reradiation. $\mathbf{\Sigma}_{\mathrm{h}}$ eventually conforms to open-circuit voltage covariance matrix with some scalar and mutual antenna resistance matrix $\mathbf{R}_{\mathrm{A}}$ defined by Eq. (2.23).

For the sake of comparison, we redefine the equivalent SNR γ of a single-input single-output (SISO) channel as,

$$\gamma = \frac{P_{\mathrm{h}}}{4k_{\mathrm{B}}T_0Br_{\mathrm{A}}}, \tag{3.49}$$

where r_{A} is the real part of the antenna impedance for SISO system. Using realistic antenna parameters and front-end noise parameters in Tables 3.1- 3.3, we compare the channel capacity performance for two scenarios of symmetrical matching and no matching.

For evaluating the designable range of the proposed symmetrical matching circuit, the ergodic channel capacity with respect to λ_{E} and λ_{O} is plotted in Fig. 3.4. The solid line denotes the contour constant curve of the closed form expression of the ergodic channel capacity given in Eq. (5.24). In this figure, the designable boundary given by Eq. (3.38) is depicted under conditions of the antenna distance $\lambda_{\mathrm{w}}/8$, NF=1dB and γ=10dB. From this figure, the optimum achievable point with highest ergodic capacity can be found with the corresponding capacity of at 5.1 bps/Hz.

The evaluation results of the ergodic capacity for multiport matching, symmetrical matching and no matching scenarios are shown in Fig. 3.5 with respect to different antenna spacing normalized over the wavelength d/λ_{w}. It can be found that the performance of the symmetrical matching is superior to identical self matching and no matching because the arbitrary impedance matrix completely matches with the optimal impedance in decoupling form. The ergodic capacity for the proposed matching is almost constant or independent of the antenna separation since SNR matrix has the degenerated eigen values. The performance discrepancy between proposed matching and other matching schemes is larger for higher NF amplifier. Figure 3.6(a) and 3.6(b) investigate the effect of matching network against equivalent SNR

γ defined in Eq. (3.49) for two different scenarios of noise figure (NF), i.e. $10\log_{10} F$, respectively. It can be found that the performance of the symmetrical matching equal to the multiport matching is superior to that without matching because the arbitrary impedance matrix completely matches with the optimal impedance in decoupling form. The multiport matching and symmetrical matching have significant gain against the identical self matching and no matching, especially at closer antenna spacing.

On a basis of the result, we can apply for asymptotic forms discussed in subsec. 2.3.1. The asymptotic approach becomes matched by each low/high SNR case compared with rigorous form provided for reference. In Fig. 3.7(a) and 3.7(b), we plot ergodic capacity as a function of equivalent SNR γ. At very small SNR and very large SNR cases, the asymptotic method is almost match with rigorous ergodic capacity result. In general, two quite different eigenvalues (λ_{E}, λ_{O}) employ the different approximated form, e.g. both large two eigenvalues apply to asymptotic form for high SNR while both small values use in low SNR one.

Table 3.1 Antenna conditions.

Content	Settings
Antenna type	Dipole antenna
Antenna length (l_{A})	$\lambda_{\mathrm{w}}/2$
Center frequency	3.5 GHz
Radius of antenna	$\lambda_{\mathrm{w}}/1000$
Antenna distance (d)	$\lambda_{\mathrm{w}}/20 \sim \lambda_{\mathrm{w}}/2$

λ_{w} : wavelength

Table 3.2 Antenna parameters.

d	S_{A12}	S_{A11}
$0.5\lambda_{\mathrm{w}}$	-0.09225 - j0.18399	0.17907 - j0.07210
$0.45\lambda_{\mathrm{w}}$	-0.04532 - j0.21141	0.19838 - j0.07874
$0.4\lambda_{\mathrm{w}}$	0.03525 - j0.23091	0.18362 - j0.09512
$0.35\lambda_{\mathrm{w}}$	0.13252 - j0.22275	0.14535 - j0.11352
$0.3\lambda_{\mathrm{w}}$	0.18391 - j0.23713	0.12331 - j0.02421
$0.25\lambda_{\mathrm{w}}$	0.31611 - j0.15925	0.03102 - j0.07953
$0.2\lambda_{\mathrm{w}}$	0.40909 - j0.13509	-0.03469 - j0.03393
$0.15\lambda_{\mathrm{w}}$	0.50119 - j0.16694	-0.09390 + j0.03442
$0.1\lambda_{\mathrm{w}}$	0.62767 - j0.11581	-0.16189 + j0.05625
$0.05\lambda_{\mathrm{w}}$	0.73840 + j0.03893	-0.21035 - j0.01394

Table 3.3 Front-end noise parameters.

Content	Value	
Noise Figure (NF)	1 dB	5 dB
Noise resistance (r_{a})	9.45 Ω	76.22 Ω
Noise conductance (g_{a})	3.24 mS	26.13 mS
Correlation impedance (z_{cor})	$35.3\angle -114°$	
Optimum impedance (z_{opt})	$55.88 + j32.25$	

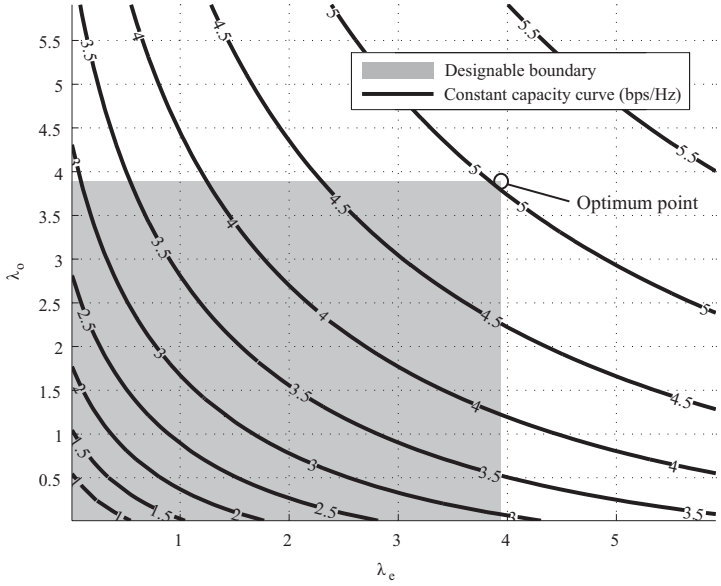


Figure 3.4 Ergodic capacity as a function of even and odd mode eigenvalues.

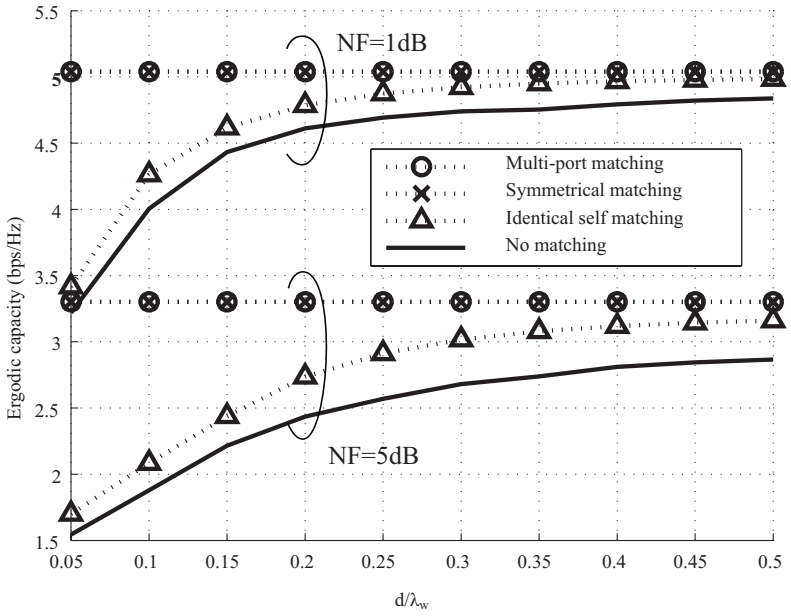
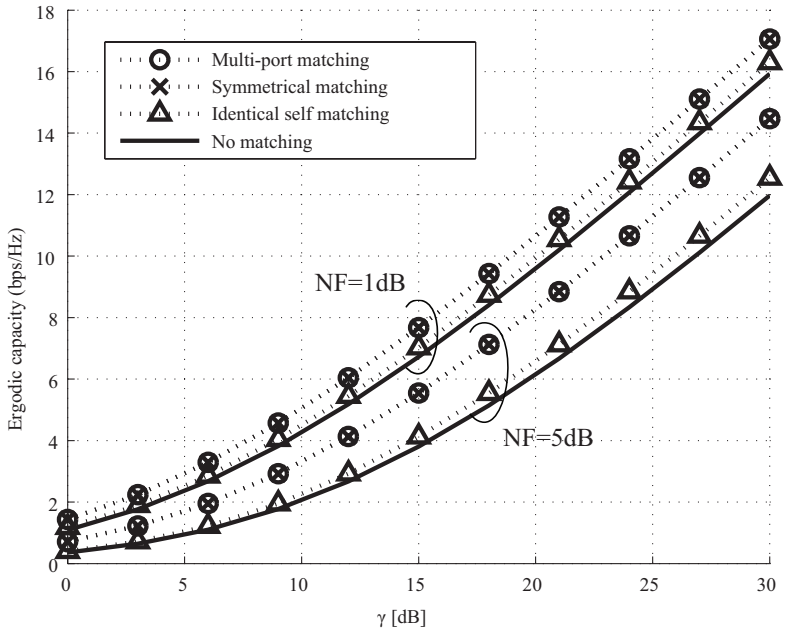
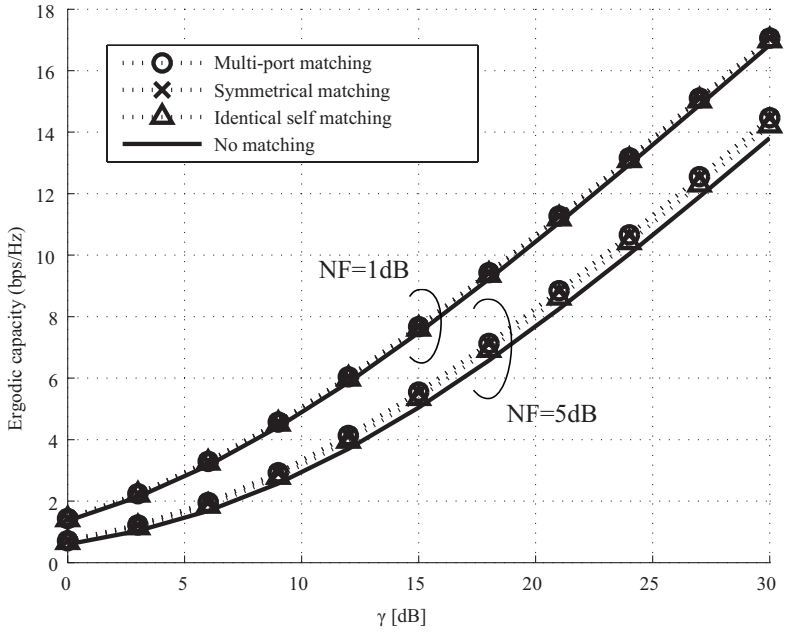


Figure 3.5 Ergodic capacity as antenna separation (γ=10dB).

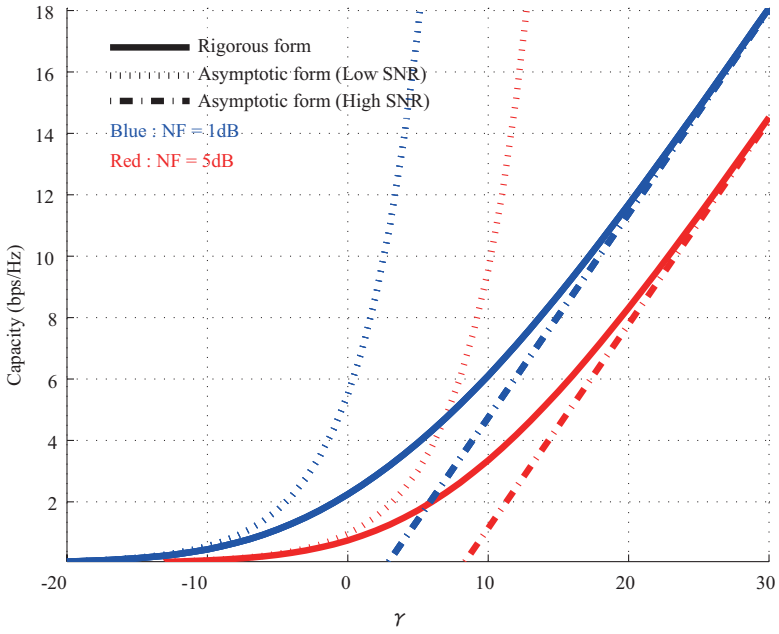


(a) $d = \lambda_{\mathrm{w}}/8$

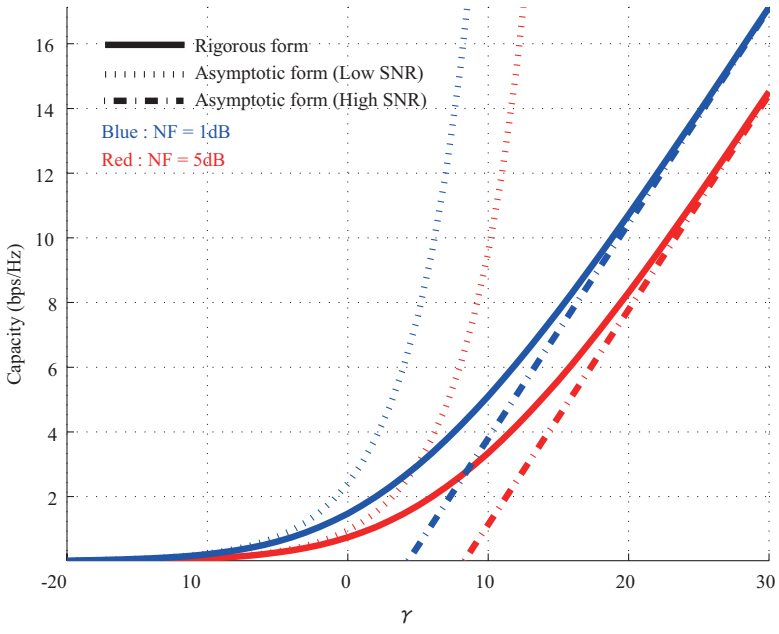


(b) $d = \lambda_{\mathrm{w}}/2$

Figure 3.6 Ergodic capacity on SNR condition



(a) $d = \lambda_{\mathrm{w}}/8$



(b) $d = \lambda_{\mathrm{w}}/2$

Figure 3.7 Capacity comparison of rigorous form and two asymptotic forms.

3.5 Summary

In this chapter we derived optimal front-end design based on a communication theory, electromagnetics and RF circuit theory perspectives. Three matching networks for maximization of ergodic capacity were presented using system model with fading correlation and noise. In particular, a simple and optimal matching network which is called as symmetrical matching was proposed under the assumption of symmetrical channel characteristic, symmetrical receive antennas and identical front-ends. At all antenna spacings, We showed that optimal multi-port matching is corresponding to symmetrical matching and these matching methods are an upper-bound than identical self and no matching cases through numerical simulations.

Chapter 4

Matching Circuit in Realization

4.1 Introduction

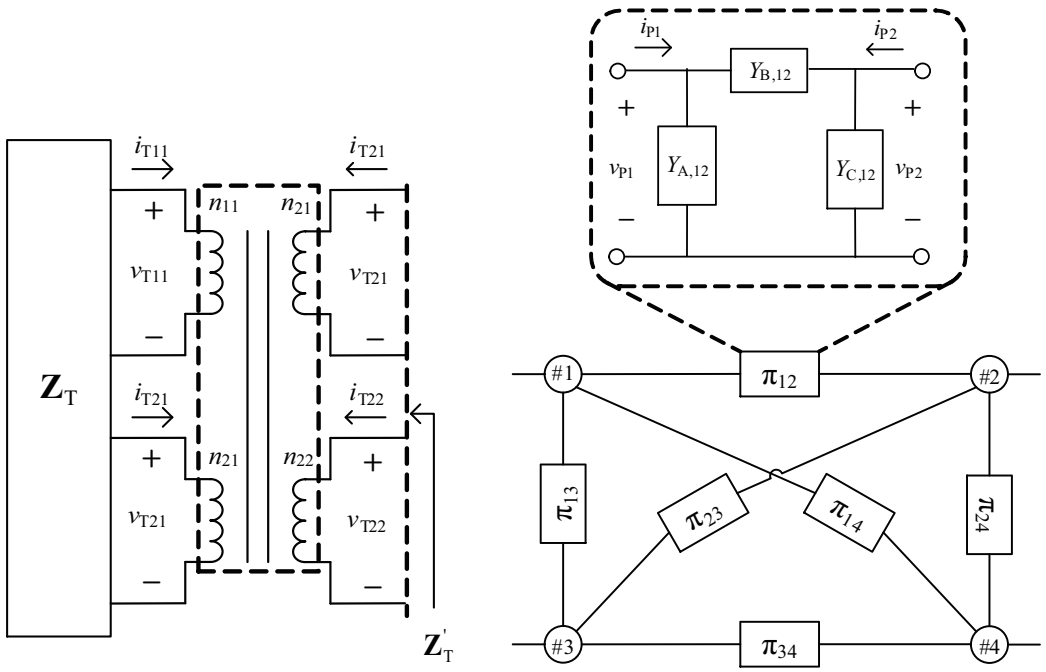
In this chapter, we theoretically derive the corresponding realization circuit parameters with reduced complexity and high performance. Furthermore, lossy condition within the desired matching circuit parameters is considered for approaching to more realistic circuit model. Finally, numerical analysis with specific simulation condition is conducted to verify the effectiveness of the proposed models.

4.2 Multi-port circuit realization

In this section, we consider multi-port circuit topology for realization of matching circuit. There are various matching structure methods, e.g. transformer based circuit and 2-port based circuit such as π, T-shape network, L-shape network and so on. Among them, we introduce multi-port circuit using transformer circuit and π network circuit for design of low noise matching.

4.2.1 Transformer circuit

We express 2×2 transformer circuit with voltage column vectors $\mathbf{v}_{\mathrm{T1}} = [v_{\mathrm{T11}}\ v_{\mathrm{T2}}]^T, \mathbf{v}_{\mathrm{T2}} = [v_{\mathrm{T21}}\ v_{\mathrm{T22}}]^T$, current column vector $\mathbf{i}_{\mathrm{T1}} = [i_{\mathrm{T11}}\ i_{\mathrm{T2}}]^T, \mathbf{i}_{\mathrm{T2}} = [i_{\mathrm{T21}}\ i_{\mathrm{T22}}]^T$ with input index T1



(a) Transformer circuit (b) π network circuit

Figure 4.1 Examples of multi-port circuit structure.

and output index T2, respectively, in Fig. 4.1(a). The multi-winding numbers become

$$\mathbf{N}_\mathrm{T} = \begin{bmatrix} \frac{n_{11}}{n_{21}} & \frac{n_{12}}{n_{21}} \\ \frac{n_{11}}{n_{22}} & \frac{n_{12}}{n_{22}} \end{bmatrix}. \tag{4.1}$$

The characteristics of the voltage and current column vector with $\mathbf{N}_\mathrm{T}$ are given by

$$\mathbf{v}_{\mathrm{T1}} = \mathbf{N}_\mathrm{T}\mathbf{v}_{\mathrm{T2}}, \quad \mathbf{i}_{\mathrm{T2}} = \mathbf{N}_\mathrm{T}^T\mathbf{i}_{\mathrm{T1}}, \tag{4.2}$$

where the total power for input and output port is given by

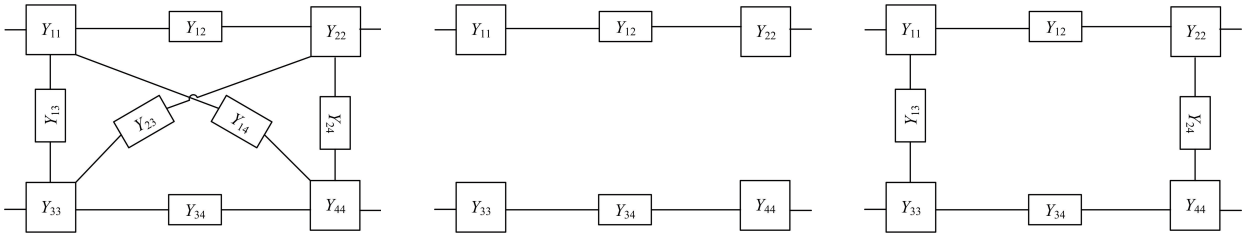
$$P_{\mathrm{T1}} = \mathbf{i}_{\mathrm{T1}}^T\mathbf{v}_{\mathrm{T1}} = \mathbf{i}_{\mathrm{T1}}^T\mathbf{N}_\mathrm{T}\mathbf{v}_{\mathrm{T2}}, \quad P_{\mathrm{T2}} = \mathbf{i}_{\mathrm{T2}}^T\mathbf{v}_{\mathrm{T2}}. \tag{4.3}$$

If the multi-winding circuit is lossless, it satisfies $\mathbf{i}_{\mathrm{T2}} = \mathbf{N}_\mathrm{T}^T\mathbf{i}_{\mathrm{T1}}$. Next, the transformer is characterized with transformer source impedance matrix $\mathbf{Z}_\mathrm{T}$ as

$$\mathbf{v}_{\mathrm{T1}} = \mathbf{Z}_\mathrm{T}\mathbf{i}_{\mathrm{T1}} = \mathbf{Z}_\mathrm{T}\mathbf{N}_\mathrm{T}^{-T}\mathbf{i}_{\mathrm{T2}}. \tag{4.4}$$

Finally, we obtain the revised transformer impedance matrix from Eq. (4.2) and (4.4) as

$$\mathbf{v}_{\mathrm{T2}} = \mathbf{Z}'_\mathrm{T}\mathbf{i}_{\mathrm{T2}}, \quad \mathbf{Z}'_\mathrm{T} = \mathbf{N}_\mathrm{T}^{-1}\mathbf{Z}_\mathrm{T}\mathbf{N}_\mathrm{T}^{-T}. \tag{4.5}$$



(a) Multi-port matching (b) Self matching (c) symmetrical matching

Figure 4.2 Classification of matching network.

Circuit synthesis for the transformer structure should be designed on IC (integrated circuit). However, multi-winding transformer is very difficult to realize. Therefore, we introduce another type of circuit using inductances and capacitances for the simple implementation in next subchapter.

4.2.2 π network circuit

We consider a 4-port matching circuit with *non-planar network* structure which mean crossing components between each ports in Fig. 4.1(b). Every sub-circuit is connected using a 2-port admittance matrix of π network. Eventually six 2-port π networks are required for the 4-port matching circuit. Imposing port numbers in each sub admittances, we note that $Y_{\mathrm{A},ij}$, $Y_{\mathrm{B},ij}$ and $Y_{\mathrm{C},ij}$ with index i, j of port number.

$$\begin{bmatrix} i_{\mathrm{P}i} \\ i_{\mathrm{P}j} \end{bmatrix} = \begin{bmatrix} Y_{\mathrm{A},ij} + Y_{\mathrm{B},ij} & -Y_{\mathrm{B},ij} \\ -Y_{\mathrm{B},ij} & Y_{\mathrm{B},ij} + Y_{\mathrm{C},ij} \end{bmatrix} \begin{bmatrix} v_{\mathrm{P}i} \\ v_{\mathrm{P}j} \end{bmatrix} \tag{4.6}$$

Defining the voltage and current for each terminal by $Kirchhoff's\ law$, the realization model shows multi-port matching structure when using four series elements and six shunt elements as shown in Fig. 4.2(a) as

$$\begin{bmatrix} Y_{11} & Y_{12} & Y_{13} & Y_{14} \\ & Y_{22} & Y_{23} & Y_{24} \\ & & Y_{33} & Y_{34} \\ & & & Y_{44} \end{bmatrix} = \begin{bmatrix} Y_1 & -Y_{\mathrm{B},12} & -Y_{\mathrm{B},13} & -Y_{\mathrm{B},14} \\ & Y_2 & -Y_{\mathrm{B},23} & -Y_{\mathrm{B},24} \\ & & Y_3 & -Y_{\mathrm{B},34} \\ & & & Y_4 \end{bmatrix}, \begin{cases} Y_1 = Y_{\mathrm{A},12} + Y_{\mathrm{A},13} + Y_{\mathrm{A},14} \\ Y_2 = Y_{\mathrm{C},12} + Y_{\mathrm{A},23} + Y_{\mathrm{A},24} \\ Y_3 = Y_{\mathrm{A},34} + Y_{\mathrm{C},13} + Y_{\mathrm{C},23} \\ Y_4 = Y_{\mathrm{C},14} + Y_{\mathrm{C},24} + Y_{\mathrm{C},34} \end{cases} \tag{4.7}$$

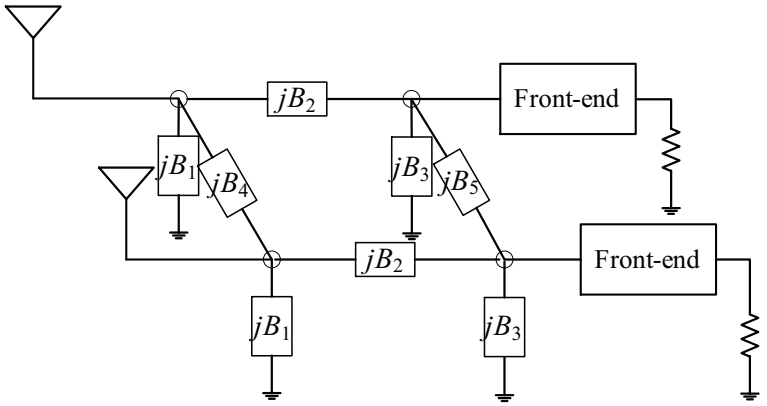


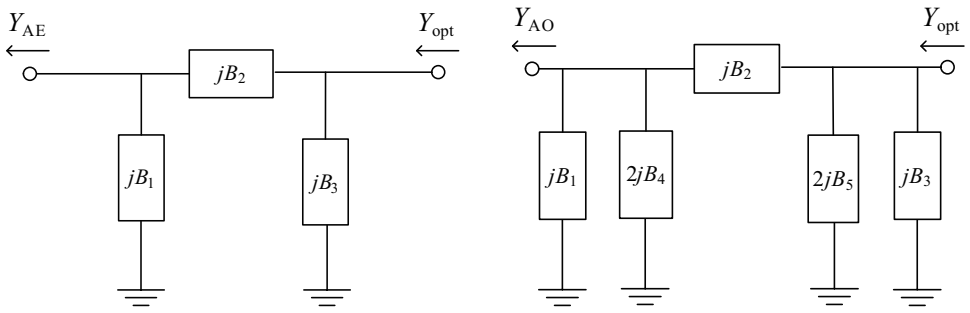
Figure 4.3 Receiver model of symmetrical matching.

where off-diagonal components are determined by four series elements of each π network.

On the other hand, the self matching with two series elements separately connected as shown in Fig. 4.2(b) defined by

$$\begin{bmatrix} Y_{11} & & Y_{13} & \\ & Y_{22} & & Y_{24} \\ Y_{13} & & Y_{33} & \\ & Y_{24} & & Y_{44} \end{bmatrix} = \begin{bmatrix} Y_1 & & -Y_{\mathrm{B},13} & \\ & Y_2 & & -Y_{\mathrm{B},24} \\ -Y_{\mathrm{B},13} & & Y_3 & \\ & -Y_{\mathrm{B},24} & & Y_4 \end{bmatrix}, \tag{4.8}$$

where design degree difference between self matching and multi-port matching has with usable parameters 6 and 10, respectively. For maximization of ergodic capacity, we assume a limited of number of controllable parameters. If the multi-port matching case, we can realize arbitrary 2-port matrix with antenna impedance matrix from Eq. (3.8) satisfying $\mathbf{Z}_{\mathrm{A}}^{'} = z_{\mathrm{opt}}$. The circuit may be difficult to fabricate with large dynamic design range, e.g. multi-port matching network size is larger than self matching size from six 2-port to two 2-port network. However, self matching can not realize the arbitrary impedance matrix by confined design area. Therefore, for deriving optimal matching with reduced circuit complexity, symmetrical matching is proposed using four series elements without two crossover components as shown in Fig. 4.2(c).



(a) Even mode (b) Odd mode

Figure 4.4 Circuit model for even-odd mode.

4.3 symmetrical matching circuit

Figure 4.3 shows the realization model of symmetrical matching structure. For each terminal by *Kirchhoff's law*, the overall admittance matrix is defined with four series and shunt elements,

$$\begin{bmatrix} Y_{11} & Y_{12} & Y_{13} & \\ & Y_{22} & & Y_{24} \\ & & Y_{33} & Y_{34} \\ & & & Y_{44} \end{bmatrix} = \begin{bmatrix} jB_1 & jB_2 & jB_4 & \\ & jB_3 & & jB_5 \\ & & jB_1 & jB_2 \\ & & & jB_3 \end{bmatrix}, \tag{4.9}$$

where, even and odd mode decomposition of the matching network can be employed with open and short circuit, respectively, by the shunt components (Y_{13}, Y_{24}) of the middle way to be open or short based on *Bartlett's bisection theorem*. Two 2-port lossless circuits for respectively symmetrical matching are represented in Fig. 4.4(a) and 4.4(b), respectively. They are composed by pi network of susceptance parameters (B_1, B_2, B_3) and (B_1', B_2, B_3') with $B_1' = B_1 + 2B_4$ and $B_3' = B_3 + 2B_5$. The doubling shunt admittances ($2B_4$,$2B_5$) are included to convert the desired susceptance parameters (B_1',B_3') in the odd mode case.

To facilitate the analysis, the antenna impedance are represented in the admittance form as,

$$Y_{AE} = \frac{1}{z_{AE}}, \quad Y_{AO} = \frac{1}{z_{AO}}. \tag{4.10}$$

For the symmetrical matching, the revised input admittances are defined as,

$$Y_{AE}' = j(B_2 + B_3) + \frac{B_2^2}{Y_{AE} + j(B_1 + B_2)}, \tag{4.11}$$

$$Y'_{\mathrm{AO}} = j(B_2 + B'_3) + \frac{B_2^2}{Y_{\mathrm{AO}} + j(B'_1 + B_2)}. \tag{4.12}$$

From the optimal impedance matching theorem of Eq. (**??**), the revised even and odd mode admittance resulted by the symmetrical matching network are simultaneously equal to the desired impedance $Y_{\mathrm{opt}} = 1/z_{\mathrm{opt}}$ characterized by noise property of front-end, i.e. $Y'_{\mathrm{AE}} = Y'_{\mathrm{AO}} = Y_{\mathrm{opt}}$.

First, the real and imaginary parts of the even mode are respectively given by,

$$G_{\mathrm{opt}}G_{\mathrm{AE}} - \{B_{\mathrm{opt}} - (B_2 + B_3)\}\{B_{\mathrm{AE}} + (B_1 + B_2)\} = B_2^2, \tag{4.13}$$

$$G_{\mathrm{AE}}\{B_{\mathrm{opt}} - (B_2 + B_3)\} + G_{\mathrm{opt}}\{B_{\mathrm{AE}} + (B_1 + B_2)\} = 0, \tag{4.14}$$

where $Y_{\mathrm{AE}} = G_{\mathrm{AE}} + jB_{\mathrm{AE}}$ and $Y_{\mathrm{opt}} = G_{\mathrm{opt}} + jB_{\mathrm{opt}}$, respectively.

On the other hand, those of the odd mode of Eq. (4.12) are as follows,

$$G_{\mathrm{opt}}G_{\mathrm{AO}} - \{B_{\mathrm{opt}} - (B_2 + B'_3)\}\{B_{\mathrm{AO}} + (B'_1 + B_2)\} = B_2^2, \tag{4.15}$$

$$G_{\mathrm{AO}}\{B_{\mathrm{opt}} - (B_2 + B'_3)\} + G_{\mathrm{opt}}\{B_{\mathrm{AO}} + (B'_1 + B_2)\} = 0, \tag{4.16}$$

where $Y_{\mathrm{AO}} = G_{\mathrm{AO}} + jB_{\mathrm{AO}}$. For the condition in Eqs. (4.13)-(4.16), B_2 is set as a free parameter for arbitrary susceptances. From the above discussion, the design procedure for symmetrical matching can be summarized as follows:

1. B_2 is set as a free parameter for arbitrary susceptances. Lower bound conditions $|B_2|^2 \geq G_{\mathrm{AE}}G_{\mathrm{opt}}$, $|B_2|^2 \geq G_{\mathrm{AO}}G_{\mathrm{opt}}$ of even-odd mode, then

$$|B_2|^2 \geq \max[\mathrm{G_{AE}}, \mathrm{G_{AO}}]\mathrm{G_{opt}}. \tag{4.17}$$

2. For B_2 to satisfy the necessity condition in step 1, B_1 and B_4 are given by

$$B_1 = \pm\sqrt{\frac{B_2^2 G_{\mathrm{AE}}}{G_{\mathrm{opt}}} - G_{\mathrm{AE}}^2} - B_{\mathrm{AE}} - B_2, \tag{4.18}$$

$$B_4 = \frac{1}{2}\left(\pm\sqrt{\frac{B_2^2 G_{\mathrm{AO}}}{G_{\mathrm{opt}}} - G_{\mathrm{AO}}^2} - B_{\mathrm{AE}} - B_2 - B_1\right) \tag{4.19}$$

3. The remaining parameters B_3 and B_5 are given by

$$B_3 = -\left(\frac{G_{\text{opt}}G_{\text{AE}} - B_2^2}{B_{\text{AE}} + B_1 + B_2}\right) + B_{\text{opt}} - B_2, \tag{4.20}$$

$$B_5 = \frac{1}{2}\left\{\left(\frac{G_{\text{opt}}G_{\text{AE}} - B_2^2}{B_{\text{AE}} + B_1 + B_2}\right) - \left(\frac{G_{\text{opt}}G_{\text{AO}} - B_2^2}{B_{\text{AO}} + B_1' + B_2}\right)\right\}. \tag{4.21}$$

In Eqs. (4.17)-(4.19), as both positive and negative values satisfy the conditions, there are totally 8 cases for deriving B_1, B_2 and B_4. The combination families can be expanded as a function of the free parameter B_2.

4.4 Lossy matching circuit

We introduce the quality factor (Q-factor) of the reactance elements within the matching circuit for evaluating the effectiveness of the symmetrical matching circuit. As the Q-factor indicates the amount of inherent resistive loss included in the susceptance elements, it becomes an important criterion for implementation in practice.

$$R_k = \frac{1}{Q|B_k|} \quad \forall k \in \{1, \ldots, 5\} \tag{4.22}$$

In particular, since inductance element generally involves much higher lossy condition compared to capacitance, we focus on the Q-factor of the inductance among other practical parameters. The performance of the above 8 combination cases depends on the Q-factor of the inductance component which has negative value among five susceptances B_k.

We also consider a newly defined noise factor under lossy matching network. An important metric of a device is the noise factor regarding lossy matching circuit F_{L} defined as the product of the signal power loss (L) and the original noise factor (F) (cf., Appendix IV). This concept can be extended to multi-port networks using the original noise factor matrix of Eq. (3.21) by

$$\mathbf{F}_{\text{L}} = \mathbf{L}\mathbf{F} = \mathbf{U}\mathbf{\Lambda}_{\text{L}}\mathbf{\Lambda}_{\text{F}}\mathbf{U}^{\dagger}, \tag{4.23}$$

where, $\mathbf{L} = \mathbf{U}\mathbf{\Lambda}_{\text{L}}\mathbf{U}^{\dagger}$ is the signal power loss matrix and $\mathbf{\Lambda}_{\text{L}} = \text{diag}(L_{\text{E}},\ L_{\text{O}})$ is a diagonal matrix representing power loss of even and odd modes, respectively. From the discussion above, we can select the optimal combination with the best performance under lossy condition of the proposed matching circuit.

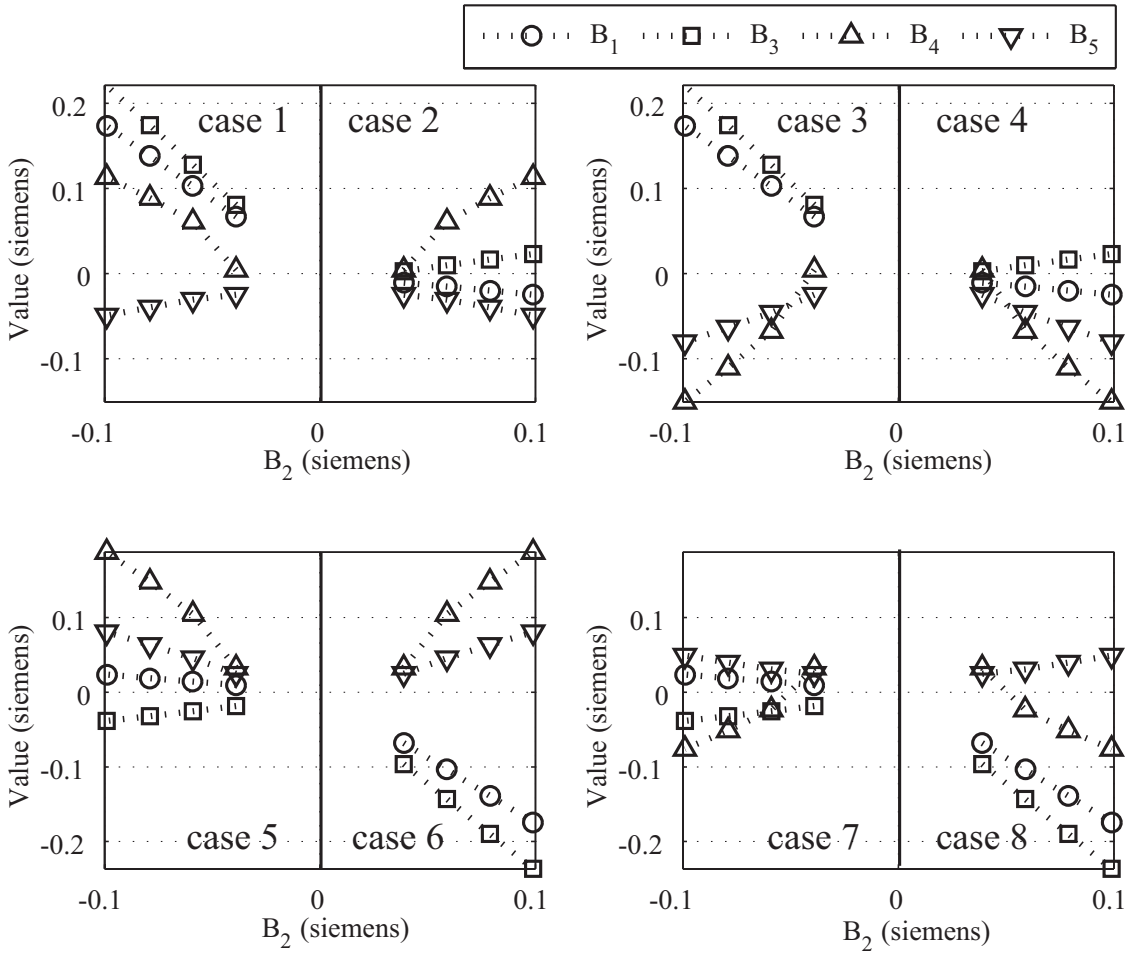


Figure 4.5 Circuit component values of symmetrical matching.

4.5 Numerical results

We now present numerical results for evaluating our designed model. On the basis of Fig. 3.6(a), Figure 4.5 shows the component parameters of the symmetrical matching circuit for the two noise factor cases at the antenna distance $\lambda_w/8$ and $\gamma = 10$dB. Table 4.1 designates various combinations of symmetrical matching circuit as plus/minus sign of the free parameter B_2. Although all case families completely satisfy the maximum point of the ergodic capacity, each case is composed of various combinations with inductance and capacitance elements.

For finding the optimal combination, we compute the ergodic channel capacity as a function of the free parameter B_2 in lossy condition ($Q = 10$) in Fig. 4.6. As the absolute value

Table 4.1 Combination of matching network components.

	$B_2(-)$	$B_2(+)$
$B_1(+)$, $B_4(+)$	case 1	case 2
$B_1(+)$, $B_4(-)$	case 3	case 4
$B_1(-)$, $B_4(+)$	case 5	case 6
$B_1(-)$, $B_4(-)$	case 7	case 8

of B_2 increases, the performance gradually deteriorates by the inherent resistive loss within the inductance component. At all ranges of $B_2(+)$, case 2 shows the best performance. Figure 4.7(a) and 4.7(b) show the realistic even and odd equivalent circuit based on L/C components of case 2, respectively. Using this circuit structure, Figure 4.8 shows the channel capacity performance of the symmetrical matching and no matching cases at different conditions of Q-factor. At that time, susceptance parameters with maximum performance are induced through a specific case 2 combination, e.g. $B_1 = 4.17$nH, $B_2 = 1.77$pF, $B_3 = 4.17$nH , $2B_4 = 391$fF and $2B_5 = 919$pF.

We also define the minimum required Q-factor $Q_{\min}$ at the cross point between the two scenarios as a criterion for evaluating the necessity of the proposed matching circuit. In this figure, the ergodic capacity of the symmetrical matching decreases as the resistive loss increases. Figure. 4.9 shows the variation of $Q_{\min}$ as a function of the equivalent SNR γ. As the equivalent SNR increases in Fig. 3.6(a), larger capacity disparity between symmetrical matching and no matching results in lower $Q_{\min}$. To analyze the physical impact of loss, from Eq. (4.23) the signal power losses (L_{E},L_{O}) of the even and odd mode operation are shown in Fig. 4.10, respectively. In the odd mode circuit of Fig. 4.7(b), both the resistive losses R_1 and $R_5/2$ affect more strongly than R_1 of the even mode circuit. It is noted that the revised antenna impedance z'_{AO} with the transfer coefficient M_{O} determined by the lossy elements can reduce the signal power loss L.

Noise figures for even mode and odd mode as a function of Q-factor are shown in Fig. 4.11. Remind that original noise figure F_{E} and F_{O} from Eq. (3.35) depend on revised antenna impedances z'_{AE} and z'_{AE} with even and odd mode matching, respectively, in contrast with the signal power losses. For noise figure of odd mode in higher NF case, the deviation against lower NF case increases due to the more sensitive impact of lossy condition. By the derived

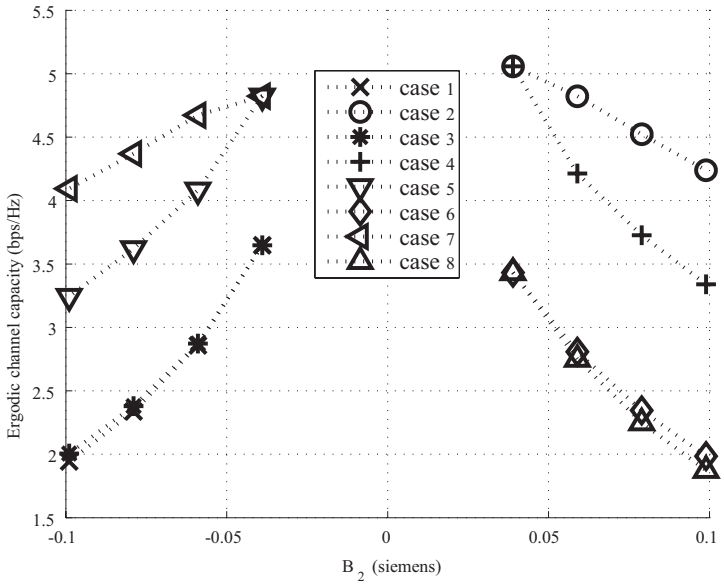
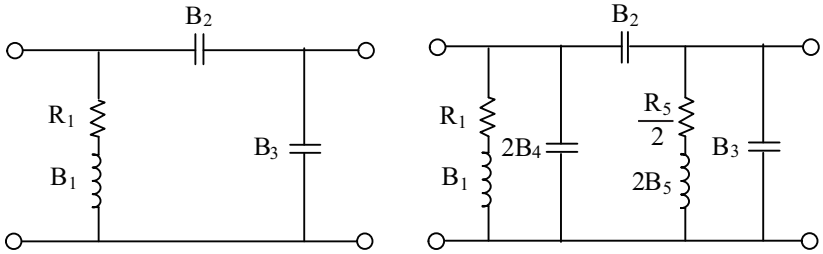


Figure 4.6 Ergodic channel capacity of 8 combinations ($Q = 10$).

circuit structure of odd mode in Fig 4.7(b), the additional inductance component ($2B_5$) affects at lower Q-factor of the inductance.

For analyzing the noise characteristic by the lossy circumstances, the noise figure circle which is a convenient format to show complex relation between antenna source impedance and noise figure (cf., Appendix III). All the lossy points by Q-factor in Fig. 4.11 as two NF scenarios are parallel to the corresponding NF cases in Fig. 4.12(a) and 4.12(b), separately. As we mentioned above, the deviated impedance is receding from optimal impedance point z_{opt} with minimum NF values as Q-factor is lower. Although the distribution lines both NF cases are identical, the NF range of color reference curves differentiate at each starting points NF=1dB and NF=5dB, respectively. Then NF circle property of 4.12(a) and 4.12(b) can be analyzed by even and odd mode as shown in fig. 4.13(a) and fig. 4.13(b), individually, through *Smith chart* of ADS simulation tool. In this sense, the lossy condition $Q = 10$ of all inductance components within symmetrical matching circuit is considered. The results show that the distortion impedance z_{D} by Q-factor cause to be deviated from optimal impedance z_{opt}.



(a) Even mode (b) Odd mode

Figure 4.7 Equivalent circuit for lossy matching network (case 2).

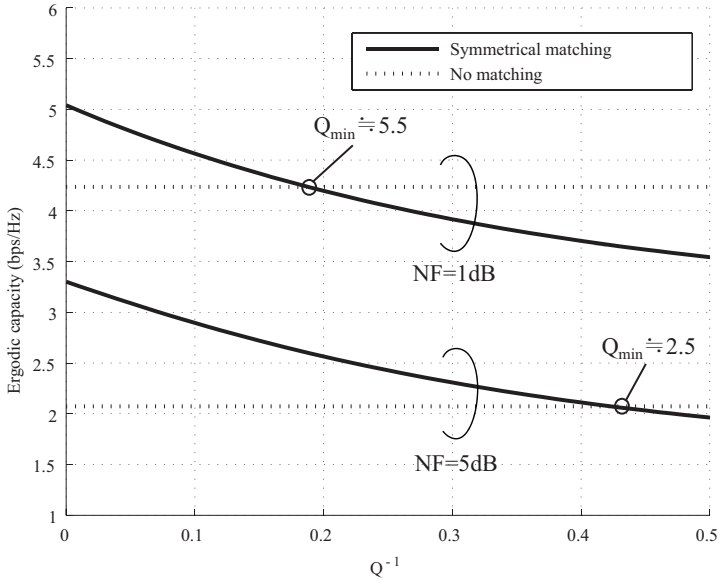


Figure 4.8 Matching circuit performance in different lossy condition.

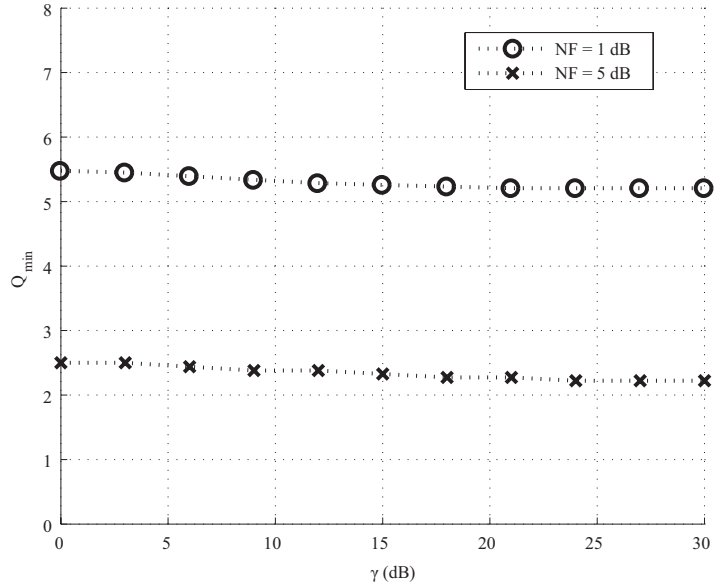


Figure 4.9 Minimum required Q-factor as γ.

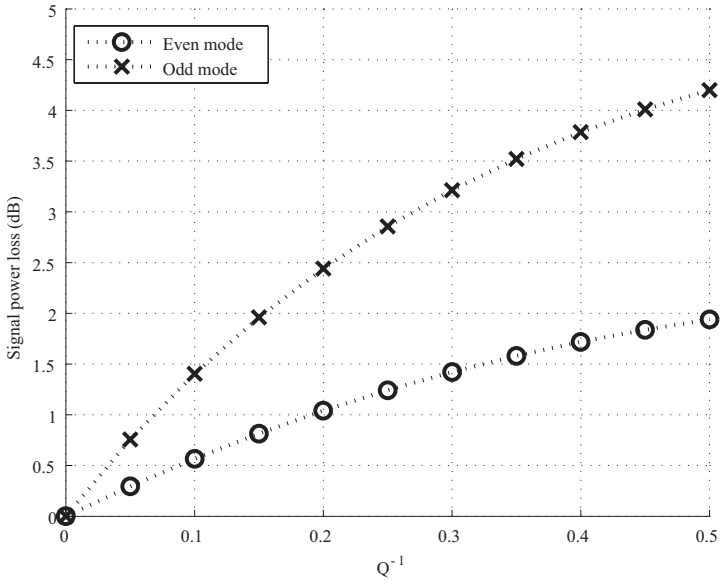


Figure 4.10 Signal degradation loss of even-odd mode.

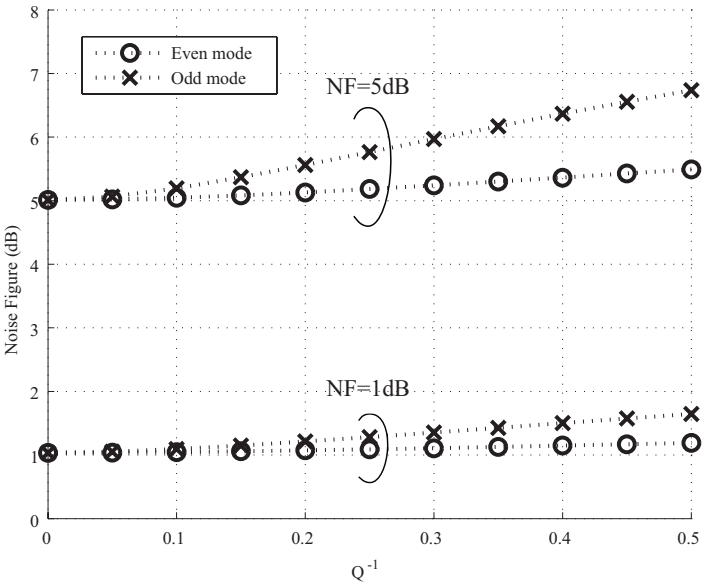
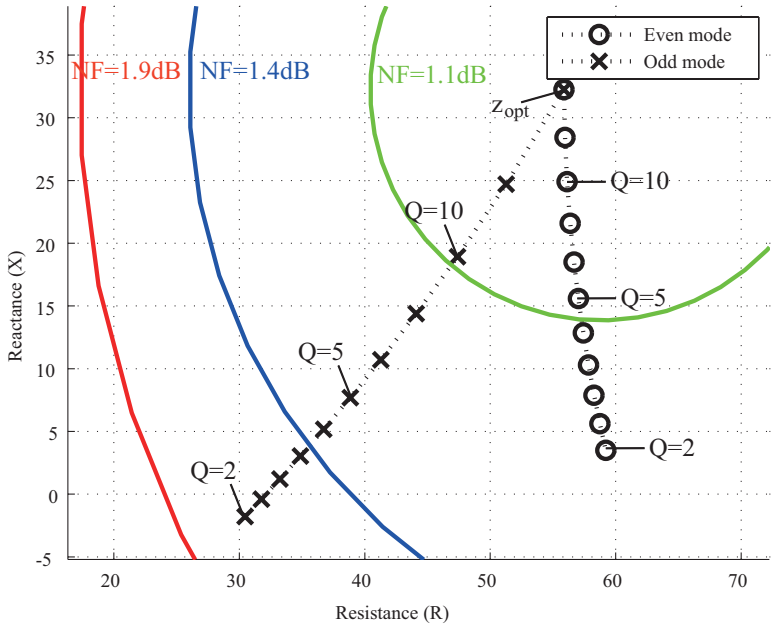
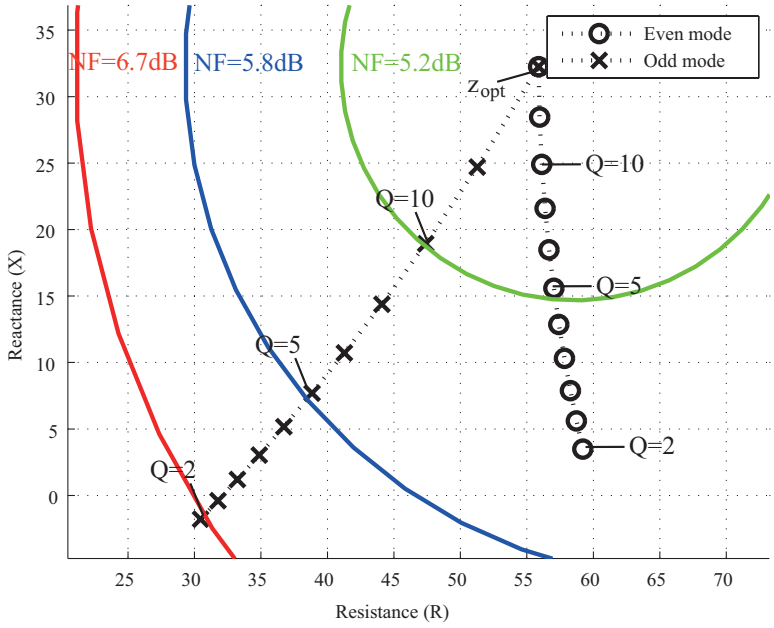


Figure 4.11 Original noise figure by lossy condition.

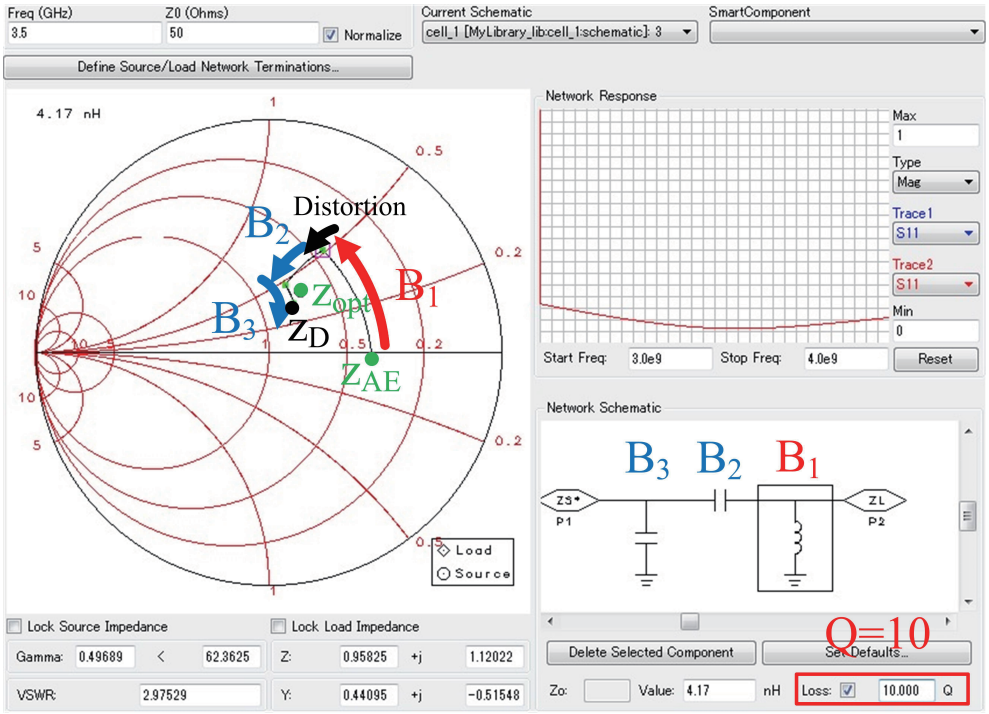


(a) NF=1dB

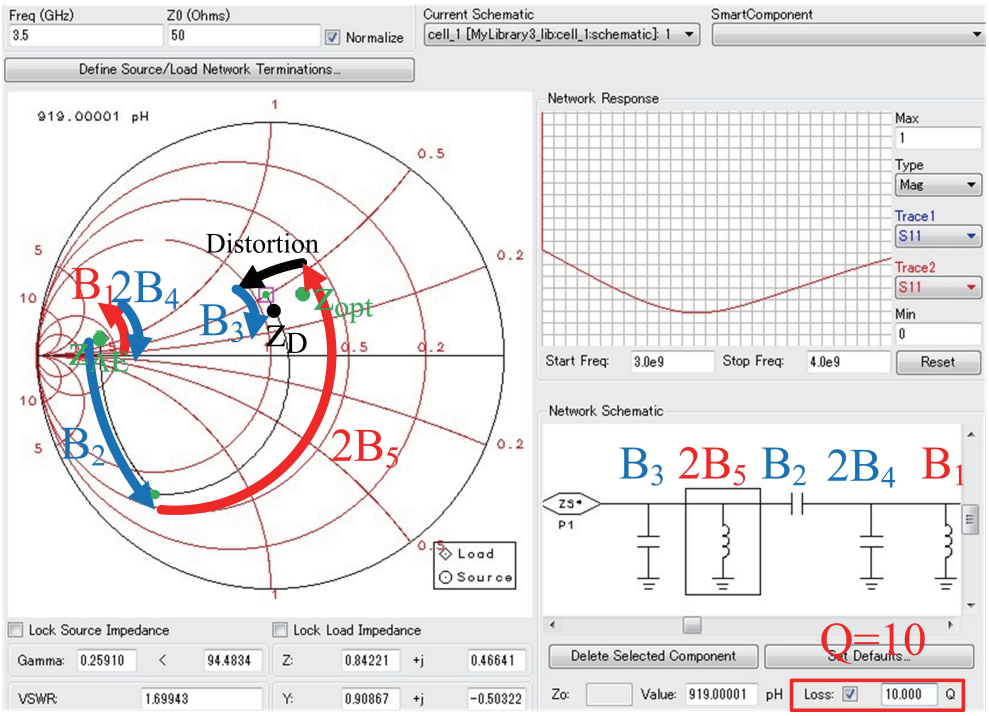


(b) NF=5dB

Figure 4.12 Noise figure circle of symmetrical matching in lossy condition.



(a) Even mode



(b) Odd mode

Figure 4.13 Smithchart of symmetrical matching on lossy condition ($Q = 10$).

4.6 Summary

Two multi-port matching structures for realization were introduced in this chapter. While conventional multi-port matching work is difficult to implement in practice due to the complexity of multi-layer realization between each ports, the proposed symmetrical matching can accomplish reduced complexity and high performance using practical L/C based circuit components. The various combinations satisfied with the optimal requirement were generated. Most optimum combination was selected by lossy condition of equivalent series resistance (ESR) for practical usage of the proposed matching method. Finally, physical analysis using NF circle and Smith chart was conducted to verify the effectiveness of the proposed models.

Chapter 5

Single Front-end Receiver with Parasitic Antenna Element

5.1 Introduction

In this chapter, we propose a novel architecture low noise design for compact MIMO receiver system. It is assumed that high spatial correlation and mutual coupling by compact antenna separation cause a problem of device miniaturization and high cost of RF circuit in compact MIMO system. The conventional MIMO architecture has technical problems with the device ' s miniaturization and high cost. In previous work, Weber investigated the matching circuit design for reducing the effect of spatial correlation between antennas [34, 35]. Nishimori evaluated channel capacity in MIMO antenna with decoupling and matching network [36]. Also, Wallace showed the capacity as optimal mutual information which matching network was constructed by Hermitian conjugation in free space [16]. On the other hand, in these days of software defined radio for realization, the flexible design methods all over analog region are required strongly. In other words, it needs vertical integrated designing and evaluation method from analog region to digital region. For example, conventional MIMO architecture required a transceiver per an antenna, which increases the cost of RF front-end, low spatial correlation environment among the antennas. However, Kalis proposed a MIMO transmitter for MIMO wireless communications using a single RF front end by mapping multiple symbol streams transmitted simultaneously on a set of basis radiation patterns [37]. Therefore, Single front-end architecture can be a suitable solution as an ideal architecture to alleviate this problem [38, 39].

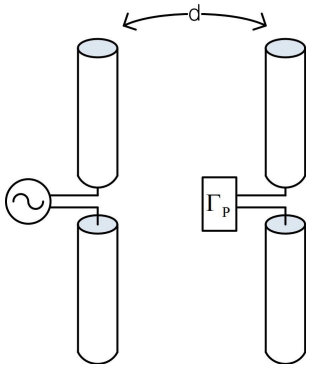
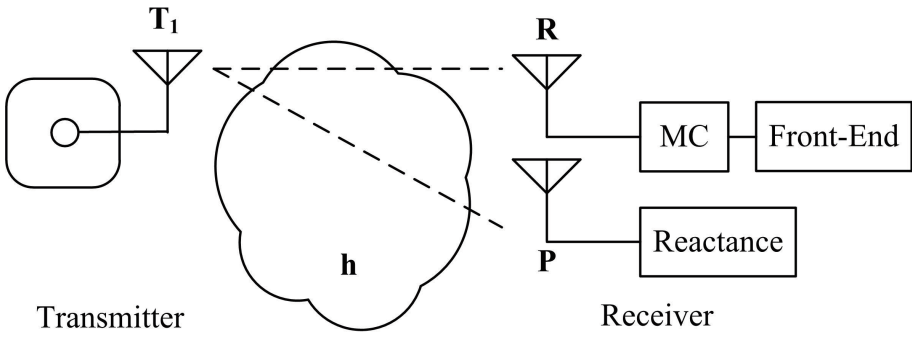


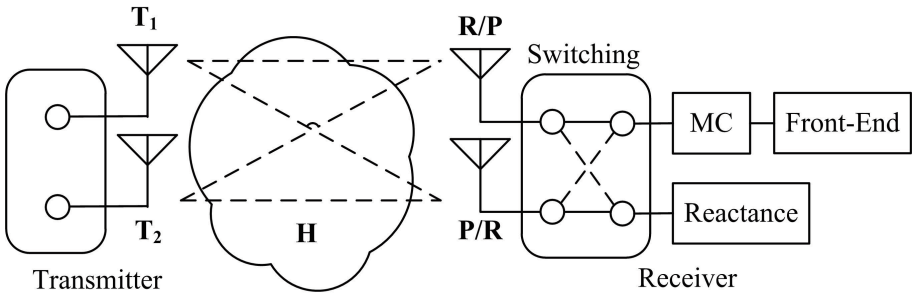
Figure 5.1 Parasitic antenna elements system.

One important characteristic facilitating the SF architecture is parasitic antenna element parasitic antenna elements(PAE) which are another characteristic of proposed system can improve transmission capacity by the mutual coupling actively using parasitic elements [40] in Fig. 5.1. Since PAE can change the directivity of antennas, independent spatial resources can be obtained instead of multiple receivers due to the orthogonality of directivity patterns. In other words, adaptive beamforming is realized by optimizing directivity corresponding to radio channel. In this chapter, PAE which changes the antenna directivity using terminated variable reactance enables adaptive directivity control on radiation environment and also adaptive antenna input impedance for optimizing the channel capacity.

Another important characteristic is required by antenna switching scheme for SF-MIMO structure. The received signals recovered by fast switching are fed to the receiver circuit for signal multiplexing [41]. Since the antenna switching operates at a frequency faster than the signal bandwidth, multiplexing signal can be recovered according to the sampling theory. Although the SNR performance deteriorates due to the switching, PAE can compensate for the switching penalty owing to analog beamforming gain. On the other hand, recent works have paid attention to the noise and the mutual coupling effect at the receiver [24]. The realistic noise model considered noise coupling in which the noise sources includes sky noise (external noise) and front-end noise (internal noise) [25,26]. The system with matching circuit examined on the impact of the channel capacity by signal mutual coupling. The realistic noise model also was employed for noise coupling with noise covariance matrix. In [16], they demonstrates that the matching for minimizing noise figure is superior to matching for maximizing power transfer.



(a) SIMO PAE system



(b) MIMO PAE system

Figure 5.2 Single front-end system with PAE.

In this chapter, we propose a low noise model for single front-end MIMO receiver system with PAE which includes arbitrary signal and noise coupling. We first introduce the single SF-SIMO PAE receive system with single Tx antenna and no switching mechanism in Fig. 5.2(a). Then, we expand SF-MIMO PAE receiver system by fast switching for multiplexing as shown in Fig. 5.2(b). Based on the equivalent circuit of proposed systems, the matching circuit to minimize noise figure is also introduced. After deriving optimal PAE value for maximizing channel capacity, the matching circuit is employed for minimum noise figure. Finally, numerical analysis is conducted to verify the proposed systems.

5.2 Channel model for SF-SIMO with PAE

In this section, the channel model for the proposed SF-SIMO architecture is discussed. At first, we express revised channel representation using PAE by the adaptive beam-forming effect. The PAE connected to a variable reactance affects its antenna directivity which is controlled by changing the reactance value. The re-radiation characteristic of the PAE influences the

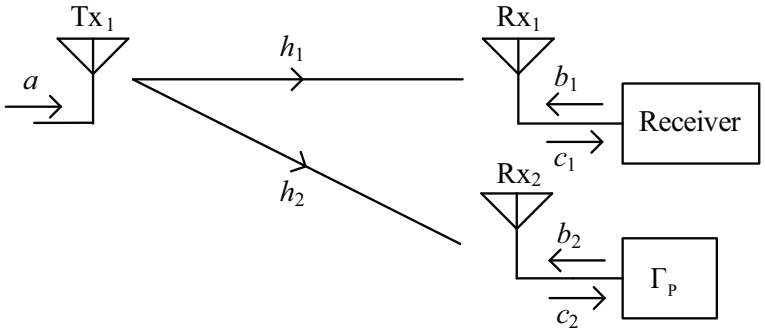


Figure 5.3 Channel representation for SIMO PAE system.

RF front-end receiver.

5.2.1 Channel representation for SIMO PAE system

We suppose a single front-end receiver with PAE considering propagation channel as Fig. 5.2. Assume a transmitter, a receiver and PAE Γ_{P} with propagation channel $\mathbf{h} = [h_1 \ h_2]^T$. At the receiver side, the mutual coupling of the antenna network can be generally expressed using a 2×2 scattering matrix $\mathbf{S}_{\mathrm{A}}$ as follows

$$\mathbf{S}_{\mathrm{A}} = \begin{bmatrix} S_{\mathrm{A11}} & S_{\mathrm{A12}} \\ S_{\mathrm{A12}} & S_{\mathrm{A22}} \end{bmatrix}, \tag{5.1}$$

where the vectors $\mathbf{b} = [b_1 \ b_2]^T \in \mathbb{C}^2$ and $\mathbf{c} = [c_1 \ c_2]^T$ denote the complex envelopes of the inward and the outward propagating waves, respectively, satisfied with $\mathbf{c} = \mathbf{S}_{\mathrm{A}}\mathbf{b}$. Also note that the reflection condition of unfed elements is $b_2 = \Gamma_{\mathrm{P}} c_2$. On this condition, the propagation channel with re-radiation from unfed element as follows

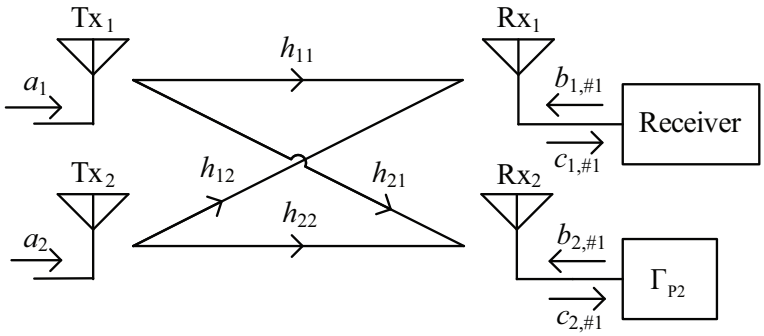
$$\tilde{h} = h_1 + D h_2, \tag{5.2}$$

where $D = S_{\mathrm{A21}}(\Gamma_{\mathrm{P}}^{-1} - S_{\mathrm{A11}})^{-1}$.

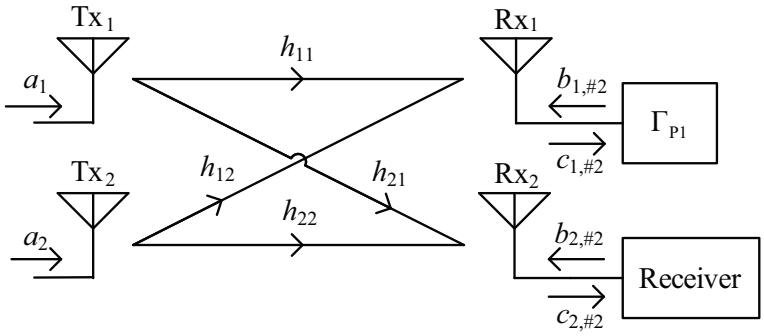
5.2.2 SIMO PAE capacity with fading

We consider a frequency-flat and Rayleigh fading SISO system with PAE. The received signal $\tilde{r}$ with external noise $\tilde{n}$ is given as

$$\tilde{r} = \tilde{h}a + \tilde{n}, \tag{5.3}$$



(a) Switched antenna port 1



(b) Switched antenna port 2

Figure 5.4 Channel model representation for SF-MIMO.

where $a \in \mathbb{C}$ is a transmitted signal and $\tilde{h} \in \mathbb{C}$ is a revised random complex channel gain. Also $\tilde{h}$ is complex random variable and the noise n is zero mean complex gaussian noise with variance σ^2. The ergodic channel capacity of SIMO system with PAE is given by

$$C_{\mathrm{SIMO}} = \mathrm{E}\left\{\log_2\left(1 + \frac{|\tilde{h}|^2 P_{\mathrm{T}} r_{\mathrm{T}}}{\sigma^2}|h_{\mathrm{w}}|^2\right)\right\}, \tag{5.4}$$

where $h_{\mathrm{w}} \sim \mathcal{CN}(0,1)$ and $\tilde{n} \sim \mathcal{CN}(0,\sigma^2)$.

5.3 Channel model for SF-MIMO with PAE

In this section, we present a channel model of SF-MIMO PAE system as a expanded form by SF-SIMO PAE system. The switching mechanism for spatial multiplexing is presented. In this mechanism, the single front-end is alternatively connected to one of the two antennas, and the other antenna is attached to the variable reactance for improving the SNR.

5.3.1 Channel Representation with MIMO PAE system

We assume a 2×2 transmit and receive antennas as shown in Fig. 5.4(a) and 5.4(b). In these figures, Γ_{P1} and Γ_{P2} at the receiver side represent the reflection coefficients by the PAE in the unfed antenna at each switching period, i.e. switched antenna port 1 and 2, respectively. We further represent the general propagation channel matrix $\mathbf{H}$ defined in subchapter 3.2.1 as follows,

$$\mathbf{H} = \begin{bmatrix} h_{11} & h_{12} \\ h_{21} & h_{22} \end{bmatrix} = \begin{bmatrix} \mathbf{h}_1 & \mathbf{h}_2 \end{bmatrix}, \tag{5.5}$$

where $\mathbf{h}_i$ which is a column vector of i.i.d zero mean. Using the reflection coefficients $\Gamma_{\mathrm{P1}}, \Gamma_{\mathrm{P2}}$ and the S-parameters from the scattering matrix $\mathbf{S}_{\mathrm{A}}$, we can express the received signal waves $c_{1,\sharp 1}$ and $c_{2,\sharp 1}$ at the switching port $\sharp 1$ in Fig. 5.4(a) as follows,

$$c_{1,\sharp 1} = \left(h_{11} + \frac{S_{\mathrm{A12}}}{\Gamma_{\mathrm{P2}}^{-1} - S_{\mathrm{A22}}} h_{21} \right) a_1 + \left(h_{12} + \frac{S_{\mathrm{A12}}}{\Gamma_{\mathrm{P2}}^{-1} - S_{\mathrm{A22}}} h_{22} \right) a_2, \tag{5.6}$$

$$c_{2,\sharp 1} = \left(h_{21} + \frac{S_{\mathrm{A22}}}{\Gamma_{\mathrm{P2}}^{-1} - S_{\mathrm{A22}}} h_{21} \right) a_1 + \left(h_{22} + \frac{S_{\mathrm{A22}}}{\Gamma_{\mathrm{P2}}^{-1} - S_{\mathrm{A22}}} h_{22} \right) a_2. \tag{5.7}$$

The reflection status of the unfed element satisfies $b_{2,\sharp 1} = \Gamma_{\mathrm{P2}} c_{2,\sharp 1}$ as stated by [42]. Similarly at the other switching period, in Fig. 5.4(b), the received signal waves $c_{1,\sharp 2}$ and $c_{2,\sharp 2}$ at the switching port $\sharp 2$ are described as,

$$c_{1,\sharp 2} = \left(h_{11} + \frac{S_{\mathrm{A11}}}{\Gamma_{\mathrm{P1}}^{-1} - S_{\mathrm{A11}}} h_{11} \right) a_1 + \left(h_{12} + \frac{S_{\mathrm{A11}}}{\Gamma_{\mathrm{P1}}^{-1} - S_{\mathrm{A11}}} h_{12} \right) a_2, \tag{5.8}$$

$$c_{2,\sharp 2} = \left(h_{21} + \frac{S_{\mathrm{A21}}}{\Gamma_{\mathrm{P1}}^{-1} - S_{\mathrm{A11}}} h_{11} \right) a_1 + \left(h_{22} + \frac{S_{\mathrm{A21}}}{\Gamma_{\mathrm{P1}}^{-1} - S_{\mathrm{A11}}} h_{12} \right) a_2, \tag{5.9}$$

where the re-radiation characteristic of the unfed opposite antenna satisfies $b_{1,\sharp 2} = \Gamma_{\mathrm{P1}} c_{1,\sharp 2}$.

5.3.2 Antenna switching for multiplexing

Single front-end MIMO receiver structure by fast switching of the antenna, where the period is within one symbol, is fed to the receiver for signal multiplexing. The antenna switching frequency operates faster than the signal bandwidth resources by using time-space resources. The signal can be recovered by sampling theory, even though the switched SNR deteriorates. As shown in Fig. 5.5, we now consider a two-antenna receiver impinged by a band pass filter

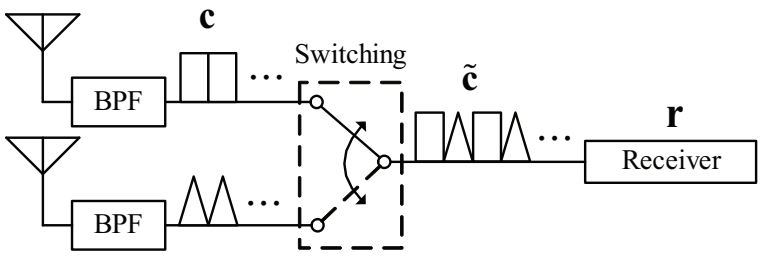


Figure 5.5 Switching mechanism for SF-MIMO.

(BPF) which is needed for anti-aliasing caused by switching operation. The switched SNR through the BPF whose bandwidth equals B deteriorates by 3dB [39].

$$\frac{\sigma_{\mathrm{S}}}{\sigma_{\mathrm{N}}} = \frac{\tilde{\gamma}}{2}, \tag{5.10}$$

where σ_{S} and σ_{N} are power spectrum density (PSD) of signal and noise, respectively. And $\tilde{\gamma}$ denotes the average branch SNR before switching Assuming symmetrical scattering parameters at the receiver side (S_{A11}=S_{A22}, S_{A12}=S_{A21}) and identical reflection coefficients (Γ_{P}=Γ_{P1}=Γ_{P2}) for easy discussion at each switching port, we derive the revised channel expresssion for switching MIMO system

$$\tilde{\mathbf{H}} = \frac{1}{\sqrt{2}}\left[\tilde{\mathbf{h}}_1 \;\; \tilde{\mathbf{h}}_2\right] = \frac{1}{\sqrt{2}}\begin{bmatrix} 1 & D \\ D & 1 \end{bmatrix}\left[\mathbf{h}_1 \;\; \mathbf{h}_2\right], \tag{5.11}$$

where $D = S_{\mathrm{A12}}/(\Gamma_{\mathrm{P}}^{-1} - S_{\mathrm{A11}})$ with reciprocal S-parameter used in Eq. (5.2).

5.3.3 SF-MIMO PAE capacity with Fading

We consider a frequency-flat Rayleigh fading model with two branch diversity system in which both fading and noise are spatially correlated as follows,

$$\tilde{\mathbf{r}} = \tilde{\mathbf{c}} + \tilde{\mathbf{n}} = \tilde{\mathbf{H}}\mathbf{a} + \tilde{\mathbf{n}}, \tag{5.12}$$

where $\tilde{\mathbf{r}}, \tilde{\mathbf{n}} \in \mathbb{C}^2$ are separately the final received signal and noise observed at the receiver circuit after switching. And $\tilde{\mathbf{c}} = [c_{1,\sharp 1} \; c_{2,\sharp 2}]^T$, which is the combined signal of $c_{1,\sharp 1}$ and $c_{2,\sharp 2}$ from the fed antenna at all consecutive switching periods, denotes the modified outward signals regarding with the effect of switching and PAE components. Similar with Eq. (3.15),

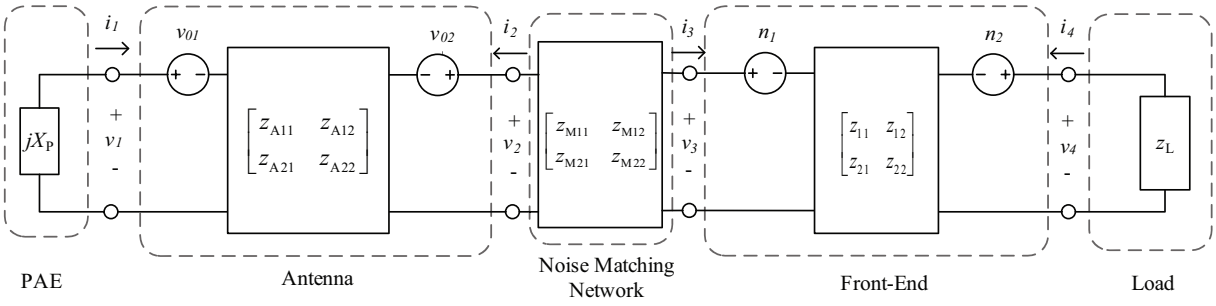


Figure 5.6 Circuit model of a single front-end receiver with PAE.

the general ergodic capacity is given by

$$C = \underset{\mathbf{H}_\mathrm{w}}{\mathrm{E}} \left[\log_2 \det \left(\mathbf{I}_2 + \mathbf{H}_\mathrm{w}^\dagger \tilde{\mathbf{\Sigma}} \mathbf{H}_\mathrm{w} \right) \right], \tag{5.13}$$

where $\tilde{\mathbf{\Sigma}} \in \mathbb{C}^{2\times 2}$ is the SNR matrix different to original formula,

$$\tilde{\mathbf{\Sigma}} = \frac{P_\mathrm{T} r_\mathrm{T}}{2} \mathbf{\Sigma}_{\tilde{\mathrm{h}}}^{1/2} \mathbf{\Sigma}_{\tilde{\mathrm{n}}}^{-1} \mathbf{\Sigma}_{\tilde{\mathrm{h}}}^{1/2}, \tag{5.14}$$

where $\mathbf{\Sigma}_{\tilde{\mathbf{n}}} = \mathrm{E}[\tilde{\mathbf{n}}\tilde{\mathbf{n}}^\dagger]$ and $\mathbf{\Sigma}_{\tilde{\mathbf{h}}} = \mathrm{E}[\tilde{\mathbf{H}}\tilde{\mathbf{H}}^\dagger]$ mean the noise covariance matrix and the receive correlation matrix of the equivalent channel, respectively. The revised channel covariance matrix is defined from Eq. (5.11) as follows,

$$\mathbf{\Sigma}_{\tilde{\mathrm{h}}} = \frac{1}{2} \begin{bmatrix} 1 & D \\ D & 1 \end{bmatrix} \mathbf{\Sigma}_\mathrm{h} \begin{bmatrix} 1 & D \\ D & 1 \end{bmatrix}^\dagger, \tag{5.15}$$

where $\mathbf{\Sigma}_\mathbf{h} = \mathrm{E}[\mathbf{H}\mathbf{H}^\dagger]$ is the receive correlation matrix of the propagation channel observed at the receiver side as defined in Eq. (2.23). The correlation condition employed in this chapter is assumed as open-circuit termination at receiver side.

5.4 Circuit model

In this section, we demonstrate an equivalent circuit model for the single front-end receiver with PAE in Fig. 5.6 assuming symmetrical antenna characteristic as well as identical PAE for SF-MIMO system with the switching mechanism. The circuit model considers that the optimal matching circuit is designed imposing the two noise characteristics equivalent to SISO system.

5.4.1 Antenna model for single front-end receiver with PAE

Let $\mathbf{v}, \mathbf{i} \in \mathbb{C}^2$ denote the voltage and the current vectors into the array antenna terminals, respectively. To easy analysis, Eq. (5.1) is transformed from the scattering matrix representation to the impedance matrix form $\mathbf{Z}_{\mathrm{A}}$ [42]. A model with Thevenin equivalent network model is

$$\mathbf{v} = \mathbf{Z}_{\mathrm{A}}\mathbf{i} + \mathbf{v}_0, \tag{5.16}$$

where $\mathbf{Z}_{\mathrm{A}} = \mathbf{R}_{\mathrm{A}} + j\mathbf{X}_{\mathrm{A}}$ and $\mathbf{v}_0 = [v_{01}\ v_{02}]^T$ which is the open-circuit voltage in Fig. 5.6. We can represent two open-circuit voltage sources $v_0', \mathbf{v}_0'$ for SF-SIMO PAE and SF-MIMO PAE system, which take the same form of Eq. (5.2) and Eq. (5.12), respectively, as follows,

$$v_0' = \tilde{h}a + n_0', \quad \mathbf{v}_0' = \tilde{\mathbf{H}}\mathbf{a} + \mathbf{n}_0', \tag{5.17}$$

where $n_0' \sim \mathcal{CN}(0, \overline{|\mathrm{n}_0'|^2})$ and $\mathbf{n}_0' \sim \mathcal{CN}(0, \mathbf{\Sigma}_{\mathrm{n}_0'})$ are the sky noises modified by PAE without and with the switching process, respectively. By Nyquist's theorem [43], the variances of $n_0', \mathbf{n}_0'$ are derived from the revised antenna impedance Z_{A}' with PAE as,

$$\overline{|n_0'|^2} = 4k_{\mathrm{B}}T_0B\Re(Z_{\mathrm{A}}'), \quad \mathbf{\Sigma}_{\mathrm{n}_0'} = 4k_{\mathrm{B}}T_0B\Re[\mathbf{Z}_{\mathrm{A}}'], \tag{5.18}$$

where $\mathbf{Z}_{\mathrm{A}}' = Z_{\mathrm{A}}'\mathbf{I}_2$. The revised antenna impedance is a function of the PAE component X_{P} as follows,

$$Z_{\mathrm{A}}' = z_{\mathrm{A}22} - Az_{\mathrm{A}21}, \quad A = z_{\mathrm{A}12}/(z_{\mathrm{A}11} + jX_{\mathrm{P}}). \tag{5.19}$$

For SF-MIMO system using each switching period, we may consider that this system is equivalently converted to a single impedance case because the virtual two branch MIMO receiver equivalent circuit has isolated antenna impedance with identical diagonal components.

5.4.2 Parasitic antenna element (PAE)

Another important parameter for low noise receiver design is to control the PAE element defined by the variable reactance X_{P}. The PAE component affects to improve the transmission capacity by adjusting analog beamforming. The reflection coefficient Γ_{P} of PAE is converted to the variable reactance X_{P} [11] as

$$jX_{\mathrm{P}} = z_0\frac{1+\Gamma_{\mathrm{P}}}{1-\Gamma_{\mathrm{P}}}, \tag{5.20}$$

where z_0 is the characteristic impedance.

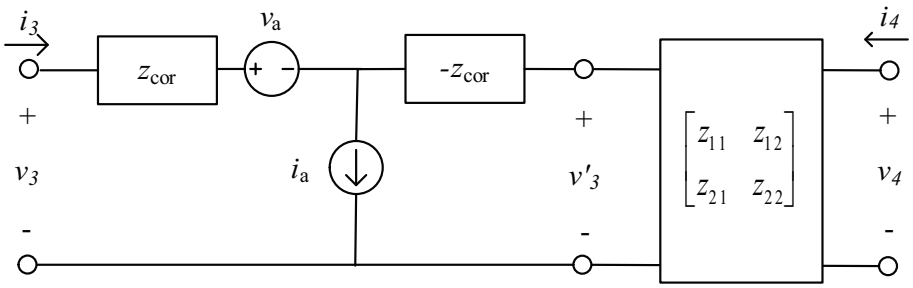


Figure 5.7 Rothe-Dahlke model of single front-end.

5.4.3 Noise matching circuit

A matching network for low noise receiver characteristic is employed between the antenna side and the single front-end side as shown in Fig. 5.6. Now consider a lossless (and therefore noise-free) matching network with impedance matrix

$$\begin{bmatrix} z_{\mathrm{M11}} & z_{\mathrm{M12}} \\ z_{\mathrm{M21}} & z_{\mathrm{M22}} \end{bmatrix} \tag{5.21}$$

The matching circuit is in turn connected to the single front-end. Ideally a matching circuit is formed with passive and reactive elements so it is noiseless, lossless, and reciprocal [44]. Extending Thevenin's theorem to the 2-port system, the modified antenna impedance taking into account the matching circuit can be represented by

$$Z'_{\mathrm{MA}} = -Mz_{\mathrm{M12}} + z_{\mathrm{M22}}, \quad M = z_{\mathrm{M21}}/(z_{\mathrm{M11}} + Z'_{\mathrm{A}}). \tag{5.22}$$

5.4.4 Front-end

We assume a specific model that an identical front-end characteristic retains during any switching period 1 and 2. Denote the voltage $v_4 \in \mathbb{C}$ and the current $i_4 \in \mathbb{C}$ at the output terminal of the single front-end, respectively. The output voltage relating all voltages to the open-circuited antenna terminals in Fig. 5.6 is given by

$$v_4 = XY(-Av_{01} + v_{02} - n_1 + X^{-1}n_2), \tag{5.23}$$

where $X = z_{21}/(Z'_{\mathrm{MA}} + z_{11})$, $Y = z_{\mathrm{L}}/(z_{22} + z_{\mathrm{L}}) - Xz_{12}$. The term XY multiplied to both the signal and noise components of the output voltage does not affect the channel capacity.

Furthermore, we apply for the well-known Rothe-Dahlke model [45] shown in Fig. 5.7 for analyzing as more practical model with internal noise source concern at the front-end. According to the applicable noise model, any linear noise two-port network can be represented by a simple noise network cascaded with a noise-free network instead of Thevenin equivalent model. The noise voltage source and noise current source at the input port, denoted by v_{a} and i_{a}, are related to the other parameters i.e. the equivalent noise resistance r_{a} and the equivalent noise conductance g_{a} with independence mutually as

$$r_{\mathrm{a}} = \frac{\mathrm{E}[|\mathrm{v_a}|^2]}{4k_{\mathrm{B}}T_0B}, \quad g_{\mathrm{a}} = \frac{\mathrm{E}[|\mathrm{i_a}|^2]}{4k_{\mathrm{B}}T_0B}, \tag{5.24}$$

where noise correlation between the input and the output port is expressed by the correlation impedance $z_{\mathrm{cor}} = r_{\mathrm{cor}} + jx_{\mathrm{cor}}$.

5.5 Optimal noise matching

5.5.1 Noise factor minimization

The total noise for both cases of SIMO PAE and MIMO PAE are parameterized by two uncorrelated noise sources with the external noise source of the antenna and the internal noise source of the front-end. Under the separated noise components of Eq. (5.23), the total noise components from Eq. (5.17) are obtained by

$$n' = n'_0 - z', \quad \mathbf{n}' \triangleq \mathbf{n}'_0 - \mathbf{z}', \tag{5.25}$$

where $\mathbf{z}' = [z' \; z']^T$ and $z' = (v_{\mathrm{a}} + (Z'_{\mathrm{MA}} + z_{\mathrm{cor}})i_{\mathrm{a}})/M$ are the internal noise from the single front-end for SIMO PAE and MIMO PAE, respectively. An important metric for evaluating a two-port network is the noise factor F_{P} for SF receiver with PAE as

$$F_{\mathrm{P}} = 1 + \frac{r_{\mathrm{a}} + |Z'_{\mathrm{MA}} + z_{\mathrm{cor}}|^2 g_{\mathrm{a}}}{\Re(Z'_{\mathrm{A}})|M|^2}. \tag{5.26}$$

The noise factor depends on the ratio of the input and output SNR of the front-end given in dB as it means the SNR drop. the SNR for the SF-MIMO system is

$$SNR = \frac{P_{\mathrm{h}}}{4k_{\mathrm{B}}T_0B\Re(Z'_{\mathrm{A}})F_{\mathrm{P}}}. \tag{5.27}$$

The noise factor for low noise design is smaller, as SNR output is larger. The minimized noise factor is obtained when the revised antenna source taking into account the matching circuit

Z'_{MA} is equal to z_{opt}. So, the minimum noise factor F_{min} and the optimum impedance z_{opt} are referred in [45], as follows

$$F_{\mathrm{min}} = 1 + 2\left\{g_{\mathrm{a}} r_{\mathrm{cor}} + \sqrt{g_{\mathrm{a}} r_{\mathrm{a}} + (g_{\mathrm{a}} r_{\mathrm{cor}})^2}\right\}, \tag{5.28}$$

$$z_{\mathrm{opt}} = \sqrt{\frac{r_{\mathrm{a}}}{g_{\mathrm{a}}} + r_{\mathrm{cor}}^2} - j x_{\mathrm{cor}}. \tag{5.29}$$

5.5.2 Capacity formula and optimum PAE

The ergodic capacity formulas of SISO, SIMO, MIMO, SIMO PAE system not having switching mechanism and MIMO PAE system with switching part are addressed for comparison of system performance. So, the normalized SNR can be employed as the equivalent SNR γ of a SISO channel defined in Eq. (3.49). The ergodic channel capacity using single transmitter case is given by [46] as

$$C_{\mathrm{SISO}} = \mathrm{E}\left\{\log_2\left(1 + \frac{\gamma}{F_{\mathrm{min}}}|h_{\mathrm{w}}|^2\right)\right\}, \tag{5.30}$$

$$C_{\mathrm{SIMO}} = \mathrm{E}\left\{\log_2\left(1 + \frac{\gamma}{F_{\mathrm{min}}}\mathbf{h}_{\mathrm{w}}^{\dagger}\boldsymbol{\Sigma}_{\mathrm{h}}^{1/2}\Re[\tilde{\mathbf{Z}}_{\mathrm{A}}^{-1}]\boldsymbol{\Sigma}_{\mathrm{h}}^{1/2}\mathbf{h}_{\mathrm{w}}\right)\right\}, \tag{5.31}$$

$$C_{\mathrm{SIMO-PAE}} = \mathrm{E}\left\{\log_2(1 + \frac{\gamma}{F_{\mathrm{min}}} U_{\mathrm{P}}|h_{\mathrm{w}}|^2)\right\}, \quad U_{\mathrm{P}} = \frac{1 + |D|^2 + 2\sqrt{\rho}\Re(D)}{\Re(Z'_{\mathrm{A}})/r_{\mathrm{A}}}, \tag{5.32}$$

where $h_{\mathrm{w}} \in \mathbb{C}$, $\mathbf{h}_{\mathrm{w}} \in \mathbb{C}^2$ are a complex channel variable and a complex channel column vector with i.i.d. normal complex elements, respectively. And $\Re[\tilde{\mathbf{Z}}_{\mathrm{A}}]$ is a normalized antenna resistance matrix with SISO antenna resistance r_{A}. The transfer function of the SIMO PAE system behaves like a random variable h_{w} multiplied by a deterministic value U_{P} which is designed to minimize the front-end noise figure for maximizing the equivalent SNR. So, we may simply conclude that the optimum value $X_{\mathrm{P-SIMO}}$ of the PAE component is decided for maximizing the ergodic capacity of SIMO PAE system.

$$X_{\mathrm{P-SIMO}}^{\mathrm{opt}} = \arg\max_{X_{\mathrm{P}}}(U_{\mathrm{P}}), \tag{5.33}$$

where U_{P} is a designable function of $\Gamma_{\mathrm{P-SIMO}}$ which converts to $X_{\mathrm{P-SIMO}}$ from Eq. (5.20).

Similarly, the ergodic channel capacity for two transmitter can be derived as,

$$C_{\mathrm{MIMO}} = \mathrm{E}\left[\log_2 \det\left(\mathbf{I}_2 + \frac{\gamma}{2F_{\mathrm{min}}}\mathbf{H}_{\mathrm{w}}^{\dagger}\boldsymbol{\Sigma}_{\mathrm{h}}^{1/2}\Re[\tilde{\mathbf{Z}}_{\mathrm{A}}^{-1}]\boldsymbol{\Sigma}_{\mathrm{h}}^{1/2}\mathbf{H}_{\mathrm{w}}\right)\right], \tag{5.34}$$

$$C_{\mathrm{MIMO-PAE}} = \mathrm{E}\left[\log_2 \det\left(\mathbf{I}_2 + \frac{\gamma}{2F_{\min}}\mathbf{H}_{\mathrm{w}}^{\dagger}\boldsymbol{\Sigma}_{\tilde{\mathrm{h}}}^{1/2}\Re[\tilde{\mathbf{Z}}_{\mathrm{A}}'^{-1}]\boldsymbol{\Sigma}_{\tilde{\mathrm{h}}}^{1/2}\mathbf{H}_{\mathrm{w}}\right)\right], \tag{5.35}$$

where $\tilde{\mathbf{Z}}_{\mathrm{A}}'$ is a revised antenna resistance matrix normalized by r_{A}. Therefore, we may conclude that the reactance $X_{\mathrm{P-MIMO}}$ of PAE affects both the resistance matrix $\Re[\mathbf{Z}_{\mathrm{A}}']$ and the reflection coefficient Γ_{P} of $\boldsymbol{\Sigma}_{\tilde{\mathrm{h}}}$, and it is clear to play an important role in maximizing the ergodic capacity of the proposed system.

$$X_{\mathrm{P-MIMO}}^{\mathrm{opt}} = \arg\max_{X_{\mathrm{P}}}(C_{\mathrm{MIMO-PAE}}). \tag{5.36}$$

5.6 Numerical results

In previous section, the normalized ergodic channel capacity formulas for conventional and proposed systems are addressed only considering spatial correlation at the receiver side using Kronecker model [7]. In this section, we numerically evaluate these systems through some specific simulation conditions. Based on the conditions of two symmetrical receive antennas with identical dipoles by a variable antenna distance parameter, we perform scattering parameters of antenna characteristic. Under the antenna parameter depicted in Sec. 3.4, the identical antenna parameter of Ansoft HFSS is used in this section. On equivalent antenna parameters in Table 3.1 and Table 3.2 of section 3.4, simulations are conducted to verify the impact of PAE effect and the proposed matching circuit compared with other systems. Using the above channel model with realistic antenna parameters and front-end noise parameters in Table 3.3, we can compute the optimal reactance value $X_{\mathrm{P-SIMO}}^{\mathrm{opt}}$, $X_{\mathrm{P-MIMO}}^{\mathrm{opt}}$ to maximize ergodic MIMO capacity in Eq. (5.33) and (5.36), respectively.

Figure 5.8 indicates the phase with optimum PAE value $X_{\mathrm{P-SIMO}}^{\mathrm{opt}}$ for maximizing deterministic value U_{P} by Eq. (5.33) for SIMO PAE system. And figure 5.9 shows the phase of the reflection coefficient $\Gamma_{\mathrm{P-MIMO}}^{\mathrm{opt}}$ corresponding to the derived optimal $X_{\mathrm{P-MIMO}}^{\mathrm{opt}}$ from Eq. (5.36). According to these figures, the reflection phase (and thus $X_{\mathrm{P-MIMO}}$) does not fluctuate largely when the antenna separation has smaller antenna spacing, On the other hand, for a larger antenna separation, the reflection phase, which it indeed means $X_{\mathrm{P-MIMO}}$), varies significantly by equivalent SNR γ of Eq. (3.49) defined in Sec. 3.4.

Furthermore, we study the dependence of capacity through these optimal phases for variability of system performance. For two NF cases, figure 5.10(a) and 5.10(b) show capacity performance with different antenna distances ($\lambda_{\mathrm{w}}/16$, $\lambda_{\mathrm{w}}/8$, $\lambda_{\mathrm{w}}/4$, $\lambda_{\mathrm{w}}/2$) , in two cases i.e. a fixed value of reactance for each antenna separation which is optimized at equivalent SNR

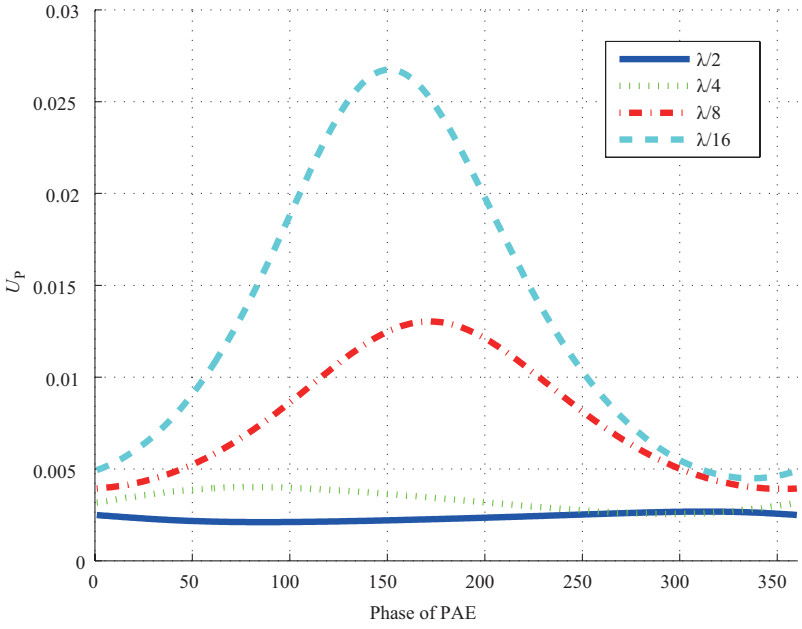


Figure 5.8 Optimum PAE value for SIMO PAE system.

γ = 15dB in Fig. 5.9, and optimal reactance values corresponding to each SNR as given in Fig. 5.9. It can be observed that the difference between these two cases is negligible. As a result, this simulation employs the fixed value of reactance optimized at equivalent SNR γ=15dB.

Using this sub-optimal fixed value of PAE, we compare the performance of SISO, SIMO, SF-SIMO PAE without switching and SF-MIMO PAE with switching under two noise figure scenarios introduced by Table 3.3 of previous chapter as shown in Fig. 5.11(a) and 5.11(b) for $\lambda_w/8$ and Fig. 5.12(a) and 5.12(b) for $\lambda_w/2$, respectively. Although the SIMO PAE system shows little worse performance than the SIMO case, the proposed MIMO PAE system performance almost reaches to the conventional MIMO system one at tight antenna spacing with strong mutual coupling. These results show that the proposed PAE system is tolerant against high spatial correlation condition while the conventional system deteriorates due to the mutual coupling effect between the two receive antennas.

Figure 5.13 shows the ergodic channel capacity performance with respect to different carrier frequencies. Both cases of fixed and optimal PAE value are considered. The figure shows

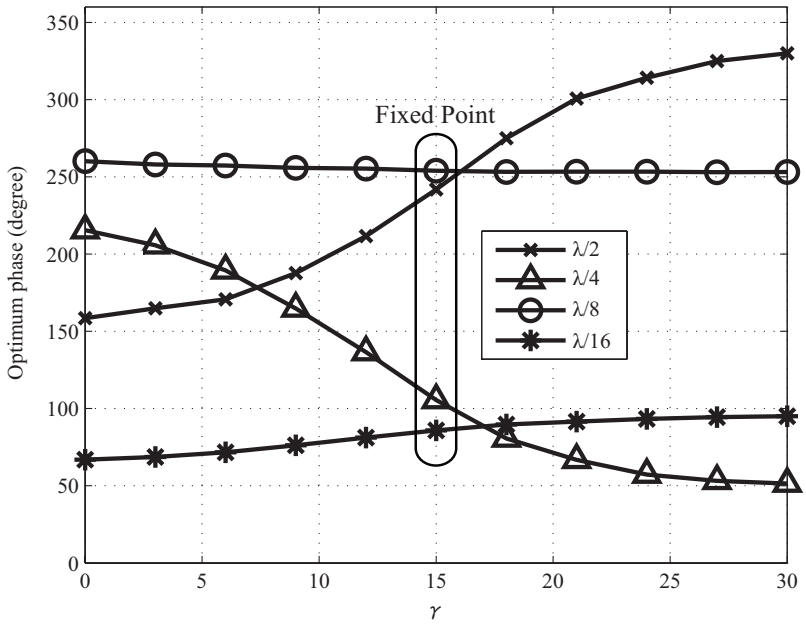
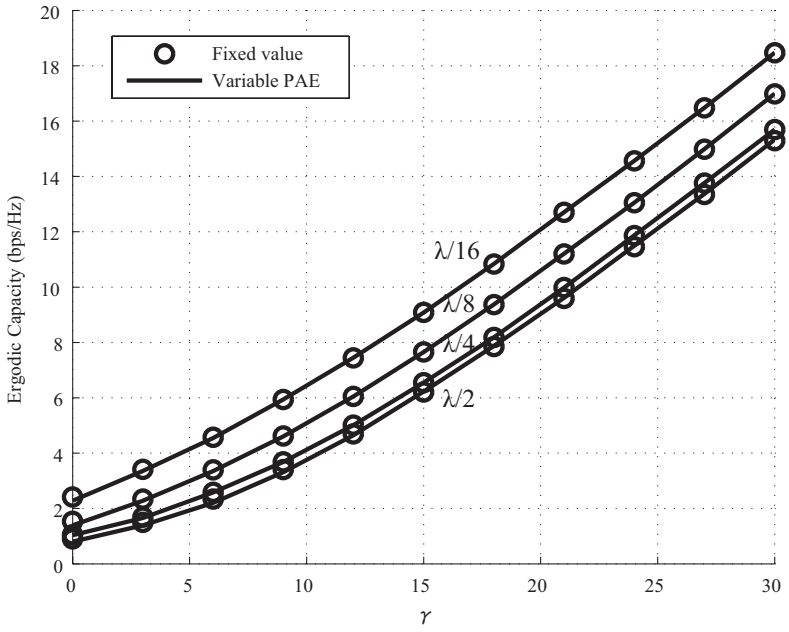
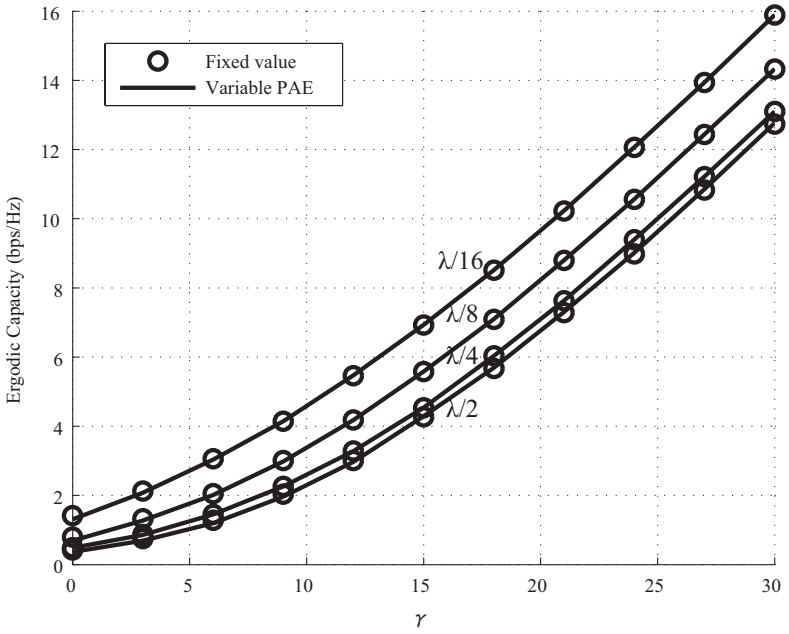


Figure 5.9 Optimum PAE value for MIMO PAE system.

that the SF-MIMO system with optimal PAE value realizes the flat channel capacity in a bandwidth range of ±3% of the central frequency. On the other hand, the SF-MIMO system with fixed value of PAE optimized at 3.5GHz only attains maximum capacity at 3.5GHz. Capacity performance gradually degrades at the other frequencies, which is similar to that of the conventional MIMO system. Although the SF-MIMO system with fixed PAE value is more practical in terms of realization, it does not have a narrowband characteristic in the relative bandwidth. We now compare the channel capacity of the SF-MIMO and the conventional MIMO system as a function of antenna distance at SNR=10dB in Fig. 5.14. It can be found that the ergodic capacity increases at closer antenna separation. Under both front-end noise figure scenarios, the SF-MIMO system shows better performance when the antenna distance is closer than $0.1\lambda_{\mathrm{w}}$. This gain is achieved owing to the optimal PAE value which can improve the mutual coupling effect and thus compensate for the switching penalty in terms of SNR loss.

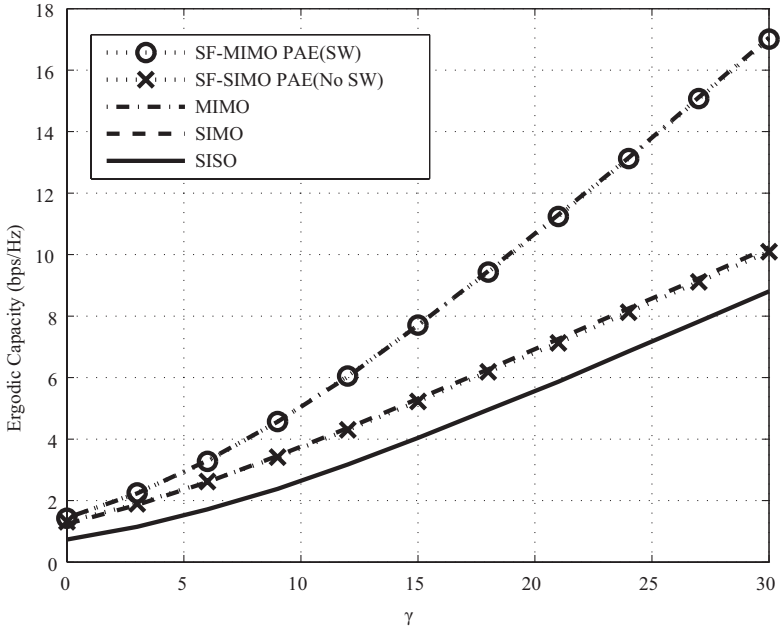


(a) NF=1dB

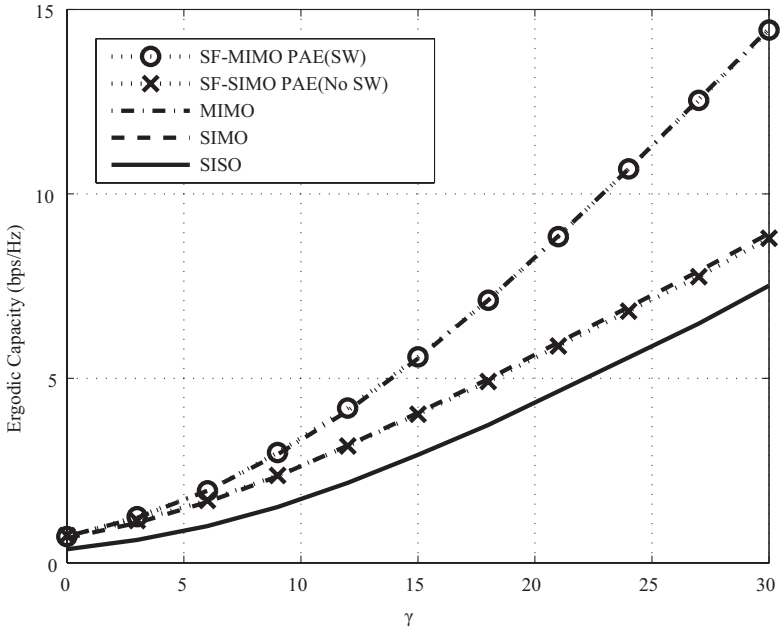


(b) NF=5dB

Figure 5.10 Capacity comparison for fixed and optimal PAE in SF-MIMO PAE.

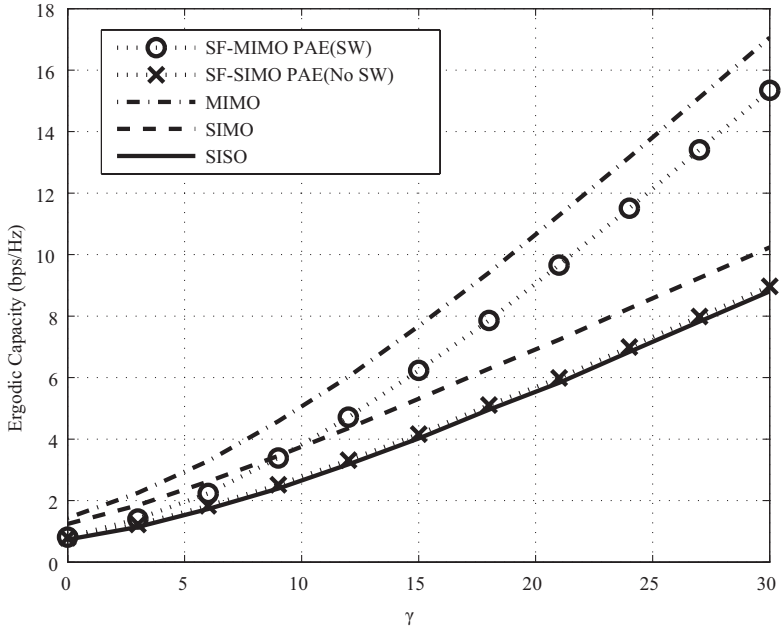


(a) NF=1dB

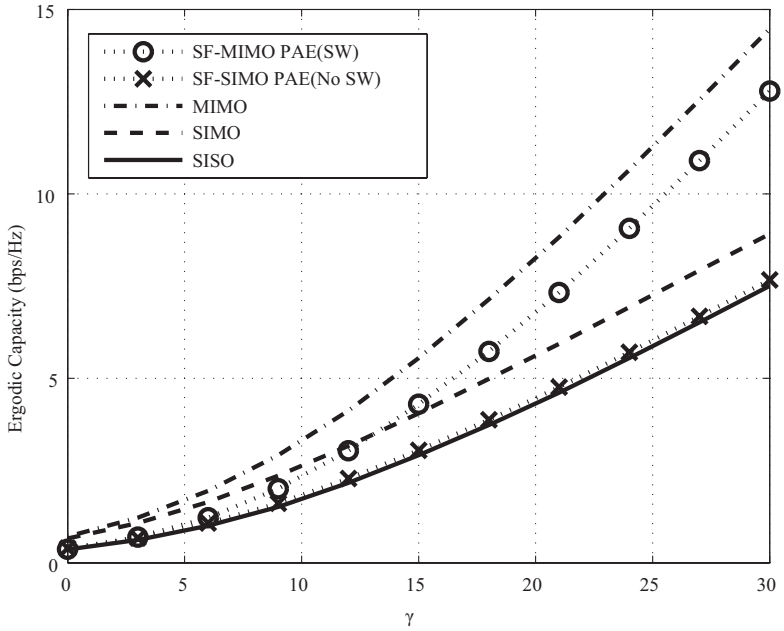


(b) NF=5dB

Figure 5.11 Capacity comparison with other systems (d=$\lambda_w/8$).



(a) NF=1dB



(b) NF=5dB

Figure 5.12 Capacity comparison with other systems (d=$\lambda_w/2$).

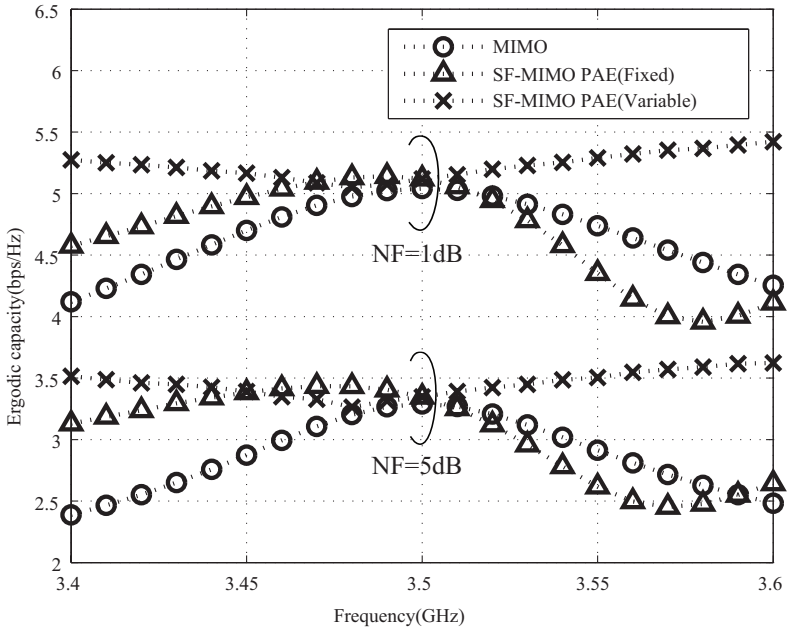


Figure 5.13 Frequency characteristic (d=λ_w/8, γ=10dB).

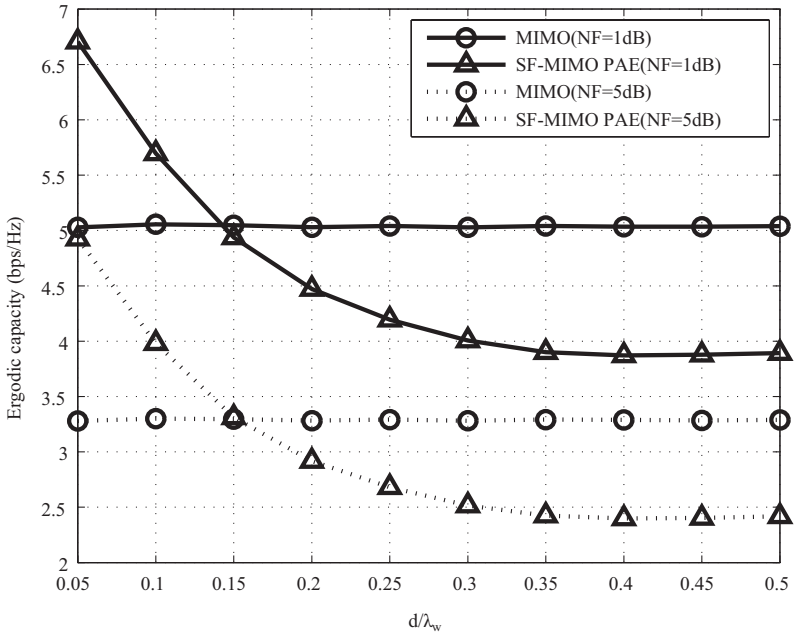


Figure 5.14 Capacity versus antenna distance (γ=10dB).

5.7 Summary

This chapter considered novel single front-end architecture with PAE for improving capacity and miniaturizing receiver in compact two receive antennas. SF-MIMO PAE system depending on switching mechanism can realize signal multiplexing by the orthogonality of directivity patterns. Different from conventional works, SF system using only one receiver can be compensated by PAE for the switching penalty due to analog beamforming. Finally, for the entire SF-MIMO system, we derived the optimal PAE value which affects both noise and reflection effect for maximizing capacity. Numerical results showed that the proposed architecture improves system performance due to tolerance against high spatial correlation as closer antenna spacing, whereas conventional MIMO system deteriorates by strong mutual coupling.

Chapter 6

Conclusion

This thesis has been concerned with design and performance evaluation of optimal low noise MIMO receiver systems. This chapter will draw together the results of previous chapters and highlight the main conclusions and limitations of this thesis. Some suggestions for possible future research extensions are also discussed.

6.1 Summary of the research

The conclusions of the whole thesis can be summarized as follows:

- Chapter 2 : We began our study the MIMO channel model which can deviate from the i.i.d. model due to insufficient antenna separation. The insufficient antenna separation induced mutual coupling and can significantly affect the performance of array antennas, especially at the receive end. As a result, the diversity advantage of the MIMO systems can be degraded by the correlation between the channel branches, which is called spatial fading correlation. The array performance metrics of signal correlation and MIMO capacity for a two element compact MIMO system were investigated. The simulation results showed that the signal correlation performances without mutual coupling and with mutual coupling were derived and compared. Moreover, we derived closed form approximation of the ergodic channel capacity for reduction of computation time.

- Chapter 3 : This chapter motivated the detailed study of noise modeling with external noise and internal noise from antennas and front-ends, respectively. We introduced an equivalent circuit model for compact multi-antenna receivers. The model allowed us to

examine how noise from the antennas and front-ends may become spatially correlated. The introduction of matching network between the receive antennas and front-ends can improve the performance of compact MIMO systems. In particular, optimal matching network enabled the receivers to be low noise design by matching between antenna impedance matrix and optimal impedance characterized by front-end. While the network achieves the minimum noise factor matrix, it may be difficult to realize in practice. A practical alternative matching methods such as symmetrical matching and identical matching were investigated on assumption of symmetrical channel characteristic, symmetrical array antennas and identical front-end. The symmetrical matching for capacity maximization was derived numerically with reduced complexity and high performance. Furthermore, the capacity performance of compact MIMO systems with various matching networks were simulated using multiport matching, symmetrical matching and identical self matching.

- Chapter 4 : The realistic matching scenarios discussed at Chapter 3 drew our attention in compact 2×2 MIMO system. To continue the investigation, we were able to consider possible multiport matching structures with coupled signal in realization issue. Specially, multiport circuits for symmetrical matching through π network design are studied in this chapter. Using this planar circuit with no crossing components of the coupled matching circuit, the symmetrical matching was developed to be the optimal for capacity maximization with simple design procedure and easy implementation. By applying lossy condition within matching circuit, we were able to prove the effect of the matching network based on L/C based circuit model. We also showed that the system performance with the lossy condition how the circuit was sensitive by the mismatch of the optimal impedance. The optimal symmetrical matching is a feasible solution to improve the performance and reduce RF complexity of MIMO matching system with compact terminals.

- Chapter 5 : For optimal low noise receiver design of compact MIMO system, we proposed new architecture receiver system with single front-end (FE) and parasitic antenna element (PAE) for enhancing spectral efficiency and miniaturizing the receiver in Chapter 5. Antenna switching scheme for SF-MIMO structure allowed signal multiplexing by fast switching according to the sampling theory. Although the SNR performance deteriorates due to the switching, PAE compensated for the switching penalty owing to

analog beamforming gain. After the optimal PAE value is derived to maximize channel capacity, we presented numerical analysis to verify the proposed system on certain conditions.

6.2 Future research topics

Several directions can be extended around the topics involved in this thesis. Some suggestions are listed below:

- Experiment of additional antenna model : The most important limitation of this thesis is that the most of theoretical analysis is confirmed by two identical array antenna system with same radiation pattern. More types of antennas besides dipoles with various radiation pattern can be considered as different species of antennas such as more modern antennas, e.g. *microstrip patch antenna*. Also, if the different sort of antennas with more than two elements are considered with different radiation patterns, more complicated theoretical analysis is inevitable.

- Various channel characteristic expansion : This thesis basically provides rayleigh fading channel assumptions of specific conditions with symmetrical channel characteristic. Since the channel characteristic is not designable, we sometimes should treat NLOS and partial LOS environments, e.g. *Rician fading channel*. Although the optimum design for antenna and front-end discussed in this thesis was proposed, design target may be changed as depending on the complicated channel characteristic. It needs to consider more advanced channel condition, e.g. milimeter-wave system which has been paid attention recently.

- Noise coupling of front-ends : An optimal matching for coupled front-ends should be modeled, while we applied uncoupled identical front-end. The coupled noise model with noise figure matrix which has off-diagonal components is difficult to proceed for optimal matching by multi-layer chain within circuit. It also needs to apply various front-end noise model as unknown and untreasured model such as noise correlation between two RF front-end chains, e.g. local oscillator, mixer, A/D and so on.

- Alternative matching suggestion : This thesis utilized simple L/C based lumped circuit model for optimal low noise matching. For integral circuit (IC) design, a matching circuit

with planar structure can be considered using multi-winding transformer. However, it is difficult due to the calculations of spectral fields in multilayer structures. Solving the limitation, new synthesis matching circuit will be investigated for calculating the electromagnetic fields in multilayer structures.

- Implementation of SF-MIMO PAE receiver architecture : The experimental evaluation for SF-MIMO PAE system can be carried out to confirm the capacity improvement of matching networks on compact MIMO system. Of course, fast RF switch mechanism for single front-end structure in compact MIMO system should guarantee the performance in loss, linearity and noise issues. Although the numerical examples verifying low noise matching by theoretical analysis were conducted in this thesis, the impact on the performance of real systems is an interesting next step of research.

Appendix I

SISO Channel Capacity

Consider instataneous channel capacity for SISO system.

$$C_{\text{ins}}^{\text{SISO}} = log(1 + \frac{P}{\Sigma_{\text{n}}}|h|^2) = log(1 + \gamma|h_{\text{w}}|^2), \tag{I.1}$$

where, P is the total transmit power, $h = \Sigma_{\text{h}}^{1/2} h_{\text{w}}$ with $\Sigma_{\text{h}} = \overline{|h|^2}$ and $\gamma = \frac{P}{4k_{\text{B}}T_0 B r_{\text{A}} F_{\min}}$. It need pdf to use average of the random variable $h_{\text{w}} \sim \mathcal{CN}(0, 1)$.

First, single pdf with real gaussian random variable x becomes

$$p(x) = \frac{1}{\sqrt{2\pi\sigma^2}} e^{\frac{-(x-m)^2}{2\sigma^2}}. \tag{I.2}$$

Next, complex gaussian pdf $z \triangleq |h_{\text{w}}|^2$ with independent real gaussian random variables $w = x + jy$. Joint probability at mean value $m = 0$ and variance $\sigma = 1/2$ is given

$$p(x, y) = p(x)p(y) = \frac{1}{\sqrt{\pi}} e^{-x^2} \frac{1}{\sqrt{\pi}} e^{-y^2} = \frac{1}{\pi} e^{-(x^2+y^2)}. \tag{I.3}$$

From xy-plane, redefine circle plane with radius r and phase θ as

$$p(r, \theta) = rp(r)p(\theta) = \frac{r}{\pi} e^{-r^2}. \tag{I.4}$$

The complex pdf by marginal probability is given by

$$p(r) = \int_0^{2\pi} p(r, \theta) = 2re^{-r^2}, \quad p(z)dz = p(r)dr, \quad \therefore\ p(z) = e^{-z}. \tag{I.5}$$

where, $z = |h_{\text{w}}|^2 = r^2$. Ergodic capacity can be defined from instantaneous formula as

$$\begin{aligned} C_{\text{E}}^{\text{SISO}} &= \text{E}(\text{C}_{\text{ins}}^{\text{SISO}}) = \text{E}\left\{\log(1 + \gamma|\text{h}_{\text{w}}|^2)\right\} \\ &= \int_0^{\infty} log(1 + \gamma z)p(z)dz = \int_0^{\infty} log(1 + \gamma z)e^{-z}dz \end{aligned} \tag{I.6}$$

Appendix II

Correlation Coefficient

The MIMO channel model can be defined by the i.i.d. model due to insufficient antenna separation. As a result, the diversity advantage of the MIMO systems can be degraded by the correlation between the channel branches called as spatial fading correlation. The correlation is attributed to two mechanisms such as the angular despreading of incoming wave or mutual coupling between antenna elements. Because of electromagnetic coupling the received signals by elements of the antenna array will no longer be independent, but become dependent on each other. Mutual coupling will influence the cross correlation between the received signals when antenna spacing is small.

Consider an incident wave impinging on an antenna array comprising two antennas space d apart from the direction angle θ in Fig. II.1. For simplicity, we assume identical omni-directional antenna elements with uniform amplitudes and signal phases difference ($l_{\mathrm{a}} = dsin\theta$). Related to the base difference, although the difference $l_{\mathrm{a}} = 0$, θ become 0, the phase difference become too far at $l_{\mathrm{a}} \geq \lambda_{\mathrm{w}}$. Note that λ_{w} means wavelength of the signal. On an assumption of the received signal r_1 at the first antenna, the received signal r_2 at the second antenna is given by

$$r_1 = \alpha, \quad r_2 = \alpha e^{-j\xi} \tag{II.1}$$

where $\xi = 2\pi dsin\theta/\lambda_{\mathrm{w}}$. From the definition of correlation coefficient [10], signal correlation can by expressed as

$$\rho = \frac{\mathrm{E}\left[r_1 r_2^*\right]}{\sqrt{\mathrm{E}\left[r_1 r_1^*\right]\mathrm{E}\left[r_2 r_2^*\right]}}. \tag{II.2}$$

For simple model with a random variable θ, *probability density function* (PDF) of θ become uniform with the range $[0, 2\pi]$. By the average expectation function, we can define the target

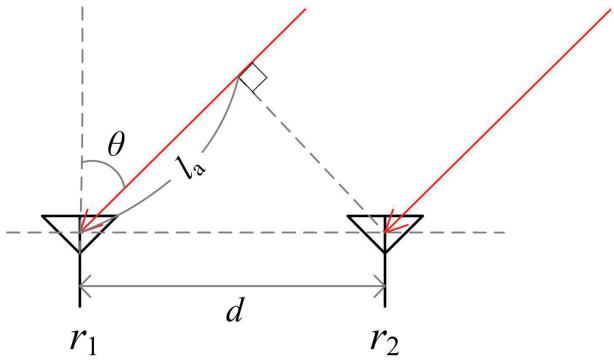


Figure II.1 Schematic of an incident wave impinging across antenna array.

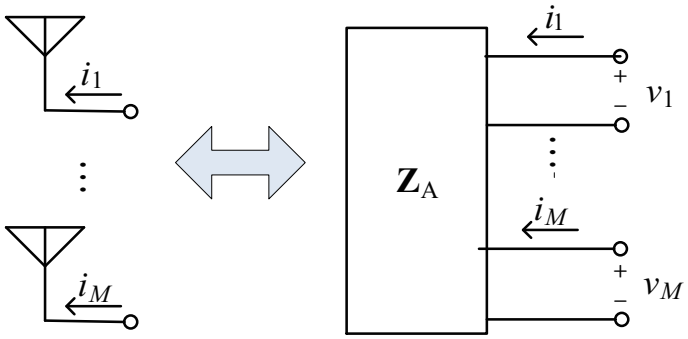


Figure II.2 Concept of mutual coupling of an array antenna.

function pdf as,

$$\rho_{\mathrm{c}} = \frac{1}{2\pi}\int_0^{2\pi} e^{j\xi}\mathrm{d}\theta = J_0\left(\frac{2\pi d}{\lambda_{\mathrm{w}}}\right) \tag{II.3}$$

where J_0 is the zeroth order *Bessel function* of the first kind. Finally, the correlation coefficient of the Clarke's model [47] becomes as a simple correlation model.

On the other hand, the mutual coupling is an important issue for the antenna property in realistic correlation model, which interacts with each other and change the currents from the isolated antennas, especially in compact array antenna [11]. Mutual coupling occurs when current flowing in one antenna induces a voltage across neighboring antenna terminals in Fig. II.2,

$$z_{\mathrm{A}ij} = \left.\frac{v_i}{i_j}\right|_{i_k=0,\forall k\neq j}, \tag{II.4}$$

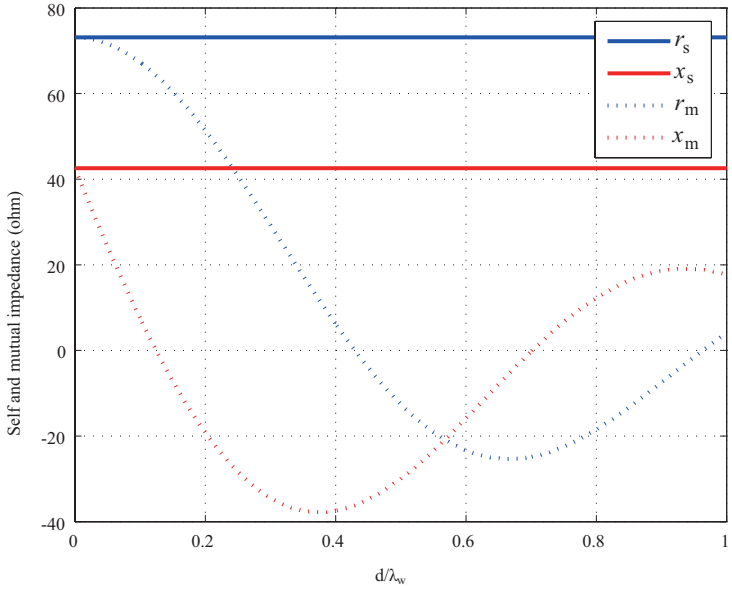


Figure II.3 Self and mutual impedance using induced EMF method.

where $z_{\mathrm{A}ii}$ is the input impedance seen looking into port i when all other ports are open-circuited, and $z_{\mathrm{A}ij}$ is the transfer impedance between ports i and j when all other ports are open-circuited. It modeled by viewing antenna array as an M-port network and defining the antenna impedance matrix $\mathbf{Z}_{\mathrm{A}}$. The antenna impedance matrix has a symmetric structure expressed by

$$\mathbf{Z}_{\mathrm{A}} = \begin{bmatrix} z_{\mathrm{A}11} & z_{\mathrm{A}12} & \cdots & z_{\mathrm{A}1j} \\ z_{\mathrm{A}21} & z_{\mathrm{A}22} & \cdots & z_{\mathrm{A}2j} \\ \vdots & \vdots & \ddots & \vdots \\ z_{\mathrm{A}i1} & z_{\mathrm{A}i2} & \cdots & z_{\mathrm{A}ij} \end{bmatrix} \tag{II.5}$$

Figure. II.3 shows self impedance $z_{\mathrm{s}} = r_{\mathrm{s}} + jx_{\mathrm{s}}$ and mutual impedance $z_{\mathrm{m}} = r_{\mathrm{m}} + jx_{\mathrm{m}}$ of two side-by-side $\lambda_{\mathrm{w}}/2$ dipoles using the *induced EMF method* [11].

For defining the correlation of the mutual coupling, we assume that two identical dipole antenna is identical with directivity D_1, D_2 and z_{L} in Fig. II.4. The antenna directivity function D' is given by

$$D'(\theta) = i_1 D_1(\theta) + i_2 D_2 = i_1 D_1(\theta) + i_2 D_1(\theta) e^{-j\xi}, \tag{II.6}$$

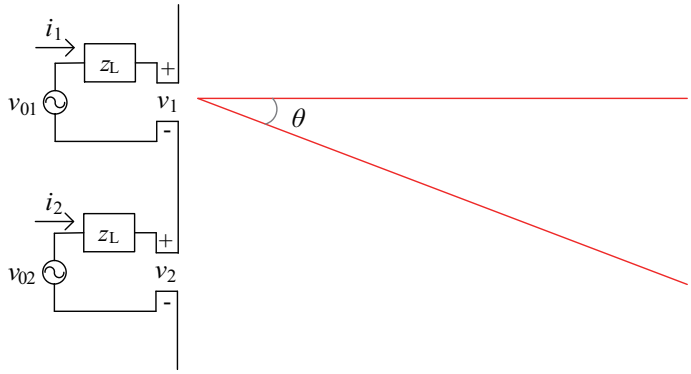


Figure II.4 Schematic of coupling paths between array antennas.

We then calculte the ratio determined by the impedance matrix and load impedance.

$$z_r = \frac{i_2}{i_1} = \frac{-z_m}{z_s + z_L}, \tag{II.7}$$

where $v_2 = z_m i_1 + z_s i_2 = -z_L i_2$. According to identical directivity $D(\theta)$, so the radiation pattern of antenna port 1,2 are expressed by

$$D_1'(\theta) = i_1 D(\theta)[1 - z_r e^{-j\xi}],\ D_2'(\theta) = i_2 D(\theta)[-z_r + e^{-j\xi}] \tag{II.8}$$

We take into account 2-D radiation pattern with uniform distribution. Using the target function pdf ρ_c from Eq. (II.3), the covariance functions of each directivity become

$$\mathrm{E}[\mathrm{D}_1'(\theta)\mathrm{D}_2'(\theta)^*] = i_1 i_2^* |\mathrm{E}[\mathrm{D}(\theta)]|^2 \left[-2\Re(z_r) + (1 + |z_r|^2)\rho_c\right], \tag{II.9}$$

$$|\mathrm{E}[\mathrm{D}_1'(\theta)]|^2 = |i_1|^2 |\mathrm{E}[\mathrm{D}(\theta)]|^2 \left[1 + |z_r|^2 - 2\Re(z_r)\rho_c\right], \tag{II.10}$$

$$|\mathrm{E}[\mathrm{D}_2'(\theta)]|^2 = |i_2|^2 |\mathrm{E}[\mathrm{D}(\theta)]|^2 \left[1 + |z_r|^2 - 2\Re(z_r)\rho_c\right], \tag{II.11}$$

Finally, we derive the correlation coefficient with mutual coupling, called as Yamada's model [48], as following

$$\rho_y^2 = \frac{|\mathrm{E}\left[\mathrm{D}_1'(\theta)\mathrm{D}_2'(\theta)^*\right]|^2}{|\mathrm{E}[\mathrm{D}_1'(\theta)]|^2 |\mathrm{E}[\mathrm{D}_2'(\theta)]|^2} = \left(\frac{\rho_c - \zeta}{1 - \zeta\rho_c}\right)^2, \tag{II.12}$$

where $\zeta = 2\Re(z_r)/(1 + |z_r|^2)$.

Similar with Yamada's correlation model, we can proceed the another approaching method using S-parameter representation by wave impedance depicted in Fig. 2.2 of Ch. 2.. If the total incident power is equal to reflected power on no power consumption system, $\mathbf{b}_L^\dagger \mathbf{b}_L = \mathbf{a}_L^\dagger \mathbf{a}_L$,

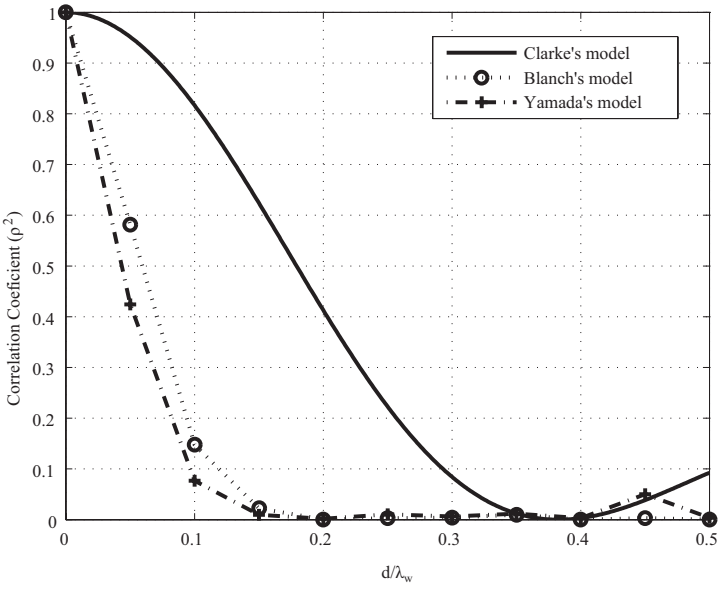


Figure II.5 Comparison of various correlation models.

then the scattering matrix satifies $\mathbf{S}_{\mathrm{L}}^{\dagger}\mathbf{S}_{\mathrm{L}} = \mathbf{I}_K$. For the correlation factor calculation, the receive antenna signals with no radiation impedance of antenna side become

$$\begin{bmatrix} b_1 \\ b_2 \end{bmatrix} = \begin{bmatrix} S_{13} & S_{14} & \cdots & S_{1K} \\ S_{23} & S_{24} & \cdots & S_{2K} \end{bmatrix} \mathbf{a}_{\mathrm{F}} \ , \tag{II.13}$$

where, the free-space incident wave vector $\mathbf{a}_{\mathrm{F}} = [a_3 \ a_4 \ \cdots \ a_K]^T$ on the assumption of random variable. The covariance elements of the receive antenna signals are defined as

$$\mathrm{E}[\mathrm{b}_1\mathrm{b}_2^*] = S_{13}S_{23}^* + S_{14}S_{24}^* + \cdots + S_{1K}S_{2K}^*, \tag{II.14}$$

$$\mathrm{E}[\mathrm{b}_1\mathrm{b}_1^*] = |S_{13}|^2 + |S_{14}|^2 + \cdots + |S_{1K}|^2, \tag{II.15}$$

$$\mathrm{E}[\mathrm{b}_2\mathrm{b}_2^*] = |S_{23}|^2 + |S_{24}|^2 + \cdots + |S_{2K}|^2, \tag{II.16}$$

From $\mathrm{E}[\mathbf{a}_{\mathrm{F}}\mathbf{a}_{\mathrm{F}}^{\dagger}] = P_{\mathrm{h}}\mathbf{I}$ with 3-D i.i.d. property of free space bound, the raw vector known $\mathbf{s}_1 = [S_{11} \ S_{12} \ \cdots \ S_{1\mathrm{K}}], \mathbf{s}_2 = [S_{21} \ S_{22} \ \cdots \ S_{2\mathrm{K}}]$ becomes

$$\mathbf{s}_1\mathbf{s}_1^{\dagger} = 1, \ \mathbf{s}_1\mathbf{s}_2^{\dagger} = 0, \ \mathbf{s}_2\mathbf{s}_1^{\dagger} = 0, \ \mathbf{s}_2\mathbf{s}_2^{\dagger} = 1, \tag{II.17}$$

Therefore, the correlation coefficient in terms of antenna S-parameter, called as Blanch's

model [49], can be derived as

$$\rho_{\mathrm{b}}^2 = \frac{|\mathrm{E}\left[\mathrm{b}_1\mathrm{b}_2^*\right]|^2}{|\mathrm{E}[\mathrm{b}_1]|^2|\mathrm{E}[\mathrm{b}_2]|^2} = \frac{|S_{11}^* S_{12} + S_{21}^* S_{22}|^2}{\left\{1-(|S_{11}|^2+|S_{21}|^2)\right\}\left\{1-(|S_{22}|^2+|S_{12}|^2)\right\}}. \tag{II.18}$$

This model is derived for high antenna correlation scenario through a simple formulation to compute the envelope correlation of an antenna diversity system. This approach has the advantage that it does not require the computation nor the measurement of the radiation pattern of the antenna system. It also offers the advantage of providing a clear understanding of the effects of mutual coupling on the diversity performance of the antenna system.

In Fig. II.5 the correlation coefficients of various models mentioned above show based on two half wave dipole antenna parameters using both no mutual coupling case with induced EMF data and mutual coupling case with HFSS data depicted in Table 3.2 of Ch. 3. Clarke's correlation coefficient of no coupling case is higher than mutual coupling ones (Yamada's and Blanch's model) due to the radiation pattern distortion effect of antenna array coupling in compact antenna spacing. The mutual coupling may increase the system performance.

Appendix III

Thermal Noise Characteristic

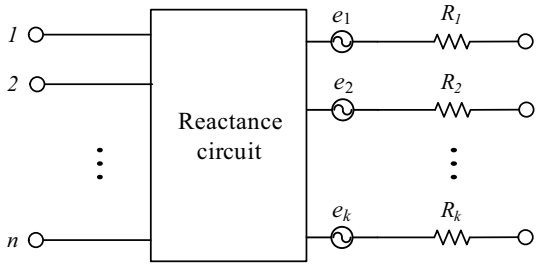


Figure III.1 Schematic of loss property with impedance matrix.

Theorem : The thermal noise covariance matrix $\mathbf{\Sigma}$ is given by real part of impedance matrix $\mathbf{Z}$ times $4k_{\mathrm{B}}T_0B$. where $k_{\mathrm{B}} = 1.38 \times 10^{-23}\mathrm{J/K}$ is the Boltzman's constant, $T_0 = 290\mathrm{K}$ is the standard noise temperature, and B is the bandwidth in Hz.

Proof : It is assumed that n port passive and reciprocal circuit contans k resistances inside. First, we define $(n+k)$-port reactance circuit whose impedance matrix is.

$$j\begin{bmatrix}\mathbf{X}_{11} & \mathbf{X}_{12}\\ \mathbf{X}_{21} & \mathbf{X}_{22}\end{bmatrix}, \tag{III.1}$$

where $\mathbf{X}_{11} : n \times n$ (real) matrix, $\mathbf{X}_{12} : n \times k$ matrix, $\mathbf{X}_{21} : k \times n$ matrix, $\mathbf{X}_{22} : k \times k$ matrix. At k-port, k resistances $(R_1, R_2, \cdots, R_k)$ are connected respectively. We can derive the $n \times n$ impedance matrix $\mathbf{Z}$ as

$$\mathbf{Z} = j\mathbf{X}_{11} + \mathbf{X}_{12}(\mathbf{R} + j\mathbf{X}_{22})^{-1}\mathbf{X}_{21}, \tag{III.2}$$

where $\mathbf{R} = diag(R_1, R_2, \cdots, R_k)$ is diagonal $k \times k$ matrix. Thus the real part of $\mathbf{Z}$ becomes

$$\Re[\mathbf{Z}] = \frac{1}{2}\mathbf{X}_{12}\left[(\mathbf{R} + j\mathbf{X}_{22})^{-1} + (\mathbf{R} - j\mathbf{X}_{22})^{-1})\right]\mathbf{X}_{21} \quad \text{(III.3)}$$

$$= \mathbf{X}_{12}\left[(\mathbf{R} + j\mathbf{X}_{22})^{-1}\mathbf{R}[\mathbf{R} - \mathbf{j}\mathbf{X}_{22}]^{-1}\right]\mathbf{X}_{21}. \quad \text{(III.4)}$$

Next, we will consider a thermal voltage e_i generated by resistance R_i of which second order moment is given by

$$\mathrm{E}[|e_i|^2] = 4k_{\mathrm{B}}T_0BR_i. \quad \text{(III.5)}$$

Defining a thermal noise vector $\mathbf{e} = (e_1, e_2, \cdots, e_k)^T$ with independent e_i as

$$\mathrm{E}\left[\mathbf{e}\mathbf{e}^{\dagger}\right] = 4k_{\mathrm{B}}T_0B\mathbf{R}. \quad \text{(III.6)}$$

Finally, an open voltage vector $\mathbf{E} = (E_1, E_2, \cdots, E_n)^T$ and a covariance matrix of $\mathbf{E}$ are expressed by

$$\mathbf{E} = -j\mathbf{X}_{12}(\mathbf{R} + j\mathbf{X}_{22})^{-1}\mathbf{e}, \quad \text{(III.7)}$$

$$\mathbf{\Sigma} = \mathrm{E}[\mathbf{E}\mathbf{E}^{\dagger}] = 4k_{\mathrm{B}}T_0B\mathbf{X}_{12}(\mathbf{R} + j\mathbf{X}_{22})^{-1}\mathbf{R}(\mathbf{R} - j\mathbf{X}_{22})^{-1}\mathbf{X}_{21} = 4k_{\mathrm{B}}T_0B\Re[\mathbf{Z}], \quad \text{(III.8)}$$

where $\mathbf{X}_{21} = \mathbf{X}_{21}^T$ with reciprocity.

Appendix IV

Constant Noise Factor Circle

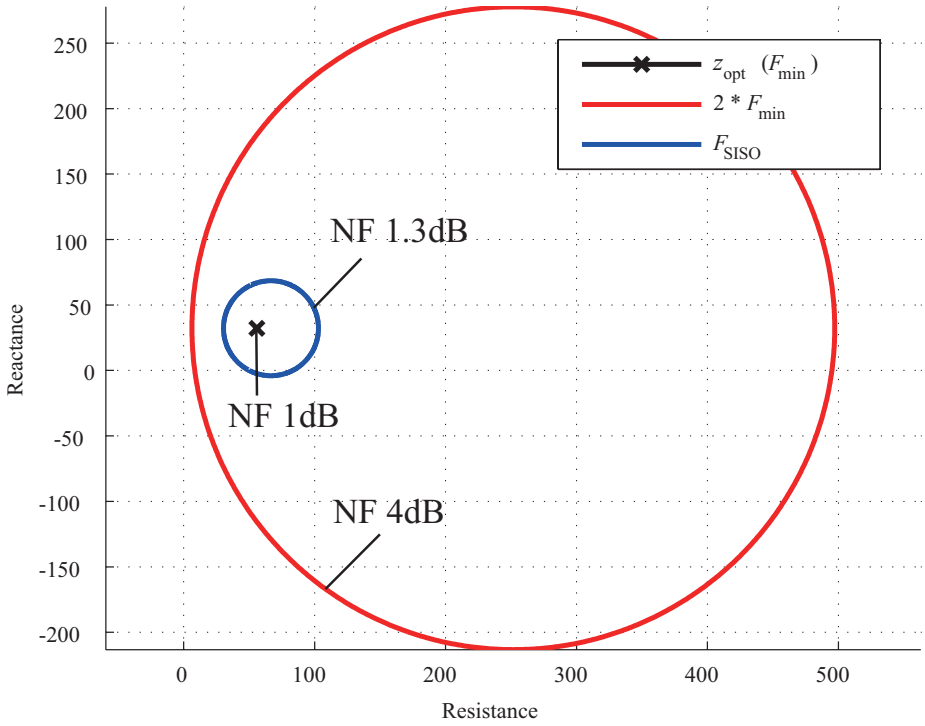


Figure IV.1 NF circle of SISO antenna receiver.

The nearest point to the z_{opt} means to solve minimization issue of noise factor (NF). By changing matching circuit, we can obtain desired position of z'_A. A constant NF circle in a

generator impedance plane for SISO receiver with a center and a radius of NF circle as a function of NF value as

$$F_{\mathrm{SISO}} = 1 + \frac{r_{\mathrm{a}} + g_{\mathrm{a}}|z_{\mathrm{A}} + z_{\mathrm{cor}}|^2}{r_{\mathrm{A}}}, \tag{IV.1}$$

$$\text{Center} : \left(\frac{F_{\mathrm{SISO}} - 1}{2g_{\mathrm{a}}}, -x_{\mathrm{cor}}\right), \quad r_{\mathrm{radius}} : \sqrt{\left(r_{\mathrm{cor}} - \frac{F_{\mathrm{SISO}} - 1}{2g_{\mathrm{a}}}\right)^2 - r_{\mathrm{cor}}^2 - \frac{r_{\mathrm{a}}}{g_{\mathrm{a}}}} \tag{IV.2}$$

The characteristics of NF circle are as following: - Constant NF circle starting point is z_{opt} satisfying with $r_{\mathrm{radius}} = 0$ and F_{min}

1) If NF increases, R also increases

2) No intersection between NF circle

Therefore, it need to consider the distance between z_{opt} and generator impedance for noise matching. Figure IV.1 shows an example of constant NF circle at $z_{\mathrm{opt}} = 55 + j32$ and $z_{\mathrm{A}} = 71 - j3$.

Appendix V

Lossy Matching Network

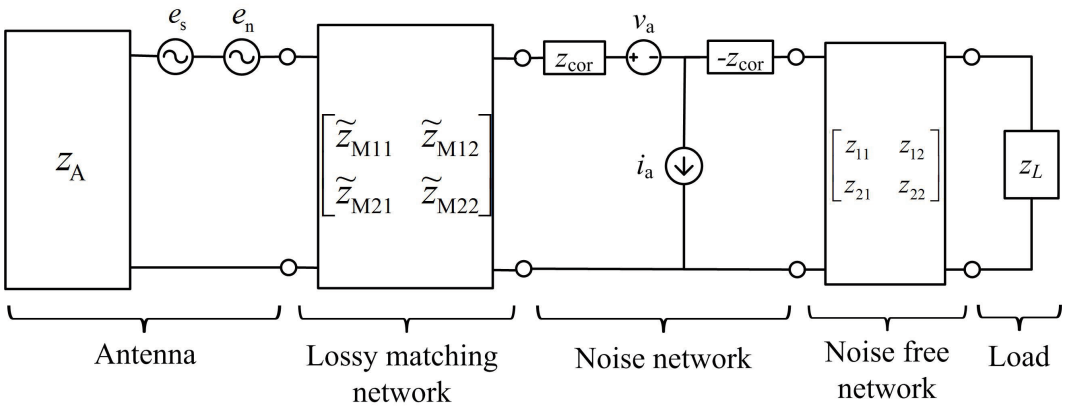


Figure V.1 Single receiver model for lossy matching network.

We briefly review a noise factor of a single receiver model for a lossy matching circuit. Equivalent series resistance (ESR) is essentially existed in practical matching circuit. The resistance brings two effects: 1) signal power degradation and 2) change of revised antenna impedance. In Fig. V.1, the desired voltage source $e_{\rm s}$ and the undesired voltage source $e_{\rm n}$ present the available signal power and the sky noise, respectively. The revised voltage sources by the transfer coefficient $\tilde{M} = \tilde{z}_{\rm M21}/(z_{\rm A} + \tilde{z}_{\rm M11})$ are as follows,

$$e'_{\rm s} = \tilde{M} e_{\rm s}, \quad e'_{\rm n} = \tilde{M} e_{\rm n} + z, \tag{V.1}$$

where the internal noise $z = v_{\rm a} + (z'_{\rm A} + z_{\rm cor}) i_{\rm a}$ with the revised antenna impedance $z'_{\rm A} = r'_{\rm A} + j x'_{\rm A} = -\tilde{M}\tilde{z}_{\rm M12} + \tilde{z}_{\rm M22}$. The noise factor $F_{\rm L}$ of the lossy matching circuit denotes the

ratio of the input and output signal-to-noise ratios as follows,

$$F_{\mathrm{L}} = \frac{S_{\mathrm{i}}/N_{\mathrm{i}}}{S_{\mathrm{o}}/N_{\mathrm{o}}} = LF, \tag{V.2}$$

where signal power loss (L) and original noise factor (F) are given by

$$L = \frac{|e_{\mathrm{s}}|^2/4k_{\mathrm{B}}T_0B\Re(z_{\mathrm{A}})}{|e'_{\mathrm{s}}|^2/4k_{\mathrm{B}}T_0B\Re(z'_{\mathrm{A}})}, \quad F = 1 + \frac{r_{\mathrm{a}} + g_{\mathrm{a}}|z'_{\mathrm{A}} + z_{\mathrm{cor}}|^2}{\Re(z'_{\mathrm{A}})}. \tag{V.3}$$

The signal power loss denotes as the ratio of input and output available power in the matching circuit. The characteristics of the lossy matching circuit are as follows: 1) inequality of signal power loss $L \geq 1$ and 2) noise figure inequality by the revised antenna impedance $F_{\mathrm{L}} \geq F$ where equality holds if and only if lossless condition is satisfied $z'_{\mathrm{A}} = z_{\mathrm{opt}}$.

Appendix VI

List of Publications

Journal papers

- J. Jeong, G. K. Tran and K. Araki, "Optimal low noise single front-end MIMO receiver system with parasitic antenna element," *IEICE Transactions on Electronics, Recent Progress in Microwave and Millimeter-Wave Technologies*, Vol.E95-C, No.10, pp.1620-1626, Oct. 2012

- J. Jeong, G. K. Tran and K. Araki, "Complexity-reduced low noise matching design for realizaion in compact MIMO receivers," *IEICE Transactions on Electronics, Recent Progress in Microwave and Millimeter-Wave Technologies*, Vol.E97-C, No.10, pp.-, Oct. 2014

Conference papers with review

- J. Jeong, Y. Miao, K. Sakaguchi and K. Araki, "Optimal low noise design for single front-end receiver with PAE," *2011 Korea-Japan Microwave Conference*, FR2-4-4, Nov. 2011

- J. Jeong, G. K. Tran and K. Araki, "Ergodic capacity with optimal matching for spatially correlated 2×2 MIMO systems in 3-D isotropic scattering environment," *APMC2014*, Nov, 2014

Conference papers without review

- J. Jeong and K. Araki, "Optimal low noise design for SF-MIMO receiver with parasitic antenna element(PAE)," *IEICE General Conference*, B-1-223, Mar, 2012
- J. Jeong, G. K. Tran and K. Araki, "A study of matching circuit on a lossy condition for compact symmetrical MIMO receiver," *IEICE General Conference*, B-1-207, Mar, 2013
- J. Jeong, G. K. Tran and K. Araki, "Noise figure of matching circuit on lossy condition in 2x2 symmetrical MIMO receiver system," *IEICE Society conference*, BS-6-27, Sep, 2014

Technical report

- J. Jeong, G. K. Tran and K. Araki, "A design of self noise matching circuit for compact MIMO system," *IEICE Technical Report*, MW2012-80, pp83-88, Sep, 2012

Reference

[1] S. M. Alamouti, "A Simple Transmit Diversity Technique for Wireless Communications ," *IEEE Journal on select areas in communications*, vol 16, no 8, Oct. 1998.

[2] V. Tarokh, N. Seshadri, and A. R. Calderbank, "Space-time codes for high data rate wireless communication: Performance analysis and code construction," *IEEE Trans. Inform. Theory*, vol. 44, pp. 744-765, Mar. 1998.

[3] W. C. Y. Lee, " Mutual coupling effect on maximum-ratio diversity combiners and application to mobile radio," *IEEE Trans. Commun. Technol.*, vol. COM-18, pp. 779-791, Dec. 1970.

[4] I. J. Gupta and A. A. Ksienski, " Effect of mutual coupling on the performance of adaptive arrays," *IEEE Trans. Antennas Propag.*, vol. AP-5, pp. 785-791, Sep. 1983.

[5] D. Shiu, G. J. Foschini, M. J. Gans and J. M. Kahn, "Fading correlation and its effect on the capacity of multielement antenna systems," *IEEE Trans. Commun.*, vol. 48, pp. 502-513, Mar. 2000.

[6] G. J. Foschini and M. J. Gans, "On limits of wireless communications in a fading environment when using multiple antennas," *Wireless Personal Commun.*, vol. 6, pp. 311-335, 1998.

[7] C. N. Chuah, D. N. C. Tse, J. M. Kahn, and R. A. Valenzuela, "Capacity scaling in MIMO wireless systems under correlated fading," *IEEE Trans. Inf. Theory*, vol. 48, pp. 637-650, Mar. 2002.

[8] K. Yu, M. Bengtsson, B. Ottersten, D. McNamara, P. Karlsson, and M. Beach, "Second order statistics of NLOS indoor MIMO channels based on 5.2 GHz measurements," *in Proc. Globecom01*, pp. 156-160, Nov. 2001

[9] M. Arai, M. Iwabuchi, K. Sakaguchi and K. Araki, "Optimization of diversity antenna directivities based on spherical mode expansion," *APMC2010*, pp. 1577-1580, Dec 2010.

[10] M. K. ¨ ozdemir, E. Arvas, and H. Arslan, "Dynamics of spatial correlation and implications on MIMO systems," *IEEE Communications Magazine*, pp. 514-519, 2004.

[11] C. A. Balanis, Antenna Theory: Analysis and Design, 3rd ed. New York: Wiley, 2005.

[12] M. C. Leifer, "Signal correlations in coupled cell MIMO antennas," *Proc. IEEE Antennas Propag. Soc. Intern. Symp.*, pp. 194-197, Jun. 2002.

[13] T. S. Svantesson and A. Ranheim, "Mutual coupling effects on the capacity of multielement antenna systems," *Proc. IEEE ICASSP*, pp. 2485-2488, 2001.

[14] C. Waldschmidt, J. v. Hagen and W. Wiesbeck, "Influence and modeling of mutual coupling in MIMO and diversity systems," *Proc. IEEE Antennas Propag. Soc. Intern. Symp.*, pp. 190-193, Jun. 2002.

[15] R. G. Vaughan and J. B. Andersen, "Antenna diversity in mobile communications," *IEEE Transactions on Vehicular Technology*, vol. VT-36, no. 4, pp. 149-172, Nov. 1987.

[16] J. W. Wallace and M. A. Jensen, "Termination-dependent diversity performance of coupled antennas: Network theory analysis," *IEEE Trans. Antennas Propag.*, vol. 52, no. 1, pp. 98-105, Jan. 2004.

[17] R. Janaswamy, " Effect of element mutual coupling on the capacity of fixed length linear arrays," *IEEE Antennas and Wireless Propagation Letters*, vol. 1, pp. 157-160, 2002.

[18] J. W. Wallace and M. A. Jensen, "Mutual coupling in MIMO wireless systems: A rigorous network theory analysis," *IEEE Trans. Wireless Commun.*, Vol. 3, No. 4, pp. 1317-1325, Jul. 2004.

[19] A. Paulraj, R. Nabar and D. Gore, Introduction to Space-Time wireless Communications, Cambridge University Press, 2003

[20] A. Goldsmith, Wireless Communications, Cambridge University Press, 2005

[21] R. G. Vaushan and J. B. Andersen, "Antenna diversity in mobile communications," *IEEE Trans. Veh. Tech.*, vol. 36, pp. 149-172, Nov 1987.

[22] W. Wasylkiwskyj, W. K. Kahn, "Theory of mutual coupling among minimum scattering antennas," *IEEE Tras. Ant. Propg.*, vol. 18, pp. 204-216, 1970.

[23] C. A. Desoer, "The maximum power transfer theorem for n-ports," *IEEE Trans. Circuit Theory*, vol. 20, pp. 328-330, May 1973.

[24] M. L. Morris and M. A. Jensen, "Network model for MIMO systems with coupled antennas and noisy amplifiers," *IEEE Trans. Antennas Propag.*, vol. 53 pp. 545-552, Jan. 2005.

[25] M. J. Gans, "Channel capacity between antenna arrays Part I: Sky noise dominates," *IEEE Trans. Commun.*, vol. 54, pp. 1586-1592, Sep. 2006.

[26] M. J. Gans, "Channel capacity between antenna arrays Part II: Amplifier noise dominates," *IEEE Trans. Commun.*, vol. 54, pp. 1983-1992, Nov. 2006.

[27] C. P. Domizioli, B. L. Hughes, K. G. Gard, G. Lazzi, "Optimal front-end design for MIMO receivers," *in Proc. IEEE Global Commun. Conf.*, Dec. 2008.

[28] C. P. Domizioli and B. L. Hughes, "Front-End Design for Compact MIMO Receivers: A Communication Theory Perspective," *IEEE Transactions on Commun.*, vol. 60, pp. 2938-2949, Oct. 2012.

[29] C. E. Shannon, "A mathmatical theory of communication," *Bell Systems Technical Journal*, pp. 379-423, 623-656, 1948.

[30] W. C. Y. Lee, " Effect of mutual coupling on a mobile-radio maximum ratio diversity combiner with a large number of branches," *IEEE Transactions on Communications*, pp. 1188-1193, Dec. 1972.

[31] Y. Fei, Y. Fan, B. K. Lau, and J. S. Thompson, "Optimal single port matching impedance for capacity maximization in compact MIMO arrays," *IEEE Trans. Antennas Propag.*, Vol. 56, No. 11, pp.3566-3575, 2008.

[32] B. K. Lau, S. M. S. Ow, G. Kristensson, and A. F. Molisch, "Capacity analysis for compact MIMO systems," *Vehicular Technology Conference, VTC 2005-Spring.*, Vol. 1, pp.1550-2252, May. 2005.

[33] B. K. Lau, J. B. Anderson, G. Kristensson, and A. F. Molisch, "Impact of matching network on bandwidth of compact antenna arrays," *IEEE Trans. on antennas and propagation.*, Vol. 54, No. 11, pp.3225-3238, Nov. 2006.

[34] J. Weber, C. Volmer, K. Blau, R. Stephan, and M. A. Hein, "Miniaturized antenna arrays using decoupling networks with realistic elements," *IEEE Trans. Microwave Theory Tech.*, vol. 54, no.6, pp.2733-2740, Jun. 2006.

[35] J. Weber, C. Volmer, K. Blau, R. Stephan, and M. A. Hein, "Implementation of a miniaturised antenna array with predefined orthogonal radiation patterns," *In European Conference on Antennas and Propagation*, pp.1-5, Nov. 2006.

[36] K. Nishimori, N. Honma, and K. Cho, "Evaluation of channel capacity in mimo terminal antenna considering decoupling and matching network," *IEICE technical report. Antennas and propagation*, vol. 109, no. 183, pp. 17-22, Aug. 2009.

[37] A. Kalis, A. Kanatas, and C. Papadias, "A novel approach to mimo transmission using a single RF front end," *IEEE Journal on Selected Areas in Communications*, vol.26, no.6, pp. 972-980, Aug. 2008.

[38] M. Yoshida, K. Sakaguchi, and K. Araki, "Single RF Front-end MIMO transceiver with parasitic antenna elements," *Proceedings of the IEICE General Conference*, Mar. 2010.

[39] M. Yoshida, K.Sakaguchi, and K.Araki, "Single Front-end MIMO Architecture with Parasitic Antenna Elements", *IEICE Trans. Commun.*, vol.E95-B, no.03, pp. 882-888, Mar. 2012.

[40] T. Ohira and K. Gyoda, "Electronically steerable passive array radiator antennas for low-cost analog adaptive beamforming," *IEEE International Conference on Phased Array Systems and Technology*, pp. 101-104, May. 2000.

[41] J. D. Fredrick, Y. Wang, and T. Itoh, "A smart antenna receiver array using a single RF channel and digital beamforming," *IEEE Tras. Microw. Theory Tech.*, vol.50, no.12, Dec. 2002

[42] D. M. Pozar, Microwave Engineering, 3rd ed. New York: Wiley, 2005

[43] R. Q. Twiss, "Nyquist's and Thevenin's therorems generalized for nonreciprocal linear networks," *J. Applied Physics*, vol. 26, pp. 599-602, May 1955.

[44] H. A. Haus and R. B. Adler, Circuit Theory of Linear Noisy Networks. New York: Wiley, 1959

[45] H. Rothe and W. Dahlke, "Theory of noisy fourpoles," *Proc. IRE*, vol. 44, pp. 811-818, Jun. 1956

[46] J. Jeong, Y. Miao, K. Sakaguchi and K. Araki, "Optimal low noise design for single front-end receiver with PAE," *KJMW2011*, Nov. 2011.

[47] R. H. Clarke, "A statistical theory of mobile radio reception", *Bell Systems Technical Journal*, 47, pp.957-1000, 1968.

[48] Y. Yamada, K. Kagoshima and K. Tsunekawa, "Diversity antennas for base and mobile stations in land mobile communication systems", *IEICE Trans.*, vol. E74, pp.3202-3209, 1991.

[49] S. Blanch, J. Romeu and I. Corbella, "Exact representation of antenna system diversity performance from input parameter description," *IEE Eletronics Letters*, vol. 39, pp. 705-707, May 2003.

[50] I. E. Telatar, "Capacity of multi-antenna gaussian channels," *AT & T Bell labs Internal Tech. Memo.*, Jun, 1995.